THE FORMATION AND DECAY OF THE COMPOUND NUCLEUS Ge^{68}

BY

FRANCIS HENRY RUDDY

A.B. CLARK UNIVERSITY, 1963

A.M. WASHINGTON UNIVERSITY, 1965

A DISSERTATION SUBMITTED IN PARTIAL FULFILLMENT

OF THE REQUIREMENTS FOR THE DEGREE OF

DOCTOR OF PHILOSOPHY

IN THE DEPARTMENT

OF

CHEMISTRY

SIMON FRASER UNIVERSITY

APRIL, 1968

EXAMINING COMMITTEE

Professor B. D. Pate, Head
Department of Chemistry
Simon Fraser University
Research Supervisor

_____ Professor E. Vogt
Department of Physics
University of British Columbia
External Examiner

___ Professor E. J. Wells
Department of Chemistry
Simon Fraser University
Examining Committee

Professor R. G. Korteling
Department of Chemistry
Simon Fraser University
Examining Committee

__ Professor J. M. D'Auria
Department of Chemistry
Simon Fraser University
Examining Committee

PARTIAL COPYRIGHT LICENSE

I hereby grant to Simon Fraser University the right to lend my thesis or dissertation (the title of which is shown below) to users of the Simon Fraser University Library, and to make partial or single copies only for such users or in response to a request from the library of any other university, or other educational institution, on its own behalf or for one of its users. I further agree that permission for multiple copying of this thesis for scholarly purposes may be granted by me or the Dean of Graduate Studies. It is understood that copying or publication of this thesis for financial gain shall not be allowed without my written permission.

Title of Thesis/Dissertation:

_____

_____

_____

_____

Author: _____

(signature)

_____

(name)

_____

(date)

ABSTRACT

Experimental excitation functions have been measured by radiochemical means for a number of reactions proceeding through the compound nucleus Ge^{68}. The target-projectile pairs were: $He^{4}+Zn^{64}$, $C^{12}+Fe^{56}$, and $O^{16}+Cr^{52}$ leading to the following reactions: (α,γ), (x,p), (x,n), (x,pn), and $(x,2n)$. Recoil ranges were measured for products of the alpha-induced reactions in order to determine those reactions which proceeded by compound nucleus formation and decay. It has been found that the "independence hypothesis" is verified for reactions induced by different target-projectile pairs but proceeding through compound nuclei of nearly equal angular momentum.

Excitation functions have been calculated with the SFU IBM System 360/40 computer via the statistical theory of nuclear reactions according to a formalism containing the explicit dependence of nuclear emission probabilities on angular momentum. Probabilities for γ-ray emission were calculated according to the single-particle model coupled with enhancement functions chosen to reflect experimentally observed collective effects.

Agreement between experiment and calculations was found to be good for the $Zn^{64}+He^{4}$ excitation functions. The "high energy tails" of the excitation functions were found to be accounted for by effects of γ-ray competition with particle emission when the latter was surpressed by angular

momentum effects. Agreement in the $Fe^{56}+C^{12}$ case was found to be very encouraging, considering the complexity of the target-projectile system and attendant theoretical difficulties.

RESUME

Les fonctions d'excitation expérimentales ont été mesurées par les moyens radiochimiques pour plusieurs réactions qui ont lieu comme résultat de la formation du noyau composé Ge^{68}. Les paires de projectile-cibles étaient: $He^{4}+Zn^{64}$, $C^{12}+Fe^{56}$, et $O^{16}+Cr^{52}$ qui produisent les réactions suivantes: (α,γ), (x,p), (x,n), (x,pn), et (x,2n). On a mesuré les distances d'atomes reculants pour les produits des réactions alpha-induites pour déterminer ces réactions qui ont résulté de la formation et de la décomposition de noyaux composés. On a vérifié "l'hypothèse d'indépendance" pour les réactions, induites par de différentes paires de projectile-cibles, mais qui résultent de noyaux composés d'à peu près la même quantité de mouvement angulaire.

On s'est servi de l'ordinateur SFU IBM Système 360/40 pour calculer les fonctions d'excitation par moyen de la théorie statistique de réactions nucléaires et selon le formalisme, qui contient la dépendance explicite, des probabilitiés d'émission nucléaire, du quantité de mouvement angulaire. On a calculé les probabilités d'émission de rayons γ selon le modèle à une seule particule en conjonction avec les fonctions d'augmentation, qui ont été choisies pour démontrer les effets collectifs observés par de différents expérimentateurs.

L'accord entre l'expérience actuelle et les calculs pour les fonctions d'excitation $Zn^{64}+He^{4}$, était bon. On pourrait expliquer la persistance de grandes valeurs pour la section efficace aux hautes énergies par les effets de la concurrence entre les rayons γ et l'évaporation de particules quand celle-la fut supprimée par les effets de quantité de mouvement angulaire. L'accord au cas de $Fe^{56}+C^{12}$ était très encourageant, si l'on tient compte de la complexité du système de projectile-cibles et des difficultés théoriques.

TABLE OF CONTENTS

page

LIST of TABLES

LIST of FIGURES

page

page

ACKNOWLEDGEMENTS

The Author wishes to express his sincere gratitude to Professor Brian D. Pate for his guidance, advice, and patience during the course of this work.

Thanks are also due to:

Dr. A. H. Sher for providing Ge(Li) detectors and for assistance with several experiments;

Professor E. Vogt for many helpful discussions;

Professors M. Blann and J. M. Miller for valuable advice;

Drs. I. Preiss, I.-M. Ladenbauer-Bellis, H. Bahkru, and A. Ewart for assistance during the HILAC runs, and the Chemistry Department and Physics Department of Yale University for their hospitality during the summer of 1966;

Professor R. Vandenbosch for providing laboratory facilities during the University of Washington runs;

Dr. J. Heagney and the late Dr. T. Morgan for cooperative scheduling at the University of Washington, and Miss J. Beechel and Mr. J. Orth for skillfull cyclotron operation;

Professors A. C. Wahl and J. B. Reynolds for assistance during the early phases of this work;

Dr. J. Hood and Mr. R. Head for cooperative scheduling and assistance with the Washington University runs;

Mr. E. Miller and the staff of the Simon Fraser University Data Processing Centre for assistance in carrying out calculations at the SFU Computing Centre, supported in part by National Research Council Grant Number E-997;

Dr. T. W. Donnelley for providing use of his optical model program and to the University of British Columbia Computing Centre for carrying out the calculations;

Miss Ann Rice, Miss Lorna Bennett, and Mr. W. A. Nelles for highly competent processing of data;

Mr. F. Wick, Mr. A. Stuart, Mr. W. Hall and the staffs of the SFU Workshops for providing excellent equipment;

Mr. and Mrs. T. S. R. Bennett for providing diagrams and for accurate typing of the manuscript of this thesis;

The Faculty and Staff of the Chemistry Department of Simon Fraser University and, in particular, the Nuclear Chemistry Group for providing fellowship and encouragement;

And; The National Research Council for providing generous support of this work.

I. INTRODUCTION

A. Nuclear Reaction Mechanisms

1. Compound Nucleus Reactions

The term nuclear reaction is applied to a variety of processes involving the collisions of nucleons or groups of nucleons.

One of the simplest types of nuclear reaction is the interaction of a neutron with a target nucleus. Early workers[1], measuring the variation of neutron reaction cross-sections over small bombarding energy ranges, found large flucuations (termed "resonances"), the widths ($\approx$0.1 eV) of which are small compared to the spacing (1 - 10^3 eV) between them. Bethe[2] attempted to explain neutron reactions in terms of a potential-well model, but was unable to account for the narrowness of the resonances. The postulate that the resonances corresponded to many-particle excited states of the product nucleus rather than virtual single-particle states of a neutron in a nuclear potential well led to the conclusion by Bohr[3] and by Breit and Wigner[4] that the incoming neutron rapidly shared its energy with the nucleons of the target nucleus to form a "compound nucleus".

In classical terms, Bohr visualised the reaction as a two-step process in which the bombarding energy is first distributed among all of the nucleons to form a metastable state which may then decay in a number of ways.

The excitation energy, if reconcentrated on a nucleon or group of nucleons near the surface of the nucleus as a result of random nucleon-nucleon collisions may supply enough energy to eject the particle or particles in question, or the compound nucleus could de-excite by the emission of gamma rays. In the case of higher mass nuclides, de-excitation could also occur by division of the compound nucleus into two fragments of nearly equal mass, a process called fission.

Bohr concluded that the compound nucleus lifetime must be long compared to nuclear relaxation times[3], but the validity of the model has been found to extend to short-lived reaction systems[5]. The two steps, compound nucleus formation and decay, were assumed to be independent; that is, the decay of a compound nucleus would depend only on the constants of motion of that particular compound nucleus, not on how it was formed. This is the so-called independence hypothesis; one consequence of it is that the probability for a given reaction may be factored into two parts, one corresponding to the formation probability (the cross-section for capture of the incoming particle) and a second to the decay probability as follows:

$$\sigma\,(a,b) = \sigma_{cap}\,(a)\left[\frac{P_b}{\sum_i P_i}\right]$$

The quantity in square brackets (the branching ratio) is the quotient of the probability for de-excitation via the reaction channel "b" (ie., to form a particular residual

nucleus and particle with a given kinetic energy) and the probability sum over all possible exit channels.

The principle of detailed balance must hold for compound nucleus reactions, that is, the reaction system must be symmetric with respect to the exchange of entrance and exit channels. Thus,

$$\frac{\sigma(a,b)}{\lambda^2_a} = \frac{\sigma(b,a)}{\lambda^2_b}$$

Where λ_a and λ_b are the reduced De Broglie wave lengths of the system in the entrance and exit channels[6.7].

2. Direct Interactions

A necessary condition in compound nucleus reactions is that energy equilibration be achieved after the incoming particle enters the target nucleus. However, a second group of reactions proceeds via a quite different mechanism in which much less than complete projectile momentum is transferred to the compound nucleus. These processes are called "direct interactions". In one form, for instance, the incoming particle may enter the target nucleus, excite a small number of nucleons to bound excited or unbound states and retain enough energy to leave the nucleus.

Another well characterised form of direct interaction is the Oppenheimer-Phillips reaction[8]. This reaction involves the interaction of a deuteron with a nucleus resulting in the absorption by the nucleus of a

neutron to populate single particle neutron states accompanied by the emitting of a high energy proton (with the proton energy perhaps exceeding the initial deuteron energy).

Compound nucleus reactions and direct interactions may be thought of as two opposite extreme mechanisms for low energy nuclear reactions. A particular reaction may proceed by an intermediate mechanism with more characteristics of one extreme than the other.

3. Experimental Distinction of Reaction Mechanisms

The predominant mechanism may often be deduced from experimental results. In the case of a compound nucleus reaction, the cross-section for formation of a specific product nucleus (say by means of an (α,n) reaction) should increase rapidly with bombarding energy until the threshold for a competing reaction (e.g., the emission of two nucleons instead of one) is reached; at this point the cross-section for the (α,n) reaction will begin to fall as the competing reaction cross-section rapidly rises. This follows from the strong dependence of the excitation energy of the compound nucleus on bombarding energy.

On the other hand, the incoming particle in a direct interaction deposits an excitation energy which is weakly related to the bombarding energy, thus rapid changes in the cross-section with the bombarding energy due to the competition described above would not be expected.

The statistical model predicts that the emission of particles from the compound nucleus is a stochastic process, and, therefore, that a compound nucleus (with zero angular momentum) emits particles isotropically. However, if a compound nucleus has a non-zero angular momentum, particles will be emitted preferentially in the equitorial plane. Classically, the compound nucleus may be thought of as a flywheel, emitting particles tangentially in its plane of rotation. The axis of rotation is perpendicular to the beam direction, hence preferential emission will be found at 0° and 180° to the beam direction in the center-of-mass system, with the overall distribution symmetric about 90°.

Most direct interactions, however, will show preferential emission at small angles to the incident beam direction as a result of the fact that a substantial fraction of the incident particle momentum is transferred directly to the emitted particles.

The emitted particle energy spectrum in the case of compound nucleus reactions is expected to be Maxwellian (except for coulomb barrier effects), but the energy spectrum for direct interactions will be more intense at higher energies, and often peaks may be resolved, corresponding to the low-energy single particle states which have been excited in the target nucleus.

The residual nuclei of a nuclear reaction will have more recoil energy in the compound nucleus case, since the linear momentum of the bombarding particle is transferred completely to the compound system.

If a projectile of energy E_a and mass A_a strikes a target of mass A_t to form a compound nucleus which emits a particle to form a residual nucleus with mass A_r and recoil energy E_r, then,

$$E_r = \frac{E_a\ A_a\ A_r}{(A_a + A_t)^2} = CE_a \qquad (1\text{-}a)$$

where C is a constant. Furthermore, from experiment it is found that the recoil range in matter $R_r = C'E_r$ so that $R_r = C''E_a$, or a plot of the range of recoiling nuclei vs. the bombarding energy should be a straight line.

This result would not be expected in direct interactions, on the other hand, since the amount of energy transferred to recoiling nuclei is weakly related to the bombarding energy and is always less than E_r calculated from equation (1-a). Having found proportionality between range and energy over a specific bombarding energy region, one may resort to theoretical range-energy relationships to calculate a recoil energy corresponding to an experimental range and then compare the energy with that calculated for complete momentum transfer. (see appendix I). Confidence in the theoretical calculation is gained by comparing theory to experiment at the reaction threshold where full momentum transfer must be achieved for the reaction to proceed.

B. The Statistical Model

1. Weisskopf Evaporation Formula

Bethe[10.], Weisskopf[11.], and Weisskopf and Ewing[12.] developed early statistical models to deal with compound nucleus reactions. Weisskopf[11.], comparing the emission of nucleons by an excited nucleus to the evaporation of molecules by a liquid drop (an analogy first suggested by Frenkel[13.]), performed the thermodynamic derivation which follows. If one considers a nucleus B with energy E_B and a neutron with energy between ϵ and $\epsilon + d\epsilon$ and velocity $v = \left(\frac{2\epsilon}{M} \right)^{\frac{1}{2}}$ enclosed in a volume Ω, the probability P_C per unit time that the neutron will be captured to form nucleus A with energy between E_A and $E_A + d\epsilon$ is given by

$$P_C = \sigma (E_A, \epsilon) \frac{v}{\Omega} \qquad (1\text{-b})$$

where $\sigma (E_A, \epsilon)$ is the mean cross-section for the collision of the neutron with nucleus B ($E_B = E_A - E_0 - \epsilon$) producing compound nucleus A (E_A), and E_0 is the binding energy of the neutron to nucleus B. The probability for the reverse process is obtained by dividing P_C by the number $(\omega_A(E_A)d\epsilon)$ of states into which the neutron can be captured and multiplying by the number $(\omega_B(E_A - E_0 - \epsilon))$ of states into which $A(E_A)$ can decay. In the volume Ω, there are

$$\frac{\Omega\, gm}{2\, \pi^2\, \hbar^3} \, (2m\epsilon)^{\frac{1}{2}} \, d\epsilon$$

translational states which may be occupied by the neutron (g is the spin degeneracy of the neutron), so that by detailed balance

$$P_n(\epsilon)\,d\epsilon = P_c \frac{\omega_B(E_B)}{\omega_A(E_A)} \frac{\Omega\, gm}{2\pi^2\hbar^3} (2m\epsilon)^{\frac{1}{2}}\, d\epsilon$$

or

$$P_n(\epsilon)\,d\epsilon = \sigma(E_a,\epsilon) \frac{gm\,\epsilon}{\pi^2\hbar^3} \frac{\omega_B(E_B)}{\omega_A(E_A)}\, d\epsilon \qquad (2\text{-b})$$

The entropy of a nucleus with energy between E and E + dE is defined by

$$S \equiv \log \omega(E)$$

Then,

$$P(\epsilon)d\epsilon = \sigma(E_A,\epsilon) \frac{gmE}{\pi^2\hbar^3} e^{S_B(E_A-E_O-\epsilon)-S_A(E_A)}\, d\epsilon$$

If $E_A \gg E_O$ and $E_A \gg \epsilon$ and ω_A and ω_B are assumed to be identical functions ($\omega_A(E) = \omega_B(E)$), a Taylor expansion on S_B yields

$$S_B(E_A - E_O - \epsilon) = S_A(E_A) - (E_O+\epsilon)\left(\frac{dS_A}{dE}\right)_{E_A}$$

Also $\frac{dS_A}{dE} = \frac{1}{T_A(E)}$ where $T_A(E)$ is the temperature (in units of kT) at which the most probable energy of the body A is equal to E. Thus,

$$P(\epsilon)d\epsilon = \sigma(E_A,\epsilon) \frac{gm}{\pi^2\hbar^3} e^{-E_O/T_A(E)}\, \epsilon e^{-\epsilon/T_A(E_A)} \qquad (3\text{-b})$$

Which is the usual form of Weisskopf's evaporation formula.

2. The Fermi Gas Model

Little is known about the densities of levels in highly excited nuclei; the variation of level density with energy has been derived from appropriate models. A widely used formulation may be derived from the Fermi gas model, in which the nucleus is described as a collection of degenerate fermions enclosed in a sphere of radius R. Under these restrictions, one may use the principles of statistical thermodynamics to derive a level density for the system.[14]. The number of states occupied by nucleons with momentum less than P_F (the momentum corresponding to the "Fermi energy") is given by

$$N = \frac{2}{(2\pi\hbar)^3} \frac{4}{3} \pi \Omega P_F^3 \qquad (\Omega = \frac{4}{3}\pi R^3)$$

At complete degeneracy (ie., the ground state),

$$P_F^{\text{proton}} = (3\pi^2)^{\frac{1}{3}} \hbar \left(\frac{Z}{\Omega}\right)^{\frac{1}{3}}$$

$$P_F^{\text{neutron}} = (3\pi^2)^{\frac{1}{3}} \hbar \left(\frac{A-Z}{\Omega}\right)^{\frac{1}{3}} \qquad (4\text{-b})$$

Where Z and A are the proton and mass numbers respectively. The total kinetic energy of the protons considered as a degenerate gas at absolute zero is given by

$$E_0^{\text{protons}} = \frac{2\Omega}{(2\pi\hbar)^3} \int_0^{P_F} \frac{p^2}{2m} 4\pi p^2 \, dp$$

$$= \frac{\pi \frac{4}{3} 3^{\frac{5}{3}}}{10} \left(\frac{Z}{\Omega}\right)^{\frac{2}{3}} Z \frac{\hbar^2}{m}$$

$$= \frac{3}{5} \frac{P_F^2}{2m} Z = \frac{3}{5} E_F Z$$

(m is the mass of the proton)

If the Fermi gas is heated to a temperature T (ie., the nucleus is excited), the excitation energy may be related to the temperature of the gas using formulas valid for a perfect gas of fermions of high degeneracy.[15] One obtains[14] for protons

$$(E_T - E_0)^{\text{protons}} = \frac{\pi^2}{4} Z \frac{k\ T^2}{E_F}$$

where k is Boltzman's constant. Substituting the value of E_F calculated from the P_F of equation (4-b),

$$(E_T - E_0)^{\text{protons}} = \frac{\pi^2}{72} \frac{\Omega m}{\hbar^2} \left(\frac{Z}{\Omega} \right)^{\frac{1}{3}} (kT)^2$$

Similarly, for neutrons

$$(E_T - E_0)^{\text{neutrons}} = \frac{\pi^2}{72} \frac{\Omega m}{\hbar^2} \left(\frac{A-Z}{\Omega} \right)^{\frac{1}{3}} (kT)^2$$

Summing the neutron and proton energies

$$(E_T - E_0)^{\text{total}} = 0.08 A^{\frac{2}{3}} [Z^{\frac{1}{3}} + (A-Z)^{\frac{1}{3}}](kT)^2$$

$$= a\ (kT)^2$$

Where a is called the Fermi gas constant. The density of states at a given energy is related to the entropy of the gas by

$$S = k \log \frac{\rho(E)}{\rho(0)}$$

or,

$$\rho\ (E) = \rho\ (0)\ e^{S/k} \qquad (5\text{-b})$$

Thermodynamically,

$$S(T) = \int_0^T \frac{dE}{T}$$

$$= 2\,ak^2 \int_0^T T\,\frac{dT}{T}$$

$$= 2\,ak^2\,T$$

$$= 2\,(ak^2E)^{\frac{1}{2}} \qquad (6\text{-b})$$

Equating quantities in equations (5-b) and (6-b)

$$k \log \frac{\rho(E)}{\rho(0)} = 2\,(ak^2E)^{\frac{1}{2}}$$

or

$$\frac{\rho(E)}{\rho(0)} = e^{2(aE)^{\frac{1}{2}}}$$

$$\rho(E) = Ce^{2\sqrt{aE}} \qquad (7\text{-b})$$

Many calculations have been performed using a level density of the above form (equation (7-b)) where C and a were assumed to be adjustable parameters which were varied to give a best fit to experimental data.[16,17]

The Fermi gas level density expression must, however, be corrected for nucleon angular momentum pairing. Weisskopf and Ewing[12] suggested adjustment of the pre-exponential constant as follows:

$C_{odd\text{-}odd} = 4C_{even\text{-}even}$ and $C_{even\text{-}odd} = C_{odd\text{-}even} = 2C_{even\text{-}even}$

Hurwitz and Bethe[18] concluded that it is more realistic to consider odd-even effects on level densities as arising from displacements of the ground-state energies caused by nucleon pairing.

Thus, the energy appearing in the level density expression must be measured from a virtual ground state, displaced upward from the true ground state by an amount equal to the pairing energy. For even-even nuclei, the proton and neutron pairing energies cause an additive displacement, thus,

$$\delta_{oe} \approx \delta_{eo} \qquad \text{and} \qquad \delta_{ee} \approx 2\ \delta_{oe}$$

Cameron[19] has calculated pairing energies from a comparison of results of his semi-emperical mass equation with measured atomic masses. Newton[20] has taken shell effects into account by calculating a characteristic value of $\underline{a}$ for each proton and neutron number.

Dostrovsky, Fraenkel, and Friedlander[21] have corrected for shell effects by including an additional energy shift which is positive just before and negative after closed shells.

3. Capture and Inverse Cross-Sections

A neutron, striking a target with impact parameter b, if captured, will form a system with an angular momentum vector normal to the direction of the relative momentum (p) of the neutron and target and of magnitude

$$L = pb = \frac{\hbar b}{\lambda} \qquad (8\text{-}b)$$

Where λ is the reduced De Broglie wave length of the system in the entrance channel. The angular momentum is quantized in units of $\hbar$, so that

$$L = \iota\hbar \qquad \iota = 0,1,2,3,\ldots\ldots \iota_{max} \qquad (9\text{-}b)$$

The maximum value of ℓ is limited by the maximum value of the impact parameter which is the sum of radii of the neutron and target ($b_{max} = R$), and from combination of equations (8-b) and (9-b),

$$b_{max} = \ell_{max} \lambda$$

or

$$\ell_{max} = R / \lambda$$

Classically, one may think of the probability for formation of an intermediate system with a specific angular momentum as corresponding to the probability that the neutron will hit the nucleus with a velocity and an impact parameter corresponding to that particular value, thus[9].

$$\begin{aligned} \sigma_\ell &= \pi\lambda^2 [(\ell+1)^2 - \ell^2] \\ &= \pi\lambda^2 (2\ell+1) \end{aligned} \qquad (10\text{-b})$$

The total cross-section is the sum of these partial cross-sections over ℓ[9].

$$\begin{aligned} \sigma_r &= \sum_{\ell=0}^{\ell_{max}} \sigma_\ell \\ &= \pi\lambda^2 \sum_{\ell=0}^{\ell_{max}} (2\ell+1) \\ &= \pi\lambda^2 (\ell_{max} + 1)^2 \\ &= \pi (\lambda+R)^2 \end{aligned} \qquad (11\text{-b})$$

Equation (11-b) represents an upper limit for σ_r since, in reality, not all collisions will result in capture. Barrier penetration (or transmission) coefficient must be introduced into the sum as follows:

$$\sigma_r = \pi\lambda^2 \sum_{l=0}^{l_{max}} (2l+1)\, T_l \qquad (12\text{-b})$$

where

$$T_l \leq 1$$

In the case of a charged particle interacting with a target nucleus, the value of the relative momentum at the point of contact will be

$$p = (2\mu)^{\frac{1}{2}}(\epsilon - B)^{\frac{1}{2}} = (2\mu\epsilon)^{\frac{1}{2}}\left(1 - \frac{B}{\epsilon}\right)^{\frac{1}{2}}$$

Where ϵ is the energy of charged particle, μ is the reduced mass, and the coulomb barrier, B, is given by

$$B = \frac{Z_x\, Z_T\, e^2}{R}$$

In this case, the upper limit for the cross-section may be shown[9] to be

$$\sigma_r = \pi R^2 (1 - B/\epsilon) \qquad (13\text{-b})$$

Equation (12-b) is valid for charged particle cross-sections, provided that the coulombic as well as the centrifugal barrier has been included in the calculation of the transmission coefficients.

Equations such as (13-b) have often been used for the approximate calculation of inverse reaction cross-sections and capture cross-sections.[35]

However, the development of the optical model (sec. I-C(1.)) has made possible more detailed calculation of transmission coefficients and several optical model computer programs are available for this purpose.[23-25].

C. Modern Compound Nucleus Theories

1. The Optical Model

When considering the interactions of incoming particles with target nuclei, an exact treatment of the many body problem is prohibitively complicated; many simplifying assumptions are necessary for all but two-body cases. Most treatments of particle-nucleus interactions neglect all structure of the nucleus and adopt a model which will describe the nuclear properties of interest.

Bethe[2] described the nucleus as a real potential well, characterised only by its radius and depth. However, several features of this model were found to be inadequate; the magnitude of predicted neutron capture cross-sections, the wide spacing of resonances, and the slow change of cross-sections with energy were not in agreement with experimental results.

Compound nucleus theories, alone, were also found to be inadequate, since no account is taken of direct interaction contributions.

The addition of an imaginery term to the potential of the well in Bethe's model was found to extend its range and accuracy. Early work by Serber[26] and by Fernbach, Serber, and Taylor[27] resulted in the proposal that the elastic scattering of neutrons be compared with the scattering of a wave by a refracting and absorbing sphere of refractive

index

$$\eta = \left(1 - \frac{V_{nuc}}{E}\right)^{\frac{1}{2}}$$

Where the wave-length of the light corresponds to the energy of the neutrons ($E = h\upsilon$). The nuclear potential is of the form

$$V_{nuc} = V + iW$$

Where V is the average single particle real potential deflecting particles from straight-line motion, and W is the "absorption potential" representing the particles lost in the formation of compound nuclei[28]. The nuclear potential is a function of the radial distance, r, between the centers of the interacting bodies, and spin-orbit interactions must be considered (except where both particles are of zero spin), leading to the following form:

$$V_{nuc}(r) = Vf(r) + iWg(r) + \left(\frac{\hbar}{\mu c}\right)^2 (V_{so}+iW_{so})\left(\frac{df}{r dr}\right)\sigma \cdot \iota$$

Where V and W are the depths of the real and imaginery potentials, V_{so} and W_{so} are the real and imaginary spin-orbit potentials, σ is the Pauli spin operator, ι is the orbital angular momentum in units of $\hbar$, and f(r) and g(r) are form factors.[29]

According to the Woods-Saxon[30] configuration

$$f(r) = \left[1 + \exp\left(\frac{r-R}{a}\right)\right]^{-1} \qquad \text{(c-1a)}$$

Where R is the sum of the nuclear radii of the interacting particles ($R = r_o(A_T^{\frac{1}{3}}+A_x^{\frac{1}{3}})$) and $\underline{a}$ is a parameter which measures the real radial diffusness.

Two different assumptions have been made about the form factor g(r).[29.]

(1.) $g(r) = f(r)$ This assumption corresponds to volume absorption.

(2.) Surface absorption.

In the latter case (a purely phenomenological approach) the imaginary form factor is usually assumed to be Gaussian.

$$g(r) = \exp\left[\frac{-(r-R)^2}{b^2}\right] \qquad (c\text{-}1b)$$

Where b corresponds to the imaginary radial diffusness, but is usually treated as an adjustable parameter. The real form factor is usually taken from the Woods-Saxon configuration in both cases.[29.]

The total potential is

$$V_T(r) = V_c(r) + \frac{\iota(\iota+1)\hbar^2}{2\mu r^2} + V_{nuc}(r) \qquad (c\text{-}2)$$

Where the first two terms correspond to coulombic and centrifugal potentials. The transmission coefficients for equation (12-b) may be calculated from optical model phase shifts (δ_ι)[5.]

$$T_\iota(\epsilon) \equiv 1 - \left|e^{2i\delta_\iota\epsilon}\right|$$

The phase shifts being obtained by solution of the Schrodinger equation:

$$[-(\frac{\hbar^2}{2M})\nabla^2 + V(r)]\psi = E\psi$$

using the V(r) of equation (c-1).

Since, if a spin-orbit interaction is used, the calculated transmission coefficients will be angular momentum dependent, the form of the summation to obtain the cross-section will be dictated by the way in which the angular momenta are coupled. If intermediate coupling, (see appendix II) is used, the angular momentum distribution of the compound nuclear states is given by[6].

$$\sigma_c(I,\epsilon,J_c) = \frac{\pi\lambda^2(2J_c+1)}{(2s+1)(2I+1)} \sum_{S=|I-s|}^{I+s} \sum_{l=|J_c-S|}^{|J_c+S|} T_l(\epsilon) \qquad (c\text{-}4)$$

For cases where I = s = o, (c-4) reduces to

$$\sigma_c(\epsilon,J_c) = \pi\lambda^2 \sum_l (2l+1)\, T_l(\epsilon) \qquad (c\text{-}5)$$

which is identical in form to equation (12-b) except that σ_c and T_l now refer to a specific angular momentum. The total reaction cross-section of equation (12-b) is given by

$$\sigma_r = \sum_{J=0}^{\infty} \sigma_c\ (\epsilon,J_c)$$

2. Angular Momentum Considerations

Since the impact parameter is not unique in nuclear reactions, compound nuclei will be formed with a distribution in angular momentum which is a function of the nature and energy of the reacting system. Equation (2-b) which was derived without reference to angular momentum, may be rewritten to include angular momentum effects as follows:

$$P\ (E_F, J_F; E_C, J_C)\ d\epsilon = \frac{(2s_x+1)}{\pi^2\ \hbar^3} \cdot \epsilon \cdot \mu \cdot \sigma(\epsilon, J_C, J_F)\ \frac{\omega(E_F, J_F)}{\omega(E_C, J_C)}\ d\epsilon \qquad (c-6)$$

Where, for clarity, the subscripts A and B have been changed to C and F, signifying "compound" and "final" respectively. The spin degeneracy, g, has been replaced by its equivalent, $2s_x + 1$, where s_x is the spin of the particle x in the entrance channel.

The total probability Γ_{xJ} for emission of particle x from a compound nucleus with exitation energy E_C and angular momentum J_C is the probability given in equation (c-6), summed over all possible J_F and integrated over all possible energies of emission.

$$\Gamma_{xJ}\ (E_C, J_C) = \frac{(2s_x+1)\mu}{\pi^2\ \hbar^3} \int_\epsilon \epsilon \sum_{J_F} \sigma_x(\epsilon, J_C, J_F)\ \frac{\omega(E_F, J_F)}{\omega(E_C, J_C)}\ d\epsilon \qquad (c-7)$$

The cross-section for a particular reaction, e.g. $X + b \rightarrow Y + x$ is given by

$$\sigma(b,x) = \sum_{J_C} \sigma_{cap}(\epsilon_b, J_C, I)\ \frac{\Gamma_{xJ}\ (E_F, J_F)}{\sum_i \Gamma_{iJ}\ (E_F, J_F)} \qquad (c-8)$$

Where I is the spin of the target nucleus and the sum over I includes all possible particles which may be emitted by the compound nucleus. It can be seen that factoring of the formation and decay probabilities is no longer possible, so that the independence hypotheses as previously stated is no longer valid. The independence hypothesis is valid for a particular J_c however, since

$$\sigma(b,x) = \sum_{J_C} \sigma_{J_C}(b,x)$$

where

$$\sigma_{J_C}(b,x) = \sigma_{cap}(\epsilon_b, J_C, I) \frac{\Gamma_{xJ}(E_F, J_F)}{\sum_i \Gamma_{iJ}(E_F, J_F)}$$

The capture and inverse cross-sections in equations (c-8) and (c-6) may be calculated as in section C-1.

The level density will also be affected by the inclusion of angular momentum considerations. From the general theoretical grounds of statistical mechanics, the dependence of the level density on angular momentum is expected to be[29].

$$(2J + 1) \exp\left[\frac{-(\text{rotational energy})}{(\text{temperature})} \right]$$

If M is the total angular momentum projection on a Z-axis and the number of particles, N, is large, the statistical central limit theorem predicts that the distribution of

M will be Gaussian

$$\omega(M) \alpha \exp\left[\frac{-M^2}{2\sigma^2} \right]$$

or

$$\omega(E,M) = \left[2\pi\sigma^2 \right]^{\frac{1}{2}} \omega(E) \exp\left[\frac{-M^2}{2\sigma^2} \right] \qquad (c\text{-}9)$$

Where $\sigma^2 = N\langle m^2 \rangle$ is the mean square deviation of M, m being the projection of the angular momentum of a single particle. The projections of the total angular momentum are

$M = J, J-1, \ldots\ldots, -J$, and

$$\omega(E,M) = \sum_{J=|M|}^{J_{max}} \omega(E,J)$$

so that

$$\omega(E,J) = \omega(E,M=J) - \omega(E,M=J+1) \qquad (c\text{-}10)$$

Since $\omega(E,M=J)$ and $\omega(E,M=J+1)$ may be expanded in a Taylor series about $M = J + \frac{1}{2}$,[44,45].

$$\omega(E,M=J) = \omega(E,J+\tfrac{1}{2}) + (M-J-\tfrac{1}{2}) \frac{\partial \omega}{\partial M}\Big|_{M=J+\frac{1}{2}} + \ldots$$

$$= \omega(E,J+\tfrac{1}{2}) - \tfrac{1}{2} \frac{\partial \omega}{\partial M}\Big|_{M=J+\frac{1}{2}} + \ldots$$

$$\omega(E,M=J+1) = \omega(E,J+\tfrac{1}{2}) + \tfrac{1}{2} \frac{\partial \omega}{\partial M}\Big|_{M=J+\frac{1}{2}} + \ldots$$

it follows, (neglecting terms $\leq \frac{1}{96} \frac{\partial^3 \omega}{\partial M^3}\Big|_{M=J+\frac{1}{2}}$) from (c-10) and (c-9) that

$$\omega(E,J) \approx \frac{\partial}{\partial M} \left[\omega(E,M) \right]_{M=J+\frac{1}{2}}$$

$$= \omega(E) \frac{(2J+1)}{2(2\pi)^{\frac{1}{2}}} \left(\frac{\hbar}{\sigma^2}\right)^{\frac{3}{2}} \exp\left[\frac{-\hbar^2 (J+\frac{1}{2})^2}{2\sigma^2} \right]$$

(c-11)

The derivation of equation (c-9) depends on use of the central limit theorem which requires that the number of particles involved be large, but Lang[33] has added further theoretical justification of the Gaussian form by the following derivation. For a Fermi gas with a density of single particle states g and the following equation of state

$$E = at^2 - \frac{3}{2}t + \frac{M^2}{2<m^2>g} \qquad (c-12)$$

the density of states is given by

$$\omega(E,M) = \omega(E - \frac{M^2}{2<m^2>g}, 0)$$

that is, the rotational and thermal energies are thought of as separate. Since [33]

$$\log[\omega(E,M)] \approx \log[\omega(E,0)] - \frac{M^2}{2<m^2>g} \frac{\partial}{\partial E} \log[\omega(E,0)]$$

and

$$\frac{1}{\mathcal{J}} \equiv \frac{\partial}{\partial E} \log [\omega(E,0)]$$

we obtain

$$\omega(E,M) = \omega(E,0) \exp [\frac{-M^2}{2c\mathcal{J}}]$$

The quantity c is the moment of inertia in units of $\hbar$ ($c = \frac{I}{\hbar}$) and is related to the spin cut off parameter by

$$\sigma^2 = ct$$

Where t is the thermodynamic temperature related to the "nuclear temperature" ϑ by

$$\vartheta \approx t + \tfrac{3}{4} a^{-1}$$

For a Fermi gas with the equation of state given by (c-12)[47.],

$$\omega(E) = \omega(E,0) = \frac{1}{12} \pi^{\frac{1}{2}} a^{-\frac{1}{4}} \left(E+\frac{3}{2}t\right)^{-\frac{5}{4}} \exp\left(2\sqrt{aE}\right)$$

and, substituting into (c-11),

$$\omega(E,J) = \frac{\sqrt{2}}{48} a^{\frac{1}{2}} \left(\frac{\hbar^2}{I}\right)^{\frac{3}{2}} \left(E + \frac{3}{2}t\right)^{-2} (2J + 1) \exp\left[2(aE)^{\frac{1}{2}} - \frac{\hbar^2 J(J+1)}{2It}\right] \qquad (c\text{-}13)$$

Bethe[10.] and others[35.] have arrived at similar forms for the level density. This form is unrealistic, however, in that it predicts the same proportion of high and low angular momentum states at all energies, when, in reality, higher J states appear only at higher energies.[5.] Lang[36.] has attempted to correct for the superfluity of high J states at low energies by introducing a higher order term in M as follows:

$$\omega(E,J) = \frac{\omega(E,0)}{2\pi\left(\frac{I}{\hbar^2} - \frac{3M^2}{5gt}\right)} \exp\left[\frac{-M^2\hbar^2}{2It} - \frac{M^4\hbar^2}{(2It)^2 \cdot 5gt}\right]$$

Sarantites and Pate[31.] have derived a level density of the following form:

$$\omega(E,J) = \frac{\sqrt{2}}{48} \left(\frac{\hbar^2}{2I}\right)^{\frac{3}{2}} a^{\frac{1}{2}} (E+t-E_r)^{-2}(2J+1) \exp\left\{2[a(E-E_r)]^{\frac{1}{2}}\right\} \qquad (c\text{-}14)$$

where

$$E_r = \frac{\hbar^2 J(J+1)}{2I}$$

This expression results in a much sharper decrease in the number of levels just before the highest value of J allowed (defined by $E = \frac{\hbar^2 J_{max}(J_{max}+1)}{2I}$), but does not appreciably relieve the persistance of high J levels at lower energies.

It can be seen that the value chosen for I greatly influences the angular momentum dependence of the level density. More will be said about the choice of I in the following section.

3. The Superconductor Analogy

The Fermi gas model (sec. B-2) is among the simplest of macroscopic models of the nucleus, since the nucleons are assumed not to interact. It is unrealistic, however to assume that the motions of the nucleons are completely independent within a finite nucleus.

Theories developed to describe the motion of electrons in metals have shown that even small interactions between fermions of a system may result in changes in the macroscopic properties of the system. Bardeen, Cooper, and Schrieffer[37] have shown that correlations between pairs of electrons arise from interactions with lattice vibrations in a crystal. For energies near the Fermi surface, electrons with equal and opposite angular momenta may pair to form

quasi-bound states, thus lowering the total energy of the system and causing the appearance of a gap in the originally continuous energy spectrum.[38].

The observed energy gap in the spectra of even-even nuclei led to the suggestion by Bohr, et. al.[39]. that nucleon correlations exist which are similar to the fermion correlations of the electrons of a superconductor. The theories of superconductivity have been applied extensively to the nuclear case[40,41,42]. where lattice interactions are replaced by forces between the nucleons which lead to angular momentum pairing. The strength of the nucleon interactions are proportional to the correlation function θ. Lang[42]. has shown that the energy gap is equal to 2θ in even-even nuclei which is approximately equal to 2Δ, where Δ is the energy difference between the ground state masses of even and odd nuclei corrected for surface, coulomb, and symmetry energies. A more detailed set of calculations by Vonach, et. al.[43]. led to the value

$$\theta = 1.3\Delta$$

For the ground state, the theories of Bardeen, Cooper, and Schrieffer[37]. give a condensation energy[43].

$$C_o = \tfrac{1}{4} g \theta_o^2 = 0.47 \text{ atc}^2$$

where

$$a = \frac{1}{6}\pi^2 g$$

$$t_c = \frac{4}{7}\theta$$

It is assumed that $2\theta_o$ is the energy gap for $t = 0$. "g" is the single particle level density of protons and neutrons for a nucleus without residual interactions. The quantity C_o decreases with energy and reaches zero at U_c, the energy corresponding to the critical temperature, t_c, at which all pairs are broken. Above t_c, the nucleus may be described as a Fermi gas with a ground state energy shifted upward by an amount equal to the condensation energy. The critical energy is given by[43].

$$U_c = at_c + C_o = 1.47\ at_c^2$$

Below U_c the concept of a level density begins to lose meaning, although theoretical forms have been derived.[55,56].

In the nuclear case, superconductor theories have been extended to describe changes in the rotational moment of inertia, which is expected to decrease with energy below t_c. Belyaev[40]. and others[39,44]. have derived approximate forms for the rotational moment of inertia as a function of energy below the critical energy. At higher energies, the moment of inertia is expected to be equal to the moment of inertia of a rigid body of the nuclear dimensions.

4. Isobaric Spin

Since the proton and the neutron are often thought of as different quantum states of the same particle (the nucleon), it is convenient to introduce a quantity which specifies charge state.[45] This variable, the isobaric spin or i-spin, takes on the values $t = +\frac{1}{2}$ and $t = -\frac{1}{2}$ for protons and neutrons respectively. An isobaric spin operator, $\mathfrak{I}$, may be introduced which has properties analagous to the Pauli spin operator, σ; in fact, the quantum mechanical behavior of t parallels that of s, the ordinary spin (however, spin-space and i-spin-space are completly independent).

The total i-spin of a nucleus is[46]

$$T = \sum_{i=1}^{A} t_i$$

which has $\mathfrak{Z}$ component

$$T_{\mathfrak{Z}} = \tfrac{1}{2}(\mathfrak{Z} - N)$$

For light nuclei ($A \lesssim 50$), T is a good quantum number, but as $\mathfrak{Z}^2/A$ increases or as the neutron excess increases, T becomes less valid, in the former case because of coulombic effects on commutation properties, and in the latter because different single particle shells are being filled by neutrons and protons.[29]

Isobaric spin conservation is important in the reactions between elementary particles and light nuclei. In the scattering of deuterons by helium, an intermediate system with T = 0 is expected. The first three excited states of Li^6 are the following:[7].

J = 3+ T = 0 2.19 MeV

J = 0+ T = 1 3.57 MeV

J = 2+ T = 0 4.52 MeV

Resonances are found corresponding to the T = 0 states, but the T = 1 state is not formed as a compound nucleus.[7].

The exact mass and energy regions of applicability of isobaric spin conservation are at present undefined, since most experiments to date only test relative isobaric spin relationships between neighboring isobars (charge exchange reactions), and little information is available for more complicated systems.[47].

Studies of alpha particles and protons emitted from the compound nucleus Cu^{63} produced by alpha (T = 0) bombardment of Co^{59} (T = -5/2) and proton (T = $\frac{1}{2}$) bombardment of Ni^{62} (T = -2) have yielded results, the anamolies in which have been discussed in terms of isobaric spin arguments[48,49].; however, these arguments are still in the formative stage, and the validity of isobaric spin conservation at such high energies is doubtful.

D. Present Work.

The present work is a radiochemical study of reactions proceeding through the compound nucleus Ge^{68} excited to energies of 10-50 MeV.

Previous studies[50-52.] have dealt with production of the compound nucleus Ge^{68} by bombardment of Zn^{64} with He^{4} ions, but have not included product range measurement to determine predominant reaction mechanisms. Different formalisms of the statistical model have been employed[50,21,53,31.] with varied success in describing the magnitude of the observed cross-sections. Calculations by Porile[50.], which did not include angular momentum dependence, required variation of the level density parameter between 0.8 and 2.8 MeV^{-1} to obtain agreement with experiment. From the shapes and high energy tails of some of the excitation functions Porile concluded that a sizable direct interaction contribution was probably present or that the statistical model was not completely applicable to this case.

Dostrovsky, Friedlander, and Fraenkel[21.] required anomalously low ($a = A/40$) level density parameters to obtain agreement between their non angular momentum dependent statistical model calculations and the data of Porile[50.].

Esterlund and Pate[53.] employed a primitive angular momentum dependent formalism with a variable moment of inertia. In order to obtain agreement with the data of Porile[50.], a moment of inertia of 1.2 times the rigid body

value was required; this value is in obvious conflict with physical possibility.

Saratites and Pate[31]. used Monte Carlo techniques and an angular momentum dependent formalism in their calculations. For calculations involving the emission of one particle by the compound nucleus, excellent agreement was obtained with the data of Porile[50]. using a realistic value of the level density parameter and the rigid body moment of inertia. For the two particle case, agreement was less satisfactory.

In light of the anomalies observed in previous studies of this reaction system, a reinvestigation of the reactions involved was undertaken. In order to detect any major direct interaction contributions, recoil ranges were measured. Also, the same compound nucleus was formed in three different ways; namely, He^4 bombardment of Zn^{64}, C^{12} bombardment of Fe^{56}, and O^{16} bombardment of Cr^{52}. Cross-sections were measured as function of energy for the following reactions:

Product	Target Zn^{64}	Fe^{56}	Cr^{52}
Ge^{67}	(α,n)	(C^{12},n)*	(O^{16},n)*
Ga^{67}	(α,p)	(C^{12},p)	(O^{16},p)*
Ge^{66}	$(\alpha,2n)$	$(C^{12},2n)$	$(O^{16},2n)$*
Ga^{66}	(α,pn)	(C^{12},pn)	(O^{16},pn)*
Ge^{68}	(α,γ)	———	———

(* only upper limits on the cross-sections were measurable)

At the energies of the measurements, the average angular momentum of the compound nucleus is expected to differ in the three cases when considered at equal excitation energies, providing a test for the angular momentum dependence of the excitation functions. Also, direct interaction contributions are expected to differ substantially for three such different reaction systems.

The isotopic spin is, however, invariant and plays no role for the three target projectile systems studied, since projectiles with zero isotopic spin are impinging on targets with isotopic spin -2 in all three cases considered.

A Fortran IV coding of statistical model calculations was undertaken for an IBM system 360/40 computer. Large memory capacities have made possible direct calculations and summation of reaction probabilities, and this method was chosen, rather than Monte Carlo techniques which have been used earlier[50,21,53,31].

II. Experimental Procedures

A. Targets

Thin metal foil targets were prepared from the materials described in Table I. Materials enriched in an isotope of interest were used in those cases where activities would be produced via reactions with other constituents of the natural isotopic mixture and would interfere with the radioassay of the nuclide of interest.

1. Zinc

Zinc targets were prepared by vacuum deposition of metallic zinc onto thin aluminum foils. The aluminum surface had to be pretreated; aluminum metal which has been exposed to air always has an oxide coating and zinc will not readily condense onto non-metallic surfaces[54]. This difficulty may be overcome by using high vapor intensities, but deposits thus formed are granular and uneven. In the case of zinc enriched in Zn^{64}, this would have been especially troublesome, since only small amounts of the enriched isotope were availiable.

It has been found[54], however, that a thin layer (~1 Å) of silver will provide nucleating sites for zinc on a non-metallic surface. Therefore, the aluminum foils were pre-treated by evaporating a thin deposit of silver, the thickness of which was determined by means of a quartz crystal and frequency monitor, the frequency of a crystal being proportional to the mass deposited upon it.

TABLE 1

Abundance (atomic percent)

Element	Isotope	Natural[56]	Enriched[57]
Cr	50	4.31	—
	→ 52	83.76	—
	53	9.55	—
	54	2.38	—
Fe	54	5.82	0.1 ± 0.02
	→ 56	91.66	99.7 ± 0.1
	57	2.19	0.1 ± 0.05
	58	0.33	0.1 ± 0.02
Zn	→ 64	48.89	99.85 ± 0.04
	66	27.81	0.14 ± 0.04
	67	4.11	<0.01
	68	18.57	0.01
	70	0.62	<0.01

In all cases, the overall average thickness of the silver deposit was less than the atomic radius, and the amount deposited was known to ±10%[55]. The zinc deposits evaporated onto a foil thus pretreated were examined by means of a microscope fitted with a calibrated eyepiece, and the grain size was found to be much less than the thickness of the deposit in all cases.

High purity, commercially available[58], natural zinc foils of .0005 inch thickness were used at higher energies when the beam energy loss in such foils was less than 1 MeV.

2. Enriched Iron

Iron foils, enriched in Fe^{56}, were prepared by electroplating iron onto aluminium foil from basic tartrate solutions. The methods of Blann et. al.[59] were modified by lowering the pH to 9.5 to avoid reaction of the basic solution with the aluminium substrate. A 5 cm. diameter tantalum disc was used as the cathode at a distance of 0.5 cm. from the aluminium foil anode. Foils were cut from the center of the plated area to avoid variations in the deposit thickness at the edges of the foils.

3. Natural Iron and Chromium

Natural iron and chromium foils were prepared by vacuum evaporation onto aluminium foil using standard techniques[54].

4. Uniformity

The uniformity of all foils was checked by accurately weighing segments of the foil which had been cut with a small die of known area (7.55 mm^2). None of the foils used for bombardment had a thickness which varied by more than 3%.

B. Bombardments

1. He^4

Bombardments were performed at the Brookhaven National Laboratory 60-inch Cyclotron, the University of Washington (Seattle) 60-inch Cyclotron, and the Washington University 45-inch Sector-focused Cyclotron.

Incident alpha-particle beam energies were measured via the observed ranges in stacks of aluminium plus blue cellophane foils. An amount of aluminium was used corresponding to most of the range, with blue cellophane used downstream for the final few percent. A brief ($\sim$1 μA-sec) passage of charged particles through blue cellophane causes ionization-induced bleaching, and the thickness beyond which bleaching no longer occurs corresponds to the range of the incident beam. The energy was then calculated from the previously measured[60.] range-energy relationship for aluminium and blue cellophane.

The incident beam energies were found to be:

U. of Washington 60-inch Cyclotron	41.6 ± 0.5 MeV
Brookhaven N.L. 60-inch Cyclotron	41.0 ± 0.3 MeV
Washington U. 45-inch Cyclotron	25.7 ± 0.3 MeV

The target configuration used on the U. of Washington 60-inch cyclotron consisted of a water-cooled aluminium plate onto which were clamped the foil stacks to be irradiated. The beam itself was not well collimated; therefore collimation at the target was effected by means of a thick aluminium mask clamped around the edges of the foil stack. In most cases, a special target chamber was used to avoid overheating of the target foils. This so-called "bell jar" assembly, (see figure 1.) allowed a flow of helium to pass across the face of the target stack, but lowered the incident beam energy to 37.4 ± 0.5 MeV.

A similar target block was used on the Washington U. 45-inch cyclotron, but no special cooling was required, because of smaller beam intensity and more efficient water-cooling of the block.

In both of the above cases, the beam intensity was measured by means of the production of Zn^{65} in copper foils. The excitation function for the combined Cu^{63} $(\alpha,2n)$ Ga^{65} and Cu^{63} (α,pn) Zn^{65} reactions was determined in a separate experiment (see appendix III) and found to be in agreement with the results of Houck and Miller[61].

The projectile energy at various positions through the foil stack was calculated using the range-energy curves due to Atkinson and Willis[62]. The range of alpha particles in zinc was determined relative to aluminium by a series of blue cellophane experiments in which different portions of the beam were intercepted by zinc or aluminium degraders before entering the cellophane stack. From the relative positions of the stopped beams in the stack, the range in zinc was calculated from the range difference and beam energy.

In the Washington University bombardments, during which the Zn^{64} (α,γ) Ge^{68} excitation function was determined, only thin foils (<2 mg/cm^2) were used. The more accurate incident energy determined from the average of an extensive series of range measurements by Reeder[63] was used in calculations (25.9 ± 0.1 MeV).

A detailed description of the Brookhaven target assembly and Faraday cup used to monitor the beam intensities is given elsewhere[64].

2. Heavy Ion (O^{16} and C^{12})

Bombardments were performed at the Yale University Heavy Ion Linear Accelerator. The most probable velocity of the fully accelerated beam particles is a constant (independent of the charge of the ions) as is the energy per projectile mass unit (10 MeV). To insure uniform energy, the C^{12} and O^{16} beams (consisting of charge +5 ions) were

passed through an analyzing magnet before being brought into focus in the experimental area.

A typical one inch diameter target stack consisted of one target foil (~250 $\mu g/cm^2$) preceded by an appropriate thickness of beam-degrading aluminium foils and followed by several thin (~200 $\mu g/cm^2$) aluminium catchers. This stack was clamped onto a brass cylinder which slipped into a $1\frac{1}{2}$ inch x 6 inch Farady cup (see figure 2). The charge from the Faraday cup was integrated by a calibrated Cary electrometer. The efficiency of the Faraday cup in retaining secondary electrons had been shown to be 100% under the influence of a strong magnetic field[65].

The energy of the beam particles at various positions through the target stack was determined from the range-energy curves of Northcliffe[66,67].

C. Chemistry and Radiation Assay Techniques

1. Chemical Separations

Standard radiochemical procedures[68,69] were adapted[50] for use on all targets in this work. Each target was dissolved in a 6N HCl solution containing known amounts of Ge(IV) and Ga(III) carrier plus Zn, Ni, Co, and Mn holdback carriers. To insure that the germanium and gallium activities were in the appropriate oxidation states, a few drops of 40% H_2O_2 solutions were added.

Germanium activities were separated by distillation as $GeCl_4$ from the above solution. The gaseous $GeCl_4$ was

dissolved in water and the germanium was precipitated as GeS_2 with H_2S, filtered and mounted for counting. Chemical yields were usually greater than 90%.

Following distillation of the germanium activity, the remaining solution was extracted with isopropyl ether to remove the gallium activities into the ether phase as $GaCl_4^-$. The ether phase was washed several times with 6N HCl before the gallium activity was back-extracted with water. The water solution was then buffered to pH 7.0 with NH_3-NH_4Cl before addition of a few drops of saturated 8-hydroxyquinoline solution to precipitate the gallium activity as $Ga(C_9H_6NO)_3$; this was heated to expel water and mounted for counting. Chemical yields varied between 45 and 70%.

2. Radiation Assay

Ge^{66} (2.4 hours) - A 7.6 cm x 7.6 cm NaI(Tl) detector was employed and the intensity of the 381.4 - keV full energy peak was measured. Efficiency data due to Heath[70]. were employed. The relative gamma-ray intensity was taken as .334 ± .045 photons/disintegration[71]. In some cases this nuclide was allowed to decay to its gallium daughter which was then assayed.

Ge^{67} (19 minutes) - Allowed to decay to Ga^{67} which was assayed.

Ge^{68} (280 days) - The 511-keV anihilation radiation from the decay of 68 - minute Ga^{68} in secular

equilibrium was assayed via a 7.6 cm x 7.6 cm NaI(Tl) detector. The anihilation radiation detection efficiency was calibrated with a Na^{22} standard source of known disintegration rate which was calibrated by conventional[9] 511-511 keV gamma-ray coincidence measurements. Positron emission was taken to occur in 87.9%[72] of the Ga^{68} disintegrations. (see appendix IV)

Ga^{66} (9.5 hour) - Anihilation radiation was assayed via 7.6 cm x 7.6 cm NaI(Tl) detectors. Positron emission was taken to occur in 56.54% of the disintegrations[73]. The decay of the nuclide was followed in some cases by means of beta proportional counters described elsewhere[65].

Ga^{67} (78 hour) - The 91.22-93.26 keV and 184.5-206 keV gamma-ray peaks were assayed via a 7.6 cm x 7.6 cm NaI(Tl) detector. The relative gamma-ray intensities were taken as 0.473 photons/disintegration and 0.274 photons/disintegration respectively[74]. Representative gamma-ray spectra were inspected for impurity activities via Ge(Li) detectors described elsewhere[71].

A series of measurements of the above specified kind spaced in time was taken for each sample and the resulting decay curves were subjected to least squares analysis via CLSQ[75], the Brookhaven computer program for radioactive decay analysis.

III Treatment of Data

A. Recoil Range Calculations

1. Influence of Particle Emission on Recoil Ranges

In a compound nucleus reaction, the energy E_R imparted to the recoiling excited compound nucleus will be determined by the conservation of linear momentum in the target-projectile system.

$$E_R = \frac{E_b A_b A_R}{(A_b + A_T)}$$

The subsequent emission of particles by the compound nucleus (symmetric about 90° to the beam direction in center of mass coordinates) will result in a distribution of recoil energies about an average value close to, but not equal to, that of the recoiling compound nucleus. Blann[76,77] has calculated that the emission of a proton by a mass 59 compound nucleus will result in no more than a 10-15% decrease from the recoil energy of the compound nucleus.

In this work recoil ranges were corrected for effects of particle emission using the approximations of Blann[76,77], namely:

(1) The evaporation energy spectrum is replaced with a unique average energy.

(2) The evaporated particle angular distribution is replaced with 50% of the particles emitted forward and 50% emitted backward along the beam direction.

Detailed calculations by Blann[76,77] have shown that these approximations produce in the recoil ranges of the product when α-particles are emitted from Ni^{59} a less than 1% error and a less than 7% error respectively.

In the present calculations, average ranges were corrected by a maximum of 16% for emission of two nucleons. It was assumed that the average neutron and proton emission energies were 3.2 and 6.5 MeV respectively. In calculations of Blann[77] a factor of two change in the assumed average particle energies was found not to effect the calculated recoil velocities by more than 1.5%.

2. Effects of Target Thickness

Projected ranges were calculated using the formalism described in Appendix I-1 (namely equation I-8) which takes into account the variation of the reaction cross-section within the target due to degradation of the beam energy. This correction never exceeded 35% in the cases considered.

3. Scattering Corrections

The experimentally measured projected ranges were converted to total path lengths using the data of Lindhard, Scharff, and Schiøtt[78] (see Appendix I-2). This correction was normally approximately one third of the projected range. Effects due to scattering of recoils at the target-catcher foil interface were assumed to be small and were ignored.

B. Excitation Function Calculations

1. Cross Section Calculations

During the bombardment, the number of product nuclei, N, present at time t is[9]:

$$N = R/\lambda \ (1-e^{\lambda t})$$

where R is the rate of formation and λ is the decay constant of the product nuclei. The rate of formation of nuclei in a reaction with cross section σ, induced by I particles per unit time impinging upon the target (of superficial atomic density N_T) is:

$$R = I\sigma N_T$$

and if I is constant throughout the bombardment,

$$\sigma = \frac{N}{N_T \ I \ (1-e^{-\lambda t})}$$

The quantity σ (which is often, as at present, that of interest) may be extracted if all the quantities on the right hand side of the equation are known or measured.

A complication may arise when one measures the number of nuclei of a particular species to determine the cross section for a particular reaction. For example, the product of the $Zn^{64}(\alpha,n)$ reaction, Ge^{67}, decays by positron emission with a 19-minute half life to an isotope, 77-hour Ga^{67} which is also the product of the $Zn^{64}(\alpha,p)$ reaction. In this

case, the amount of Ga^{67} produced both during the bombardment and before chemical separation of the gallium fraction must be calculated and subtracted from the measured total to obtain the amount of Ga^{67} formed directly in the reaction of interest. This calculation, which is described in detail elsewhere[9], was performed also for the $Zn^{64}(\alpha,pn)Ga^{66}$ reaction and the corresponding heavy ion cases.

If the beam current varies during the bombardment (as it did in the HILAC bombardments), R will not be constant. Under these conditions, the bombardment may be divided into smaller time intervals, Δt_i, during which the rate of formation, R_i, is approximately constant. Under these conditions[9]:

$$N = \frac{1}{\lambda} \sum_{i=1}^{n} R_i \, (1-e^{-\lambda \Delta t_i}) e^{-(t-t_i)}$$

where t_i is the time at the end of the i^{th} interval.

2. Excitation Energy

In order to compare the excitation functions for various target projectile systems forming the compound nucleus Ge^{68}, it is convenient to convert the bombarding energies into corresponding excitation energies of the compound nucleus.

$$E^* = E_{cm} + E_{BE}$$

$$= E_b \frac{A_T}{A_{cn}} + (A_b + A_T - A_{cn})\, c^2$$

where E* is the excitation energy of the compound nucleus, E_{cm} is the center of mass energy of the target projectile system, and E_{BE} is the binding energy of the projectile to the target. c is the velocity of light.

The projectile, target, and compound nucleus masses (A_b, A_T, and A_{cn} respectively) were obtained from the mass table of Mattauch, et al.[79].

3. Coulomb Barriers and Reaction Thresholds

Coulomb barrier energies, V, were calculated via the approximation of spherical nuclei in contact[80]., i.e.

$$V = \frac{Z_b\, Z_T\, e^2}{R_b + R_T}$$

where e is the charge of the electron and other symbols have their usual meaning with b and T designating the bombarding particle and target nucleus respectively.

Reaction threshold energies were calculated as differences between the compound nucleus and product nucleus binding energies as tabulated by Mattanch, et al.[81].

Because of the high coulomb barrier for the C^{12} and O^{16} reaction systems, all measurements were taken on these systems at bombarding energies far above the thresholds of the reactions studied (see table II).

TABLE II

System	V(MeV)	E_{BE}(MeV)
$Cr^{52} + O^{16}$	29.5	+6.423
$Fe^{56} + C^{12}$	24.6	+5.968
$Zn^{64} + He^{4}$	10.3	+2.998

Reaction	Reaction Threshold (MeV)*
$Ge^{68} \rightarrow Ge^{67}+n$	12.180
$Ge^{68} \rightarrow Ge^{67}+2n$	21.980
$Ge^{68} \rightarrow Ga^{67}+p$	7.000
$Ge^{68} \rightarrow Ga^{67}+p+n$	18.230

Compound Nucleus	Particle	Binding Energy
Ge^{68}	n	12.180
	p	7.000
	α	2.998
Ge^{67}	n	9.800
	p	6.050
	α	3.483
Ge^{66}	n	12.550
	p	5.730
	α	3.321
Ga^{67}	n	11.230
	p	5.273
	α	5.775

* All energies refer to excitation energies in Ge^{68}.

TABLE II (cont.)

Compound Nucleus	Particle	Binding energy
Ga^{66}	n	9.102
	p	5.078
	α	5.041

IV Experimental Results

A. Radiative Capture

The experimentally measured Zn^{64} (α,γ) Ge^{68} excitation function is shown in figure 3. The previously measured data of Porile[50.] are shown on the same figure for comparison. The heavy lines were drawn to fit the data of the present work.

Above 17 MeV no (α,γ) cross-sections were measurable because of the interfering Ge^{68} activity produced via the $(\alpha,2n)$ reaction on Zn^{66}.

The four lowest energy points give a fairly good definition of the Zn^{64} (α,γ) Ge^{68} excitation function. Differences between these results and those of Porile[50.] may be explained in terms of different energy resolution in the two sets of experiments. The measurements of Porile[50.] were achieved by degrading a full energy beam of 41.0 ± 0.5 MeV to energy values in the region of interest. The present data was measured at energies resulting from degradation of a 25.9 ± 0.1 MeV[63.] full energy beam. The maximum error in the energy values plotted for the present work is not expected to exceed 0.5 MeV, while the uncertainty in the energy values of Porile[50.] is expected to be many times this value. It can be seen from figure 5 that Porile's cross-section value at the highest energy he employed may have included the effects of interfering activity from the Zn^{66} $(\alpha,2n)$ Ge^{68} reaction, while his lowest energy cross-section may have extended into the energy region below the

coulomb barrier (as may the lowest energy cross-section in the present work).

The error bars on the cross-section magnitudes in this work are mainly a measure of the uncertainty in detector efficiencies during the assay of the various samples. Chemical yields were greater than 90% in most cases. The absolute uncertainty for any of the points shown in figure 3 is not expected to exceed 15% and the relative uncertainty of one value with respect to others is 5%.

Unfortunately, recoil ranges for the $Zn^{64}(\alpha,\gamma)Ge^{68}$ reaction were unmeasurable in these experiments. Long irradiation times were necessary for the production of useful activity of 280 day Ge^{68}, and only a small fraction of the Ge^{68} recoils were found in the catcher foils as a result of low recoil energies.

Aside from known collective effects[82-88]., the majority of radiative capture events are expected to proceed via a compound nucleus mechanism and complete momentum transfer. Also, the absence of either a proton or neutron excess in the bombarding particle would further hinder any possibility of direct capture[89].

The $Cr^{52}(O^{16},\gamma)Ge^{68}$ and $Fe^{56}(C^{12},\gamma)Ge^{68}$ excitation functions were unmeasurable in the present work.

B. Reactions Involving the Emission of One Nucleon by the Compound Nucleus

1. Zn^{64} (α,n) Ge^{67}

The Zn^{64} (α,n) Ge^{67} excitation function from the present study is shown in figure 4, together with the data of Porile[50]. The heavy line was drawn to fit the data of the present work.

Although the positions in energy of the excitation function peaks are in reasonable agreement for the two sets of measurements, the low and high energy ends differ considerably. Above a bombarding energy of 30.8 MeV, interference from the Zn^{66} $(\alpha,3n)$ Ge^{67} reaction is possible and may be present in the two highest energy points measured in this work.

The error bars on the cross-section magnitudes in figure 4 are due mainly to a combination of uncertainties from radioactivity assay statistics and detector efficiences as well as uncertainties in chemical yields. The uncertainty in the magnitude of any of the cross-sections does not exceed 20% and the relative uncertainty of the points is approximately 7%.

Ranges for the product of this reaction were experimentally unmeasureable directly in the present work, because of the low activities in the catcher foils. However, the long duration of bombardment for the production of Ga^{67} by the (α,p) reaction resulted in a substantial

amount of Ga^{67} formed indirectly (through the (α,n) reaction followed by β^+ decay), so that the ranges measured by determining the fraction of Ga^{67} in the catcher foils are actually combined ranges for the products of the (α,n) and (α,p) reaction. These ranges are presented and discussed in the following section.

2. Zn^{64} (α,p) Ga^{67}

The Zn^{64} (α,p) Ga^{67} excitation function for the present work is shown in figure 5 together with the data of Porile[50]. It can be seen that agreement between the two sets of data is within experimental error throughout the entire energy range of the measurements.

Sources of error in the present work include uncertainties in the chemical yields, beam currents, target thickness, incident and degraded particle energy, and radioactivity assay statistics and efficiences. The latter uncertainties account for most of the magnitude of the error bars on the cross-sections of figure 5. These error bars represent less than 20 % uncertainties in all cases. The relative uncertainties are less than 10%.

The combined Zn^{64} (α,n) Ge^{67} and Zn^{64} (α,p) Ga^{67} ranges are also shown in figure 5. Within experimental error, the ranges are directly proportional to bombarding energy. The ranges at the highest energy has the largest uncertainty and may contain an appreciable direct interaction component.

In figure 6, the experimental ranges are shown plotted together with the range-energy curve calculated by means of the formalism of Lindhard, Scharff, and Schiøtt[78]. (see Appendix I). Agreement between the data and theory is within experimental error.

On the basis of the analysis of the range data for the mixed (α,n) and (α,p) products, it may be concluded that both of these reactions proceed primarily via the compound nucleus mechanism.

3. Fe^{56} (C^{12},p) Ga^{67} and Fe^{56} (C^{12},n) Ge^{67}

Only the sum of the cross-sections for these two reactions was measurable in the present work. The cross-sections obtained are shown in figure 7 plotted as a function of the Ge^{68} excitation energy together with the sum of the experimentally measured Zn^{64} (α,p) Ga^{67} and Zn^{64} (α,n) Ge^{67} cross-sections.

Errors in the experimentally measured cross-sections arise from the same sources discussed in the previous section, but in the present work, uncertainties in the beam energy and small non-constant beam currents provide the major sources of error. The uncertainties in the cross-section magnitudes are about 60%, and the energy uncertainty is about ±1.5 MeV.

The cross-sections for the C^{12} induced reactions are seen to be in agreement within experimental error with an extrapolation of the α-induced excitation function.

This agreement is not unexpected, since the compound nucleus angular momenta resulting from the two reaction systems are calculated to be very nearly equal in this energy region. In figure 8, the average Ge^{68} angular momentum as calculated with ABACUS-2*[23,90]. is plotted vs. excitation energy for the three reaction systems: $Zn^{64} + He^{4}$, $Fe^{56} + C^{12}$, and $Cr^{52} + O^{16}$. At the two bombarding energies studied for the C^{12} case, the average compound nucleus angular momentum is expected to differ by less than $2\hbar$ from the corresponding alpha cases. It is not surprising, therefore, that behavior similar to that first observed by Ghoshal[91]. is seen for these two reaction systems.

No ranges were measured, but it may be assumed that C^{12}-induced reactions resulting in products close to the mass of the compound nucleus proceed predominantly by a compound nucleus mechanism, since a direct mechanism whereby the incident C^{12} nucleus imparts the majority of its momentum to one or two nucleons of the target nucleus, is quite improbable[92].

4. Cr^{52} (O^{16},n) Ge^{67} and Cr^{52} (O^{16}, p) Ga^{67}

Upper limits determined for the magnitude of the sum of the Cr^{52} (O^{16},n) Ge^{67} and Cr^{52} (O^{16},p) Ga^{67} cross-sections are shown plotted as a function of Ge^{68} excitation energy in figure 7. The lower energy cross-section was measured at an energy below the coulomb barrier and the low value indicated by the experimental limit is

expected. The higher energy cross-section is seen to be below the value one would expect by extrapolating the α and C^{12} excitation functions to this energy. This apparent violation of the independence hypothesis is expected, however, since the average angular momentum of the compound nucleus formed by O^{16} bombardment of Cr^{52} is lower at this energy than either the α or C^{12} induced average angular momentum (see figure 8). Excitation functions for systems with higher angular momenta are expected[9] to be shifted to higher energies, and this is seen to be consistant with the present experimental results.

C. Reactions Involving the Emission of Two Nucleons by the Compound Nucleus.

1. $Zn^{64}(\alpha,2n)Ge^{66}$

The cross-sections measured for the $Zn^{64}(\alpha,2n)Ge^{66}$ reaction are shown in figure 9, plotted together with the data of Porile[50]. The magnitudes of the latter cross-sections were adjusted by a factor corresponding to the replacement of the rather approximate Ga^{66} positron branching ratio, ~66%[93], used by Porile in his Ga^{66} assay, with the more accurate value 56.54%[73], now available. The solid line in figure 11, was drawn to fit the present data.

The main discrepancy between the two sets of data exists at energies between the threshold and the peak of the excitation function. The present data are expected to be correct to within ±20% in cross-section magnitude and within ±0.8 MeV in energy. The relative accuracy of the cross-sections is expected to be better than ±10%.

The recoil ranges measured for the product of this reaction are also shown in figure 9, plotted on a linear ordinate scale vs. bombarding energy.

Figure 10, shows the experimental and calculated recoil ranges plotted against the calculated average recoil energy for the compound nucleus. The solid line was calculated using the formalism of Lindhard, Scharff, and Schiøtt[78]. The experimentally measured projected ranges agree well within experimental error with the calculated projected ranges.

This analysis provides strong evidence that the $Zn^{64}(\alpha,2n)Ge^{66}$ reaction proceeds predominantly via the compound nucleus mechanism.

2. Zn^{64} (α, pn) Ga^{66}

The cross-sections measured for the $Zn^{64}(\alpha,pn)Ga^{66}$ reaction are shown in figure 11 plotted together with the data of Porile[63], which were again adjusted to correct for the calibration error as described in the previous section. The solid line was drawn to fit the present data.

The discrepancy between the two sets of data appears to be a displacement along the energy axis. The present data consist of a combination of data measured via bombardments at two different cyclotrons (Brookhaven, and University of Washington). The Brookhaven experiments also resulted in points on the Zn^{64} (α,p) Ga^{67} excitation function which agreed with the data of Porile[50] (see section IV-B-4). The present data are expected to be accurate to within ±20% in cross-section magnitude and within ±0.8MeV in energy. The relative accuracy of the cross-sections is expected to be better than ±10%.

The recoil ranges measured for the product of this reaction are also shown in figure 11. plotted vs. bombarding energy on a linear ordinate scale. The two highest energy ranges appear to break from the linearity established by the lower energy points.

Figure 12. shows the recoil ranges plotted against the calculated average recoil energy of the compound nucleus. The solid line was calculated using the formalism of Lindhard, Schaff, and Schiøtt.[78] The higher energy disparity between the calculated ranges and experimental ranges is quite pronounced in this graph.

On the basis of this analysis, it may be deduced that the $Zn^{64}(\alpha,pn)\ Ga^{66}$ reaction proceeds predominantly via the compound nucleus mechanism at lower energies (<32MeV). At higher energies, the lower ranges would indicate the onset of a noncomplete momentum transfer process (although this assumption is based essentially on the validity of one range measurement.)

3. $Fe^{56}\ (C^{12},2n)\ Ge^{66}$ and $Fe^{56}\ (C^{12},pn)\ Ga^{66}$

The cross-sections measured for the $Fe^{56}(C^{12},2n)Ge^{66}$ and $Fe^{56}(C^{12},pn)Ga^{66}$ reactions are shown plotted together as a function of C^{12} bombarding energy in figure 13., the dotted and solid lines were drawn to fit the cross-sections for the respective reactions.

The $Fe^{56}(C^{12},2n)Ge^{66}$ and $Zn^{64}(\alpha,2n)Ge^{66}$ cross-sections are plotted as a function of Ge^{68} excitation energy in figure 14., with the dotted and solid lines drawn to fit the two respective excitation functions. The lowest energy $(C^{12},2n)$ cross-section is seen to be in agreement with the $(\alpha,2n)$ excitation function, but, unfortunately, the higher energy portion of the $(\alpha,2n)$ excitation function is not sufficiently well-defined to enable a meaningful comparison with the higher energy $(C^{12},2n)$ cross-sections.

The $Fe^{56}(C^{12},pn)Ga^{66}$ and $Zn^{64}(\alpha,pn)Ga^{66}$ cross-sections are shown plotted vs. Ge^{68} excitation energy in figure 15. Although the high energy portion of the (α,pn) excitation function is more well-defined experimentally in this case, some uncertainty arises

from the apparent presence of a non-compound nucleus reaction component as discussed in section IV-C-2. The triangles of figure 15. represent an upper limit to the compound nucleus contribution to the cross-section. These upper limits were determined using the approximation that all catcher activity resulted from compound nuclear processes; target foil activities (and the corresponding cross-sections) were calculated with equation I-5 (Appendix I) using the range values calculated by means of the formalism of Lindhard, Scharff, and Schiøtt[78]. Again, the lowest energy heavy ion cross-section is seen to be in agreement with the (α,pn) excitation function as defined by either the measured or corrected cross-sections, but little can be inferred about agreement with the higher energy heavy ion cross-sections.

A comparison of the alpha- and C^{12}-induced results in the form of cross-section ratios is deferred to section V-C-2 to follow.

4. $Cr^{52}(O^{16},2n)Ge^{66}$ and $Cr^{52}(O^{16},pn)Ga^{66}$.

Only upper limits were measurable for the $Cr^{52}(O^{16},2n)Ge^{66}$ and $Cr^{52}(O^{16},pn)Ga^{66}$ reactions. These limits are plotted in figures 14. and 15., respectively. The decreased magnitude of these cross-sections when compared to the corresponding C^{12}- and α-induced excitation functions may be explained by arguments analagous to those used in section IV-B-4.

V Statistical Model Calculations

A. Formalism

The formalism used for the calculation of reaction cross-sections is based on the statistical model theory discussed in sections I-B and I-C.

1. Particle Emission

The probability for transitions between nuclear states was calculated via equation (c-6), namely;

$$P(E_F,J_F;E_C,J_C)\,d\epsilon = \frac{(2s_x+1)}{\pi^2\hbar^3}\,\epsilon\mu\sigma\,(\epsilon,J_C,J_F)\,\frac{\omega(E_F,J_F)}{\omega(E_C,J_C)}\,d\epsilon$$

Where

$$\omega(E,J) = \frac{\sqrt{2}}{48}\,a^{\frac{1}{2}}\,\left(\frac{\hbar}{I}\right)^{\frac{3}{2}}\,(E+\tfrac{3}{2}t)^{-2}(2J+1)\exp\left[2(aE)^{\frac{1}{2}} - \frac{\hbar^2J(J+1)}{2It}\right]$$

and

$$\sigma(\epsilon,J_C,J_F) = \frac{\pi\,\lambda^2(2J_C+1)}{(2s_x+1)(2J_F+1)}\sum_{S=|J_F-s_x|}^{J_F+s_x}\ \sum_{i=|J_C-S|}^{J_C+S} T_i(\epsilon)$$

For non-interacting free nucleons confined within a nucleus of radius $R = r_oA^{\frac{1}{3}}$, the Fermi gas model predicts the level density parameter to be the following:[35.]

$$a = 2\left(\frac{\pi}{3}\right)^{\frac{4}{3}}\,\frac{mr_o^2}{h^2}\,A$$

Experimental evidence, as interpreted by Lang[94.] indicates the value $a = \frac{A}{8.0}\,MeV^{-1}$ (corresponding to a radius parameter r_o = 1.15 f) which was used in this work.

The energy used in the level density expression was corrected for nucleon pairing with the pairing energies of Cameron[19.]. Since Ge^{68} lies far from shell closure, no

shell correction was used.

For each excitation energy, E*, a maximum value of the angular momentum, J_{max}, is expected[95.] to exist above which the level density is zero. If the excitation energy is partitioned into thermal and rotational energies and the rotational energy is taken to be[96.,33.]

$$E_{rot} = \frac{J(J+1)\hbar^2}{2I}$$

it follows that

$$E^* = \frac{J_{max}(J_{max}+1)\hbar^2}{2I}$$

For a rigid spherical body, the moment of inertia, I_r, is given by[29.]

$$I_r = \frac{2}{5} AR^2$$

For a nucleus with a constant pairing energy between particles in doubly occupied pair states (see section I-C-3) the moment of inertia is expected to be considerably less than the rigid body value for energies less than a neutron binding energy.[40.,42.,44.] For energies greater than a neutron binding energy, the rigid body moment of inertia is expected to be a good approximation to the nuclear moment of inertia.[40.,42.] To reflect these expectations, the moment of inertia was taken to vary between some value at zero energy (I_o), and the rigid body value (I_r) at higher energies as follows:

$$I = I_r(1-be^{-0.693E/c})$$

where

$$I_r(1-b) = I_o$$

It was found that the magnitude of the assumed value for I_o (which determines b) could be changed from .04 I_r to 0.4 I_r with an effect of only a few per cent on the calculated cross-sections. The value I_o = .04 I_r or b = 0.96 was used throughout the calculations. The calculation results were found, however, to be quite sensitive to the value chosen for c, which controls the rate of approach to rigidity with energy; this was taken as 3.0 MeV, resulting in a moment of inertia equal to 93% of the rigid body value at the neutron binding energy for Ge^{68} (see figure 16.)

Below a certain energy (which was also taken as 3 MeV, but was unrelated to the above choice), the level density becomes unrealistically large when compared with experiment[97.,98.] and was replaced with an extrapolation to zero energy, namely:

$$\omega'(E,J) = \left(\frac{E}{3.0}\right)^2 \omega(E=3.0,J)+\left(\frac{3.0-E}{3.0}\right)\omega_o$$

Here ω_o is the "level density" at zero energy which was chosen from the trends of experimentally measured level densities.[97.,98.]

The optical model parameters (see equations c-1, c-1-a, and c-1-b) used in calculating transmission coeficients are summarized in Table III. Parameters for p-,n-, and α-penetration were chosen for optimum agreement with the tabulations of Hodgson[99.]. The parameters for the C^{12} and O^{16} cases are those suggested by Vogt.[100.]

TABLE III*

Reaction	V	W	a,b	r_o	V_{so}	W_{so}
$Zn^{64} + He^{4} \rightarrow Ge^{68}$	-50 MeV	-11 MeV	0.59f	1.10f	0	0
$Fe^{56} + C^{12} \rightarrow Ge^{68}$	-100 MeV	-10 MeV	0.6f	1.10f	0	0
$Cr^{52} + O^{16} \rightarrow Ge^{68}$	-100 MeV	-10 MeV	0.6f	1.10f	0	0
$Ge^{68} \rightarrow Ge^{67} + n$	-52.5 MeV + 0.6E	-2.5 - 0.3E	0.6f	1.10f	-9.5 MeV	0
$Ge^{68} \rightarrow Ga^{67} + p$	-55.0 MeV + 0.7E	-0.50 - 0.45E	0.65f	1.10f	-9.5 MeV	0

* See equation c-1, c-1(a), and c-1(b) for the meaning of the symbols.

All transmission coefficients were calculated with ABACUS - 2*, the optical model program of Auerbach[23] as revised by Donnelly[90] for use on the University of British Columbia IBM 7040 computer. It has been found that the coulomb wave functions used in ABACUS - 2[23] may not give proper convergence in energy regions near coulomb barriers or at low excitation energies. The revisions in ABACUS - 2* include changes in the coulomb wave functions, however, and proper convergence is expected[101] with these changes.

2. Gamma Ray Emission

The probabilities for gamma ray emission were calculated using the formalism derived from the single particle model[101.,29] as follows:

$$P_\gamma (E_F, J_F; E_C, J_C) = C_\iota(\epsilon_\gamma) \frac{\omega(E_F, J_F)}{\omega(E_C, J_C)} \epsilon_\gamma^{2\iota+1} \qquad \text{(A-1)}$$

where ι corresponds to the multipolarity of the emitted gamma ray of energy

$$\epsilon_\gamma = E_C - E_F$$

The factors $C_\iota(\epsilon_\gamma)$ (which have been assumed to be constants by previous authors[31.,96.,103-105]) were altered from the single particle estimates to take into account experimentally observed collective effects not predicted by the single particle model.

Dipole gamma rays show in all nuclei a broad absorption resonance of 4 - 10 MeV full width at half maximum peaked at about 20 MeV.[29.] This so-called giant dipole resonance was taken to be of the Breit-Wigner[4.] form as follows:

$$C_l(\epsilon_\gamma) = C_l' f(\epsilon_\gamma) \qquad (l=1)$$

with

$$f(\epsilon_\gamma) = \frac{E_d^2 + \frac{1}{4}\Gamma^2}{(\epsilon_\gamma - E_d)^2 + \frac{1}{4}\Gamma^2}$$

where E_d is the energy at the peak of the resonance and Γ is the full energy width at half maximum. The factor C_l' $(l=1)$ is taken to be a constant the magnitude of which is determined by empirical fitting of the calculation results to the measured (α,γ) excitation function. The hydrodynamic model predicts that the energy of the resonance peak will vary as $A^{-\frac{1}{3}}$ [82.], and the following form[82.] is consistant with experimental results,[106.,107.]

$$E_d = 82A^{-\frac{1}{3}}$$

giving for Ge^{68} the value 20 MeV. The resonance width was chosen, consistant with experimental evidence, to be 5 MeV. It has been found[83.] that calculated cross-sections are "relatively insensitive" to variations of 1 MeV in the resonance peak energy and of 2 MeV in the resonance width.

Other gamma-ray resonances are known to exist,[84.,85.] but not enough experimental characterization is available

to warrant their inclusion in the present calculations.

Many experimental electric quadrupole (E2-) transition intensities are found to be strongly enhanced over single particle estimates.[29] According to the single-particle model alone, one would expect the dipole gamma-ray emission rate to be 10^2 to 10^3 times faster than the quadrupole gamma-ray emission rate,[102.,103.] but compilations of experimentally known reduced gamma-ray emission rates[108.] show many E2 emission rates are 10 - 100 times faster than single-particle estimates. This effect has been explained[86.] in terms of rapid de-excitation through intra-rotational band cascades. An attempt was made in some of the present calculations to reflect this behavior by introducing an enhancement factor into the quadrupole term for gamma emission as follows:[29.]

$$C_\iota(\epsilon_\gamma) = C_\iota' \frac{J_c(J_c+1)(J_c-2)}{2(2J_c-1)} \left[\frac{\Delta E(J_c \rightarrow J_c-2)}{\Delta E(J_c \rightarrow J_c-1)} \right]^5$$

where C_ι' is again taken to be a constant. The quantities ΔE correspond to level spacings at the excitation energy E*. The above expression was not allowed to exceed

$$C_\iota(\epsilon_\gamma) = C_\iota' Z^2$$

the theoretical upper limit.[88.]

For quadrupole transitions not involving a change of two units of angular momentum, no enhancement factor was used, ie.

$$C_\iota(\epsilon_\gamma) = C_\iota'$$

Since the present calculations did not include parity considerations, no distinction could be drawn between electric quadrupole and magnetic quadrupole transitions. The latter are not expected to be enhanced.

Although the above form for the enhancement factor has some theoretical grounds[29]. it was used only as a rough attempt to reflect experimentally observed effects, and is in no way to be considered a quantative treatment of the problem.

The factors $C_\iota(\varepsilon_\gamma)$ for $\iota = 3$ and $\iota = 4$ were taken to be constants. Higher multipoles than that corresponding to $\iota = 4$ were not considered. The constants C_ι' were chosen to reflect the single-particle estimates for each multipolarity and, since the single particle model predicts smaller contributions from higher multipoles;[29,84,102,103]. these constants were rather arbitrarily taken to decrease by factors of ten for each unit increase in ι. The magnitude of the four constants was set by fitting of the calculated value of the (α,γ) cross-section to the experimentally measured value.

B. SFUSMAP - Program Logic

The calculation was performed via direct calculation and summation of the various transition probabilities, according to a procedure similar to that of Blann.[109].

The initial emitting system was taken to be a compound nucleus with a unique excitation energy ($E^* = E_{cm} + E_{BE}$) and a distribution in angular momentum, $\sigma(Z,A,E^*,J)$, characteristic of the reaction through which it was formed.

The possible modes of de-excitation considered were gamma, alpha, proton, and neutron emission. Arrays dimensioned in residual energy and angular momentum were considered for the product nuclei formed by these respective modes of de-excitation, namely $\sigma(Z,A,E,J,)$, populated by gamma emission by the compound nucleus (Z,A); $\sigma(Z-2,A-4,E',J')$, populated by alpha emission; $\sigma(Z-1,A-1,E'',J'')$, populated by proton emission; and $\sigma(Z,A-1,E''',J''')$, populated by neutron emission. To conserve computer space these arrays were divided into bins $2\hbar$ units wide in angular momentum and 2 MeV wide in energy. Reducing the energy width to 1 MeV was found to effect the outcome of sample calculations by less than 5%.

The initial angular momentum population of the compound nucleus ($\sigma(Z,A,E^*,J)$) was calculated via ABACUS - 2*[90]. (see preceding section) and read in as input data to the program. The relative probabilities for population of bins in the arrays for the several daughter

nuclei were calculated for each angular momentum value of the compound nucleus, multiplied in turn by the capture cross-section leading to each particular compound nucleus angular momentum value, and summed to give the total population cross-section of the daughter arrays by the decay of the compound nucleus. Thus, for neutron emission,

$$\sigma(Z,A-1,E',J') = \sum_J \sigma(Z,A,E^*,J) \frac{P_n(E^*,J;E',J')}{\sum_{i=\gamma,\alpha,p,n} \sum_{E'} \sum_{J'} P_i(E,J;E',J')}$$

The populations $\sigma(Z,A-2,E,J)$, $\sigma(Z-1,A-1,E,J)$, and $\sigma(Z-1,A-2,E,J)$ are then considered in order.

The formation cross section for a particular nucleus is taken as the sum of the bins in the array populated by gamma emission in that nucleus. This approximation will overestimate the formation cross-section slightly, since some states populated by gamma emission may still emit particles; however, the contribution of these states to the total cross-section will be small (<0.1%) as a result of the fact that gamma emission is normally several orders of magnitude less probable than particle emission when the latter is energetically allowed. Thus, the cross-section for formation of the product nucleus resulting from emission of two neutrons by the compound nucleus is,

$$\sigma(x,2n) = \sum_{E'} \sum_{J'} \left[\sum_{E} \sum_{J} \sigma(Z,A-2,E,J) \frac{P_\gamma(E,J;E',J')}{\sum_{i=\gamma,\alpha,p,n} \sum_{E'J'} P_i(E,J;E',J')} \right.$$

The de-excitation process is only considered up to and including emission of three particles. This limitation is a result of lack of computer space only, and the program may easily be expanded to include the consideration of further particle evaporation.

The output of each set of calculations contains the population distribution for each nucleus considered both before and after emission of one gamma-ray, as well as the final formation cross-sections. A more detailed description of the computer program is given in Appendix V.

C. Calculation Results

1. General Features of Calculated Results

Sample results for residual nuclei resulting from particle emission are shown in figures 17, 18, and 19. The calculated quantities $\sigma(Z,A,E,J)$ are shown plotted vs. E and J in the form of contour diagrams, with successive contours representing factors of ten in cross-section magnitude. The emitting system in all three cases is Ge^{68} excited to 40 MeV and with 20$\hbar$ units of angular momentum. The verticle dotted line represents the angular momentum of the emitting compound nucleus, and the horizontal dotted line represents the excitation energy of the emitting nucleus minus the binding energy of the emitted particle. The region of no states corresponds to J values greater than J_{max} as defined in section V-A

In figures 17, and 18, representing the results of neutron and proton emission respectively, the average change in angular momentum is approximately 2.5$\hbar$ in the direction of lower angular momentum. This decrease in angular momentum is a result of the greater availability of levels at J values lower than 20$\hbar$ as compared to the availability at higher J values.

Figure 19, representing the results of alpha particle emission, shows an average decrease in angular momentum of 6$\hbar$. Furthermore, the average change in angular momentum is seen to increase sharply with increasing alpha energy. This effect is a consequence of the fact that

higher energy alpha particles are able to carry off (or carry in) many more units of angular momentum (cf. figure 8). This same effect is also seen for neutrons and protons, but to a much lesser extent because of the smaller masses of these particles. In the region bordering the rotational cutoff ($J \simeq J_{max}$), these trends are quite important.

The star in figure 20 represents a state in a compound nucleus and the verticle components of the arrows correspond in length to the binding energy of an emitted particle. For purposes of illustration, states in the daughter nucleus are represented on the same diagram. The horizontal and curved dotted lines represent a displacement of one binding energy from zero energy and the rotational cutoff, respectively. It is seen that for the compound nucleus in a state represented by the star, particle emissions with a zero or positive change in the nuclear angular momentum are inhibited (dotted arrow), but that emissions resulting in negative charges in the nuclear angular momentum are allowed (full arrow). Unless the change in angular momentum is very large indeed, the energy of the emitted particle will, of necessity, be low. For low energy particles, transmission coefficients for higher ℓ values are very small, so that the corresponding emission probability will be small. Under these conditions, gamma ray emission is expected[109.,104.] to compete favorably with particle emission.

Figures 21 and 22 illustrate a particular case where population of states near the rotational cutoff is an important consideration. In the upper right hand corner of the diagram, the cross-section (in millibarns) for population of a given compound nucleus angular momentum value during bombardment is shown plotted against angular momentum (in units of $\hbar$). The cross-section distribution is seen to be peaked at higher J values for the $Fe^{56} + C^{12}$ case (figure 21) than for the corresponding $Zn^{64} + He^{4}$ case (figure 22). The contour diagrams (which are identical to those described previously, except that now the contours represent the sum of contributions from each angular momentum value along the accompaning σ_J distribution in the emitting compound nucleus) reflect this angular momentum difference even after emission of two nucleons. It can be seen, particularly in the Ge^{66} and Ga^{66} product nuclei, that the population of states along the rotational cutoff is much more dense in the $Fe^{56} + C^{12}$ case. Since, therefore, these two product nuclei have a much higher probability for gamma ray emission in the $Fe^{56} + C^{12}$ case, one would expect the $Fe^{56}(C^{12},pn)$ and $Fe^{56}(C^{12},2n)$ reaction cross-sections to be larger at this energy than the corresponding $Zn^{64}(\alpha,pn)$ and $Zn^{64}(\alpha,2n)$ cross-sections which will be depleted by particle emission. For the same reason, reaction thresholds for emission of three nucleons should be shifted to higher energies for the higher angular momentum case. Corresponding shifts to higher energies are expected for excitation functions corresponding to reactions involving evaporation of one particle by the compound nucleus.

An even more pronounced case of highly populated states in the vicinity of the rotational cutoff is seen in figure 23 for the system $Cr^{52} + O^{16}$ at 64MeV excitation.

The effects of gamma ray competition with particle emission are well illustrated by the calculated excitation functions shown in figure 24.

The differences in slope between the two excitation functions below 40MeV are due mainly to differences in the total reaction cross-section. Above 40MeV, however, where both total reaction cross-sections change slowly with energy, the slope of the $Fe^{56}(C^{12},pn)Ga^{66}$ excitation function increases in relation to the $Zn^{64}(\alpha,pn)Ga^{66}$ excitation function; this is due to effects such as that just described following the rapidly increasing average angular momentum of the $C^{12} + Fe^{56}$ system as compared to the $He^{4} + Zn^{64}$ system (see figure 8).

2. Comparisons of Calculations with Experiment.

The calculated $Zn^{64}(\alpha,\gamma)Ge^{68}$ excitation function is shown in figure 25 together with the present experimental data. The magnitude of the calculated excitation function was set by adjustment of the gamma strength constants (C_i') in formula V-A-1. The apparent discrepancy in energy is probably due to inaccuracy in the values used for particle binding energies[81], which are subject to large uncertainties.[20,81,110] The magnitudes of the gamma strength constants obtained for Ge^{68} from this calculation were assumed to be identical for neighboring nuclei.

The calculated $Zn^{64}(\alpha,n)Ge^{67}$ excitation function is shown in figure 26 plotted together with the experimental cross-sections. Agreement is seen to be quite good above 20 MeV, whereas agreement is poor for lower energy values. This disparity is probably due to inaccuracy in the neutron binding energy used[81]. and concomittant inaccuracy of the reaction threshold.

The $Zn^{64}(\alpha,p)Ga^{67}$ excitation function is shown in figure 27. Although the cross-section magnitudes are generally lower than those measured, the excitation function shape is seen to reflect the shape of the experimental excitation function quite well.

The $Zn^{64}(\alpha,2n)Ge^{66}$ excitation function is shown in figure 28. Again there appears to be an energy shift between the experimental and calculated excitation functions which may probably be attributed to inaccurate binding energies. Otherwise, both the shape and the magnitude of the calculated excitation function reflect those of the experimental excitation function quite well.

The calculated $Zn^{64}(\alpha,pn)Ga^{66}$ excitation function is shown in figure 29. The calculated excitation function shape is seen to closely reproduce that of the experimentally measured one, but, as in the (α,p) case, the calculated cross-section magnitudes are low. This suggests possible inaccuracies in the calculated proton transmission

coefficients, although the disparity may be due to other causes.

The calculated excitation function for the sum of the $Fe^{56}(C^{12},n)Ge^{67}$ and $Fe^{56}(C^{12},p)Ga^{67}$ excitation functions are shown in figure 30 plotted together with the experimental sum cross-sections. There is a more serious lack of agreement in this case.

The calculated $Fe^{56}(C^{12},2n)Ge^{66}$ excitation function is shown in figure 31. Agreement is seen to be good between the calculated excitation function and the two higher energy cross-section values. The calculation is seen not to be in agreement with the lowest energy cross-section value. This lack of agreement is very likely due to inaccuracy of the coulomb barrier as calculated by ABACUS - 2*. The rigid sphere in contact approximation (see section III-B) predicts a much lower coulomb barrier energy, and this prediction appears to be in better agreement with experiment.

The calculated $Fe^{56}(C^{12},pn)Ga^{66}$ excitation function is shown in figure 32. Again, agreement with experiment is good for the two highest energy points, but poor for the lowest energy point. Again, the inaccurate coulomb barrier probably accounts for this discrepancy.

Some ambiguity arises when comparing cross-section magnitudes because of the different probabilities of forming the compound nucleus for different target projectile systems. This ambiguity is removed when one considers reaction cross-section ratios, however.

Figure 33 shows the calculated and experimental ratios of the $Zn^{64}(\alpha,pn)Ga^{66}$ cross-section to the $Zn^{64}(\alpha,2n)Ge^{66}$ cross-section as well as the $(C^{12},pn)/(C^{12},2n)$ ratios plotted vs. excitation energy. The discrepancy between the calculated $(\alpha,pn)/(\alpha,2n)$ ratio and experiment is probably to be attributed to binding energy errors. At higher energies the calculated and experimental ratios are seen to merge within experimental error. The calculated and experimental $(C^{12},pn)/(C^{12},2n)$ ratios are seen to agree well within experimental error.

It is interesting to note that the experimental ratios form a continuous curve for the two systems. The coincidence of the two sets of data in the region from 36 - 40MeV where the angular momenta of the two systems is very closely matched (cf. figure 8) provides strong evidence that the predominant mechanism for both of these reactions is compound nucleus formation and decay and is a convincing verification of the independence hypothesis. Since any direct interaction component would not be expected to be of the same magnitude for two such differing target-projectile systems, it must be concluded that the highest energy range measurement for the $Zn^{64}(\alpha,pn)Ga^{66}$ reaction (see figure 11.) is probably in error.

VI. Conclusions

It may be stated, on the basis of this work, that, contrary to previous observations[34,63], the compound nucleus model provides a satisfactory account of the reactions of alpha particles with Zn^{64}. This conclusion is based on experimental recoil range evidence as well as the agreement of calculated excitation functions with experiment. The "high energy tails" of the measured excitation functions may be explained in terms of angular momentum effects and gamma ray competition with particle emission, rather than by assuming large direct interaction contributions to the reaction mechanism. Furthermore, all calculation parameters employed were based on available independent experimental evidence, rather than adjusted to achieve best agreement between calculation and experiment as has been done by other workers[34,44,63,66].

The main source of difficulty in performing calculations of excitation functions was found, in the present work, to be lack of reliable optical model parameters as well as uncertainty in particle binding energies.

The outcome of the $Fe^{56}+C^{12}$ calculations seems encouraging in light of the fact that one would expect the approximations inherent in the optical model to be an oversimplification for such a complex target-projectile system. The success of the statistical model on this reaction system would suggest further such experiments for investigation of angular momentum effects (see Appendix VI).

The treatment of gamma ray emission used in this work is in obvious need of refinement. The single particle estimates are inadequate, and the nature of collective enhancement of gamma ray emission probabilities is still a largely unexplored field. The rather emperical approach used in this work was seen to be adequate only to a first approximation.

In conclusion, it may be stated that, provided one has a reasonably accurate knowledge of the constants of motion of a compound nucleus formed by a given target-projectile system, the decay of this compound nucleus may be accurately described by the statistical model.

TABLE IV

Zn^{64} and He^{4} Cross-sections.

E_α(MeV)	$\sigma(\alpha,\gamma)$	$\sigma(\alpha,p)$	$\sigma(\alpha,n)$	$\sigma(\alpha,pn)$	$\sigma(\alpha,2n)$
9.1		21.8			
9.4	.259				
11.3	.771				
11.9		115			
12.9			2.0		
13.5	.720				
14.3		269			
14.4			11.2		
15.6	.218				
15.9			67.5		
16.4		305			
18.0		404		0.64	
19.6		452			
19.7			233		
21.6				84.1	
21.8			206		
22.4		339			
24.8		225		551	
25.0					0.97
26.1			82.3		
27.2					50.9
28.3		84.8		938	
29.5					126
29.7			45.1		
31.0				969	
31.5			36.1		
32.3					129
34.5			20.0		

TABLE IV (cont'd)

E_α(MeV)	$\sigma(\alpha,\gamma)$	$\sigma(\alpha,p)$	$\sigma(\alpha,n)$	$\sigma(\alpha,pn)$	$\sigma(\alpha,2n)$
34.7					109
34.9				539	
36.9		11.7		415	
37.3					82.2

(All cross-sections are expressed in millibarns)

TABLE V

Zn^{64} and He^{4} Recoil Ranges.

E_α(MeV)	$R_o[(\alpha,n)+(\alpha,p)]$	$R_o[(\alpha,pn)]$	$R_o[(\alpha,2n)]$
8.6	87		
11.5	172		
12.9	193		
15.6	274		
17.0		145	
19.0	301		
19.7		228	
23.1	374		
24.1		256	
25.0			342
27.2			353
27.6		333	
29.5			376
30.2		361	
32.3			319
34.5		333	
34.7			435
36.3	477	272	
37.3			495

(All ranges are expressed in $\mu g/cm^2$.)

TABLE VI

Fe^{56} and C^{12} Cross-sections

$E_{C^{12}}$(MeV)	E*(MeV)	$\sigma(C^{12},n)+\sigma(C^{12},p)$	$\sigma(C^{12},pn)$	$\sigma(C^{12},2n)$
36.9	36.4	2.57	370	98.0
39.1	38.2	1.49	90.0	24.2
43.8	42.1	- - -	17.2	5.3
75.4	68.1	- - -	<0.5	<0.9

(all cross-sections are expressed in millibarns)

TABLE VII

Cr^{52} and O^{16} Cross-sections

E_{O16}(MeV)	E*(MeV)	$\sigma(O^{16},n)+\sigma(O^{16},p)$	$\sigma(O^{16},pn)$	$\sigma(O^{16},2n)$
39.2	36.4	<1.8	<0.23	<.061
47.5	42.7	<2.7	<0.34	<.090
131.0	106	<2.6	<0.33	<.088

E_{O16}(MeV)	E*(MeV)	$\sigma(O^{16},\alpha 2n)$	$\sigma(O^{16},\alpha pn)$	$\sigma(O^{16},3pn)$
39.2	36.4	<3.1	<0.70	<0.28
47.5	42.7	<2.1	<0.48	<0.19
131.0	106	<3.0	<0.69	<0.27

(all cross-sections are expressed in millibarns)

HILAC TARGET HOLDER

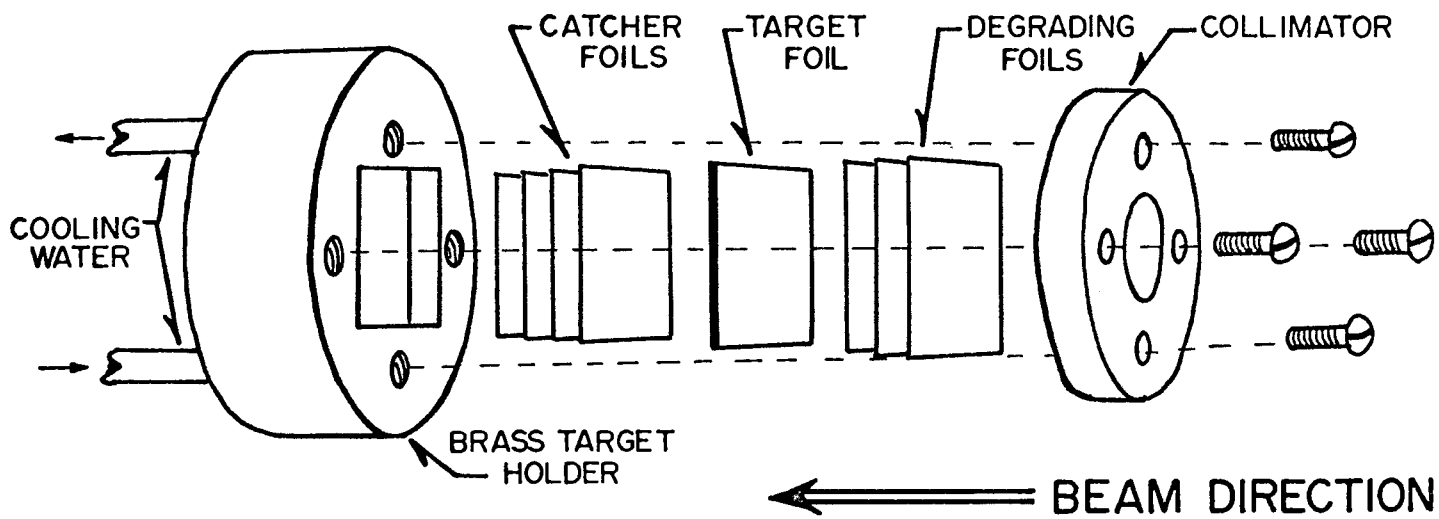

FIGURE 1

UNIVERSITY OF WASHINGTON
"BELL JAR" TARGET ASSEMBLY

(Schematic)

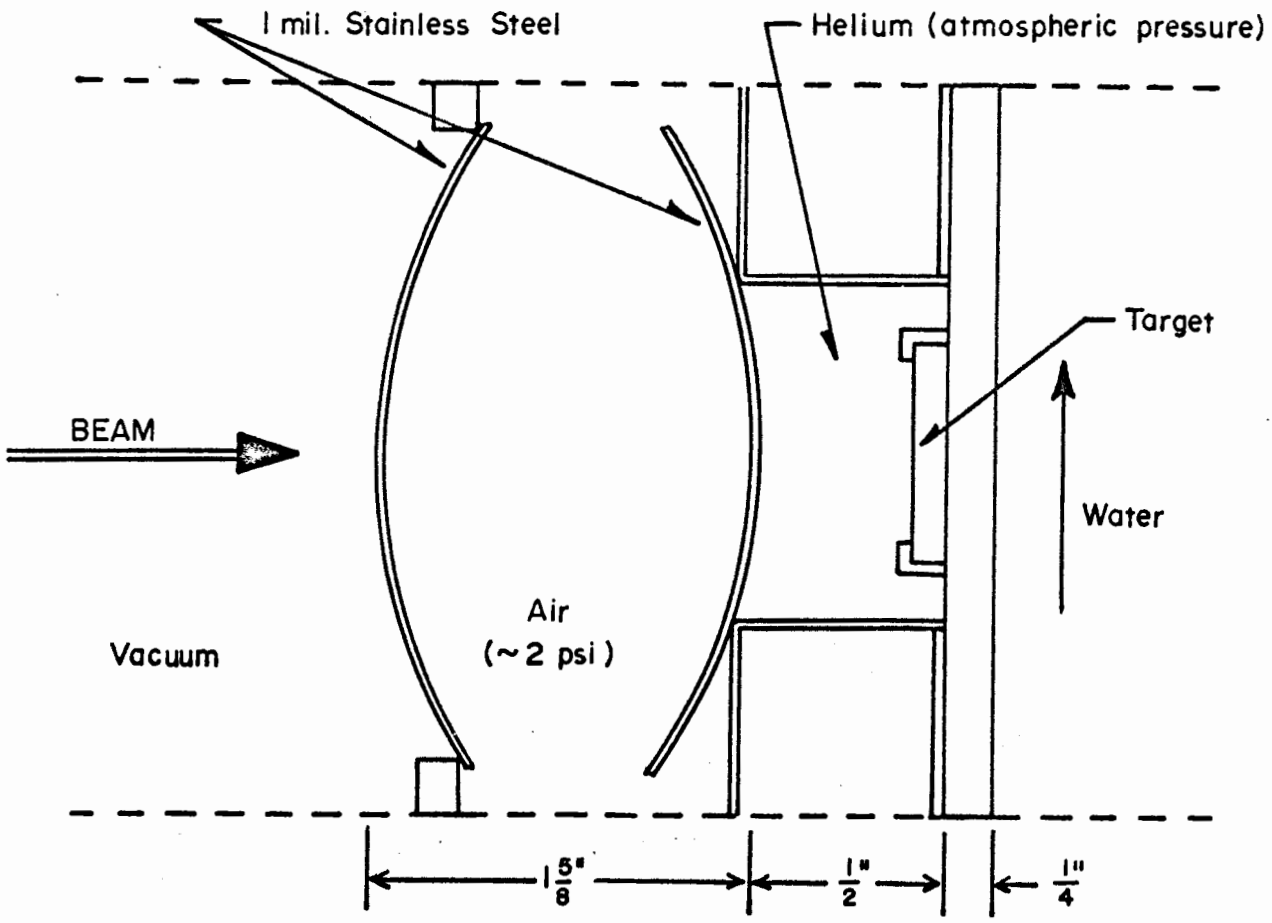

FIGURE 2

FIGURE 3

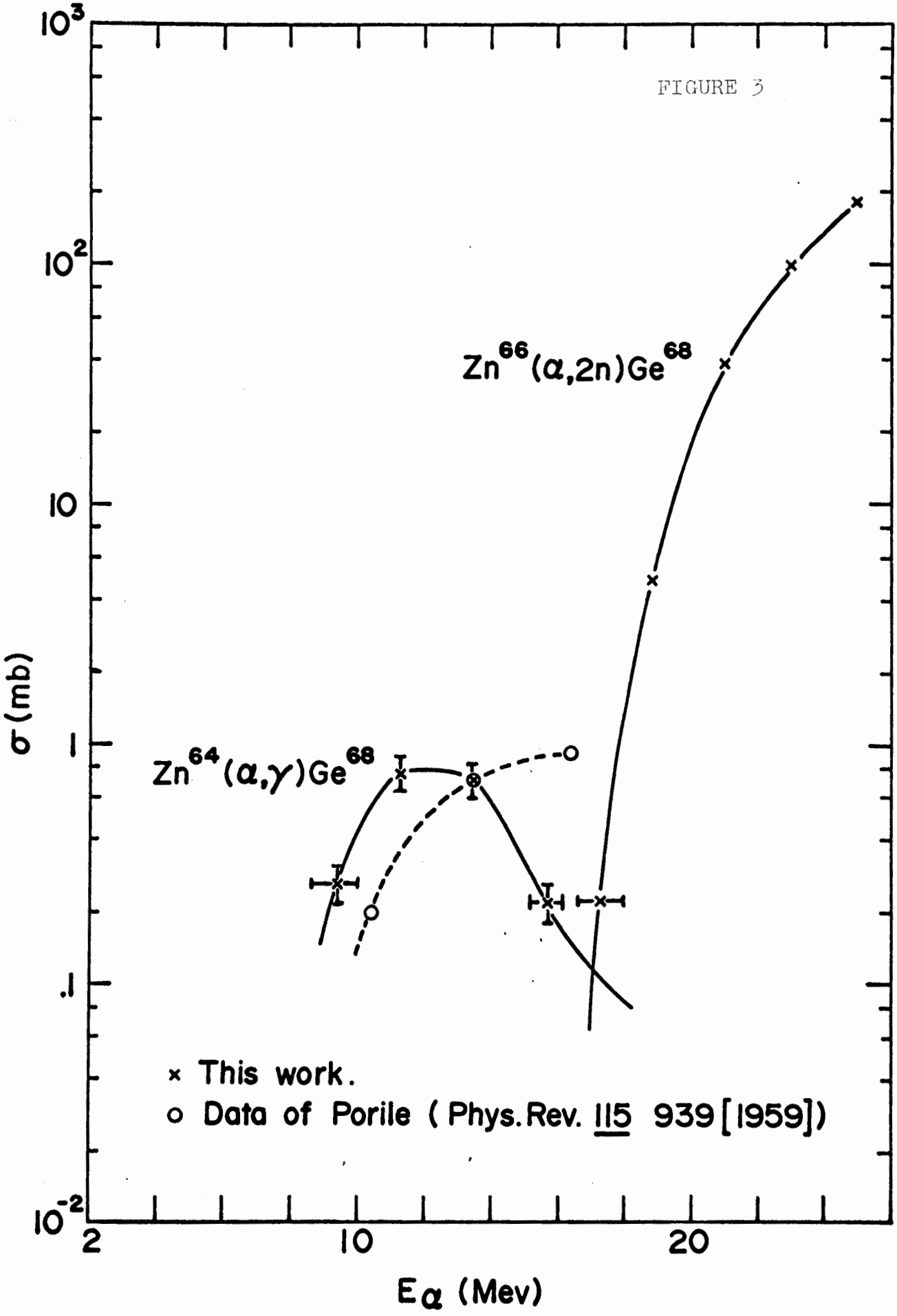
10^3
10^2
10
1
.1
10^{-2}
σ (mb)
$Zn^{66}(\alpha,2n)Ge^{68}$
$Zn^{64}(\alpha,\gamma)Ge^{68}$
× This work.
o Data of Porile (Phys.Rev. 115 939 [1959])
2
10
20
E_α (Mev)

FIGURE 4

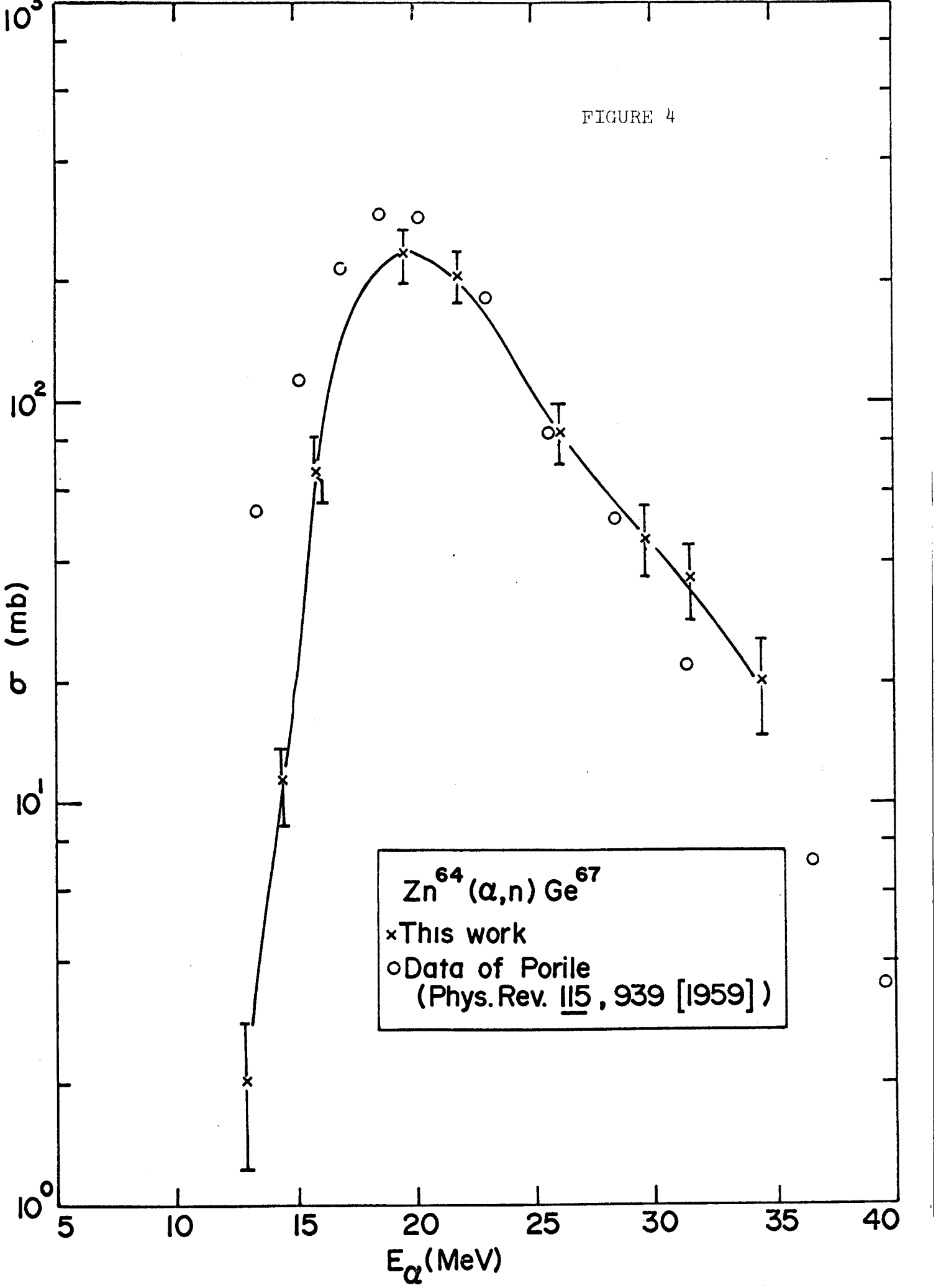
10^3
10^2
10^1
10^0
σ (mb)
5
10
15
20
25
30
35
40
E_α (MeV)
$Zn^{64}(\alpha,n)Ge^{67}$
×This work
○Data of Porile
(Phys. Rev. 115, 939 [1959])

FIGURE 5

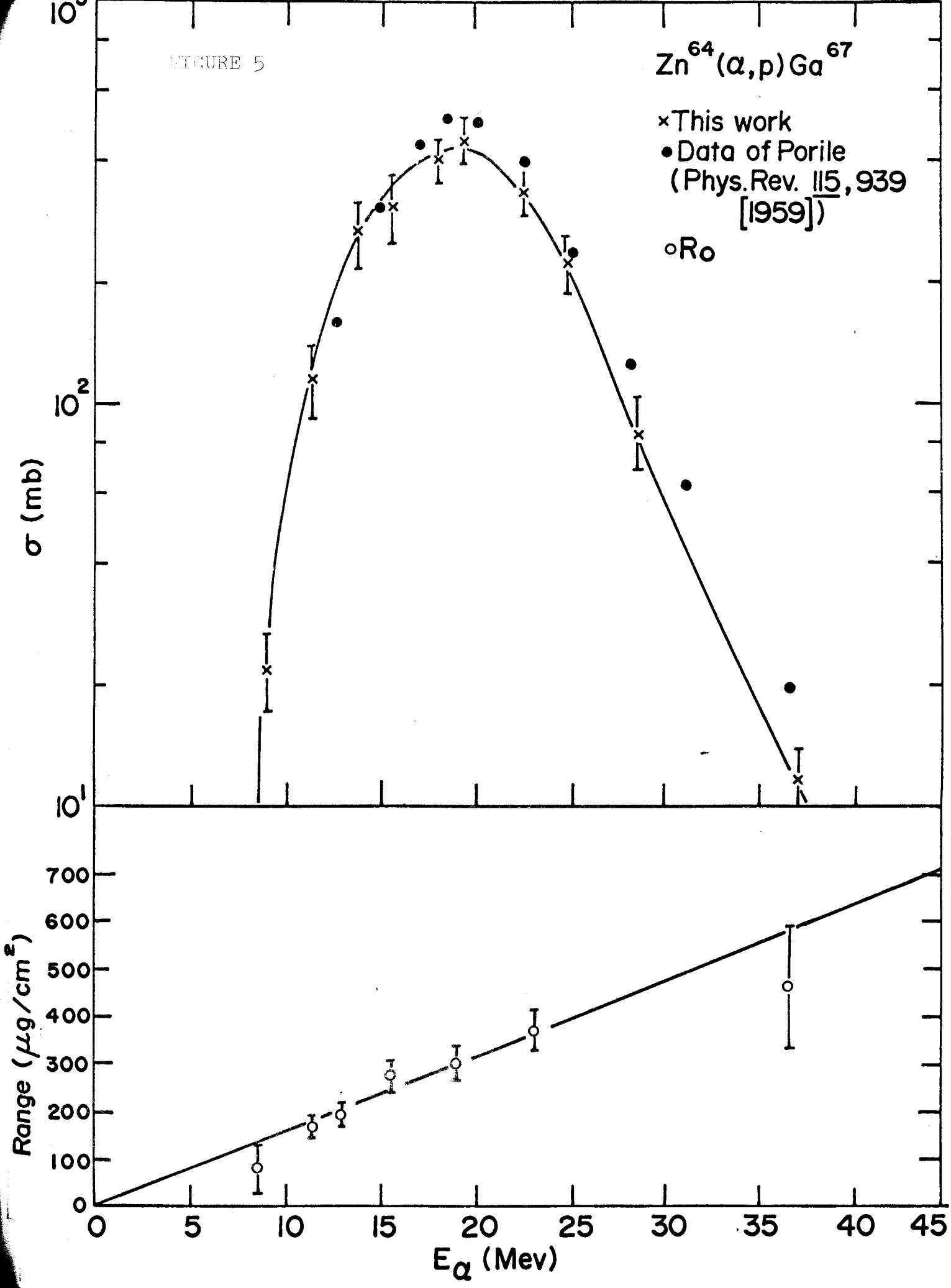
$Zn^{64}(\alpha,p)Ga^{67}$
×This work
•Data of Porile (Phys.Rev. 115, 939 [1959])
○Ro
σ (mb)
10^2
10^1
Range ($\mu g/cm^2$)
0
100
200
300
400
500
600
700
0
5
10
15
20
25
30
35
40
45
E_α (Mev)

FIGURE 6

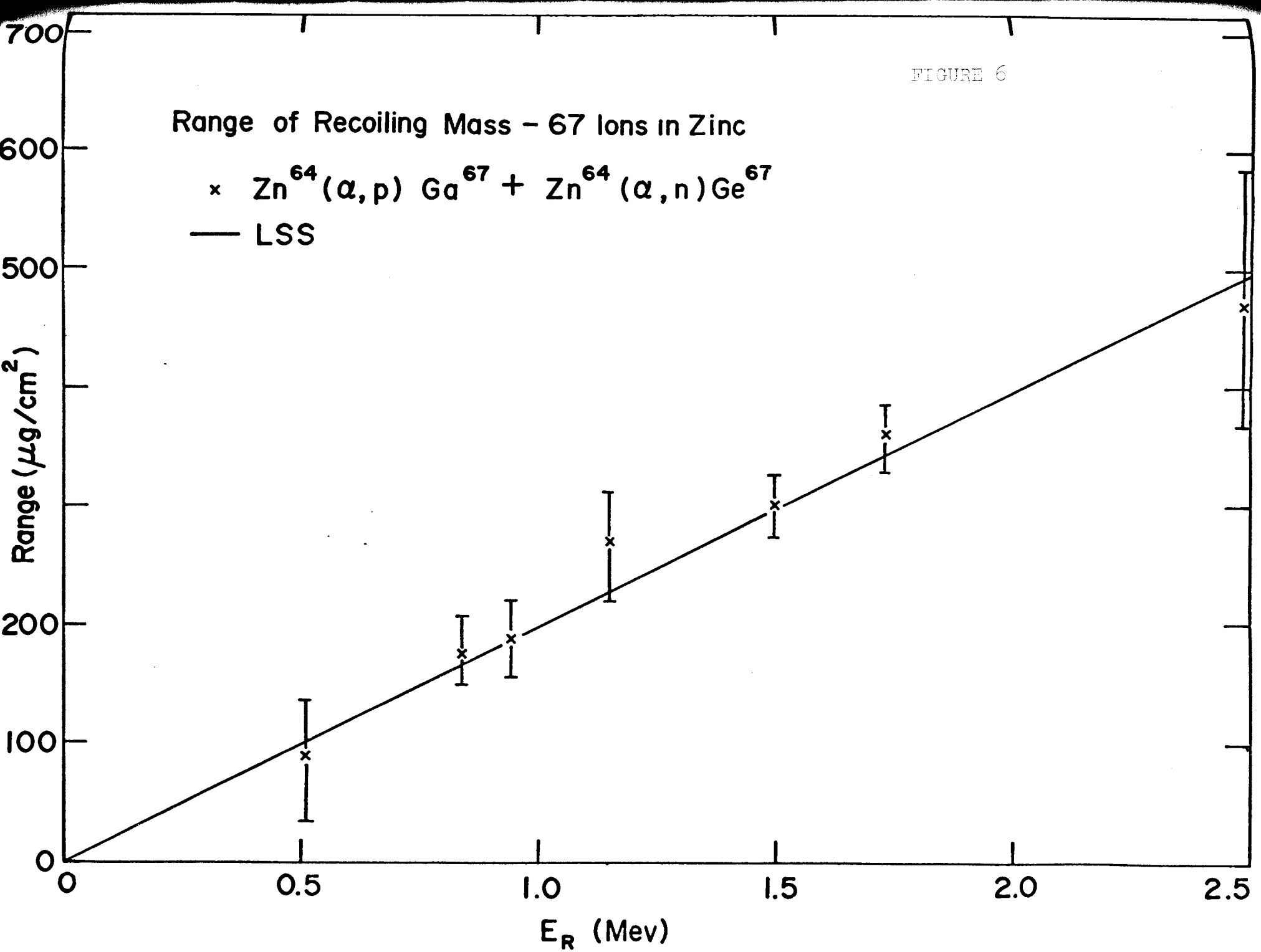
Range of Recoiling Mass – 67 Ions in Zinc
× $Zn^{64}(\alpha, p)\ Ga^{67} + Zn^{64}(\alpha, n)Ge^{67}$
— LSS
Range ($\mu g/cm^2$)
E_R (Mev)
0
100
200
500
600
700
0.5
1.0
1.5
2.0
2.5

FIGURE 7

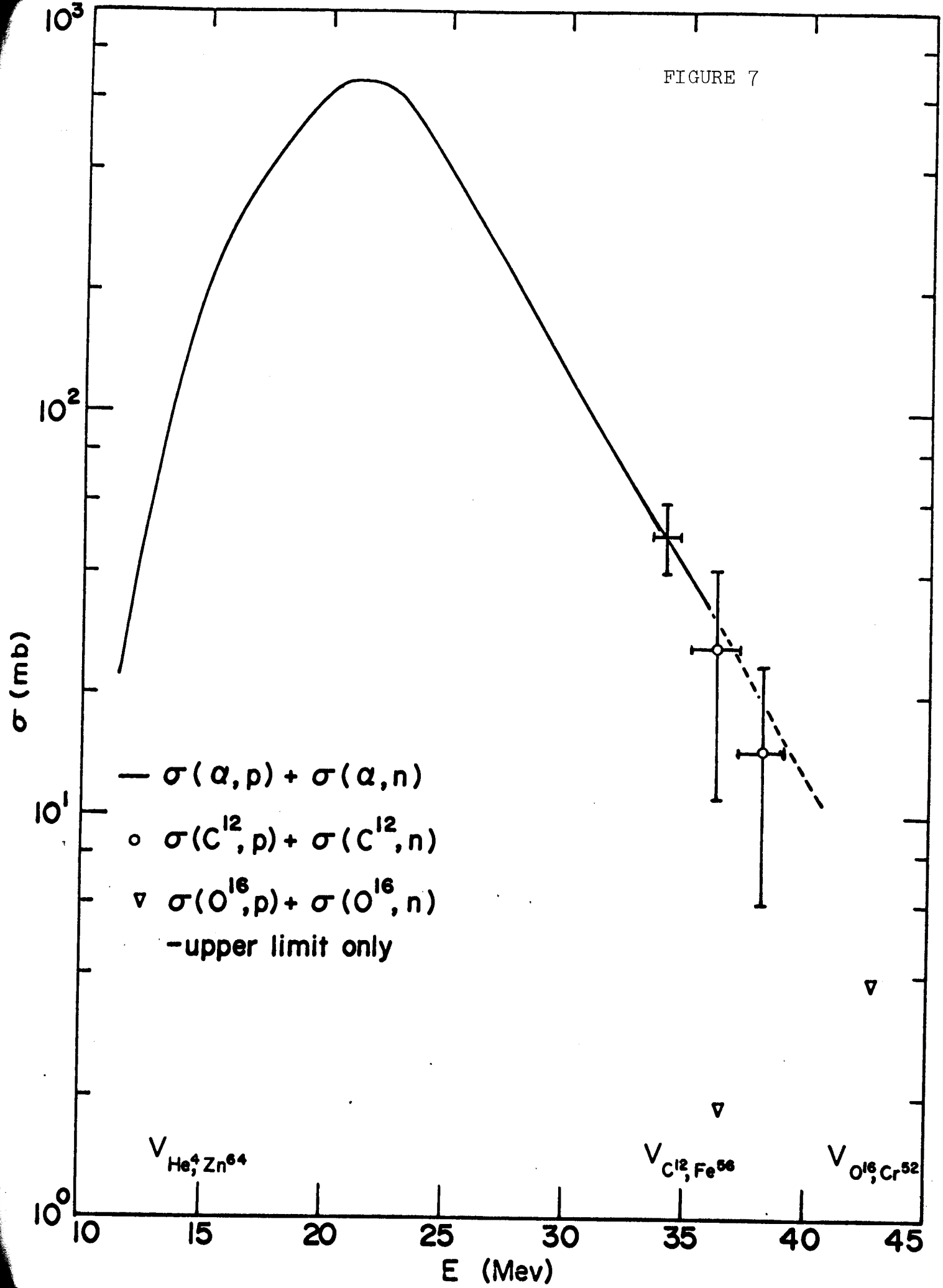
10^3
10^2
10^1
10^0
σ (mb)
— σ(α, p) + σ(α, n)
o σ(C^{12}, p) + σ(C^{12}, n)
▽ σ(O^{16}, p) + σ(O^{16}, n)
-upper limit only
$V_{He^4;Zn^{64}}$
$V_{C^{12};Fe^{56}}$
$V_{O^{16};Cr^{52}}$
10
15
20
25
30
35
40
45
E (Mev)

FIGURE 8

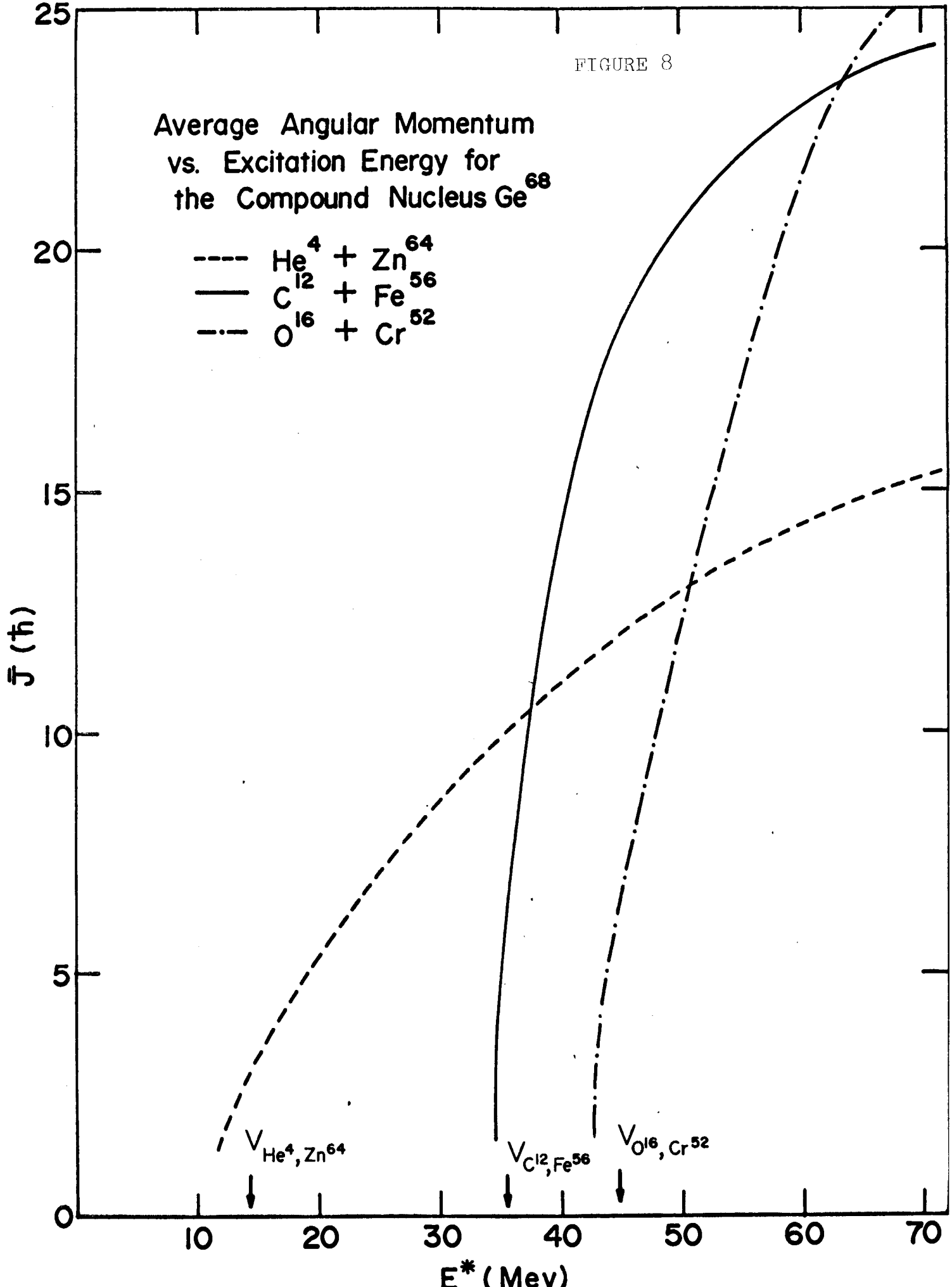
Average Angular Momentum
vs. Excitation Energy for
the Compound Nucleus Ge^{68}
---- $He^4 + Zn^{64}$
—— $C^{12} + Fe^{56}$
-·- $O^{16} + Cr^{52}$
$\bar{J}$ (ħ)
E^* (Mev)
$V_{He^4, Zn^{64}}$
$V_{C^{12}, Fe^{56}}$
$V_{O^{16}, Cr^{52}}$
0
5
10
15
20
25
10
20
30
40
50
60
70

FIGURE 9

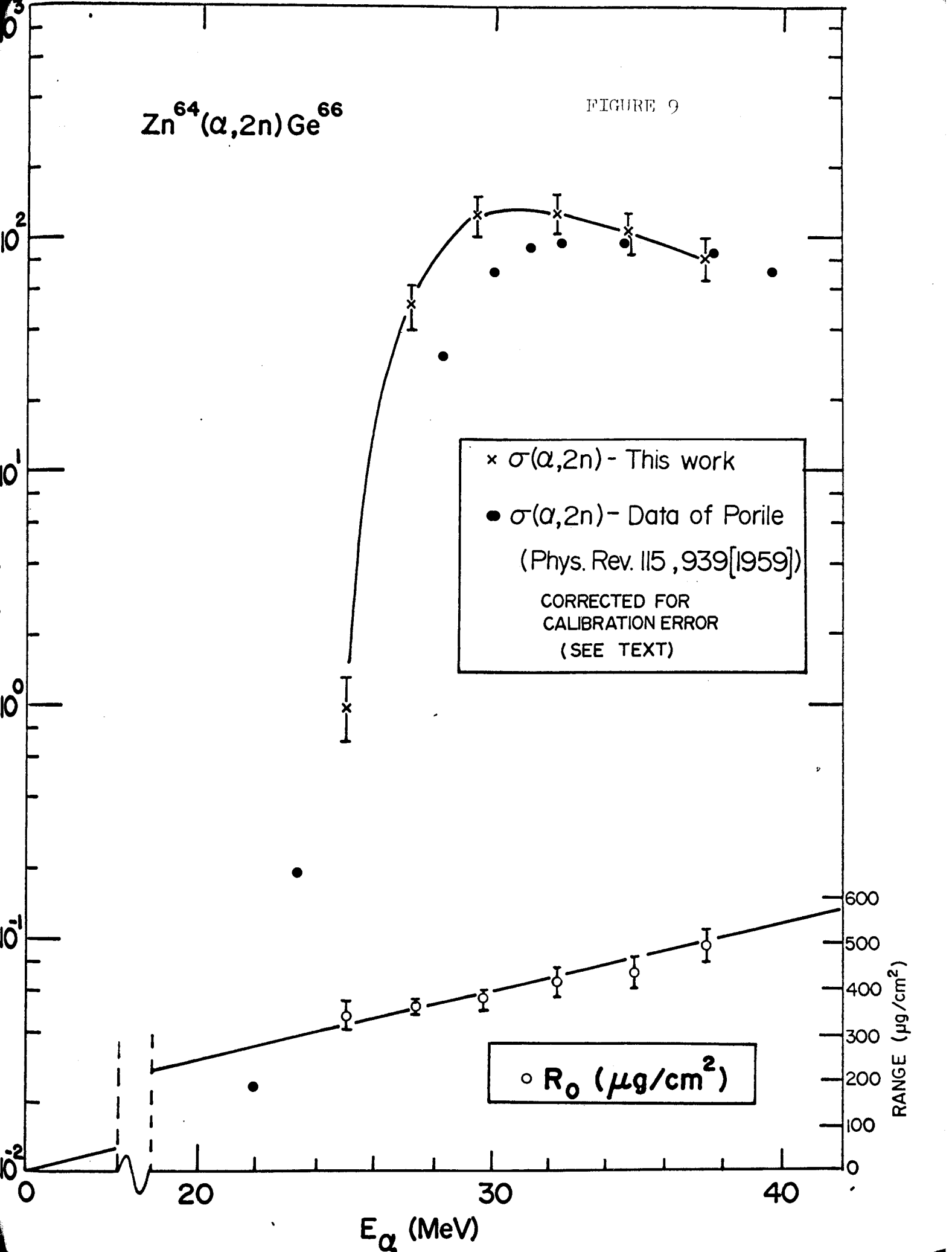
$Zn^{64}(\alpha,2n)Ge^{66}$
× σ(α,2n) - This work
● σ(α,2n) - Data of Porile
(Phys. Rev. 115, 939[1959])
CORRECTED FOR
CALIBRATION ERROR
(SEE TEXT)
○ R_0 (μg/cm²)
10^3
10^2
10^1
10^0
10^{-1}
10^{-2}
0
20
30
40
600
500
400
300
200
100
0
RANGE (μg/cm²)
E_α (MeV)

FIGURE 10

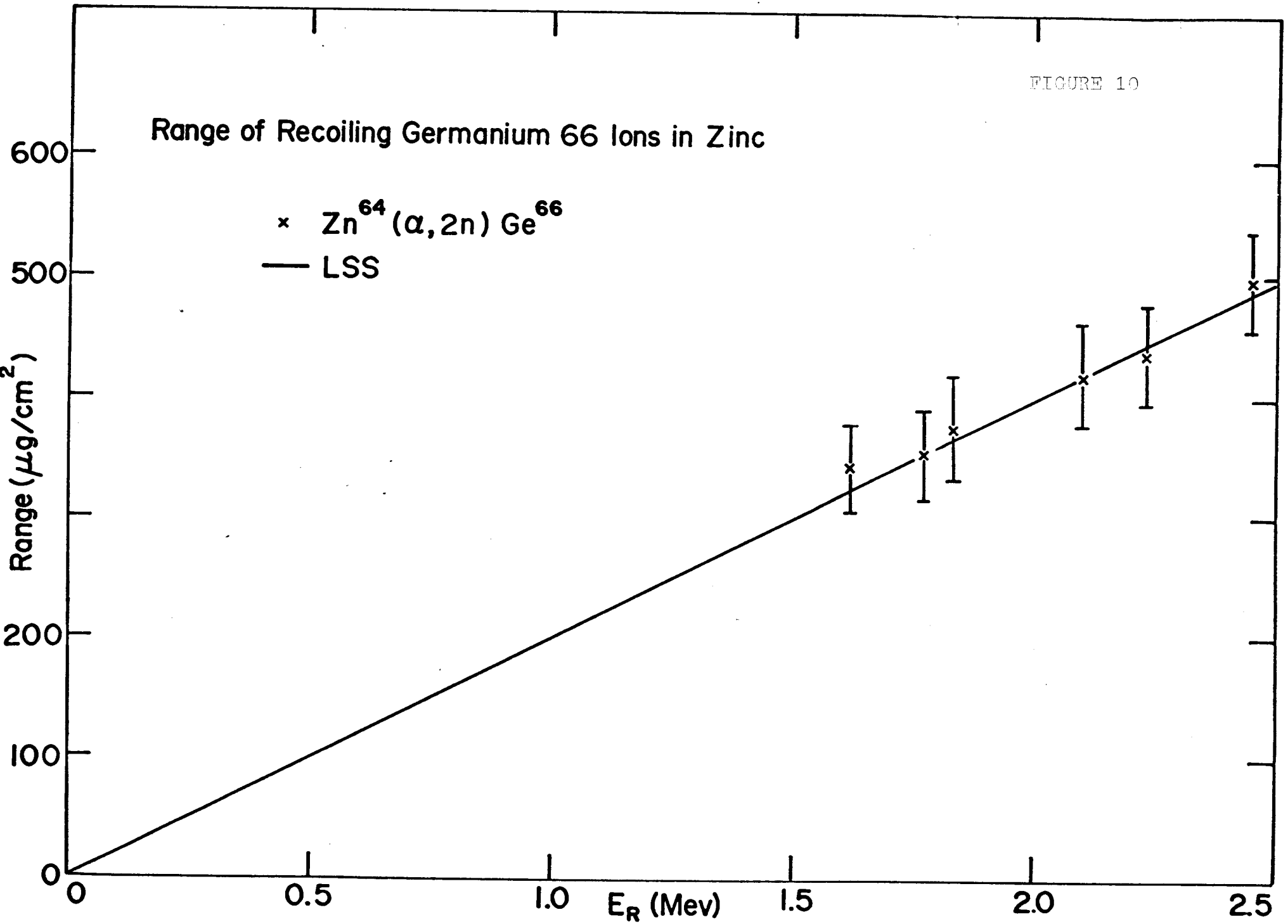
Range of Recoiling Germanium 66 Ions in Zinc
× $Zn^{64}(\alpha, 2n)\ Ge^{66}$
— LSS
Range ($\mu g/cm^2$)
600
500
200
100
0
0
0.5
1.0
E_R (Mev)
1.5
2.0
2.5

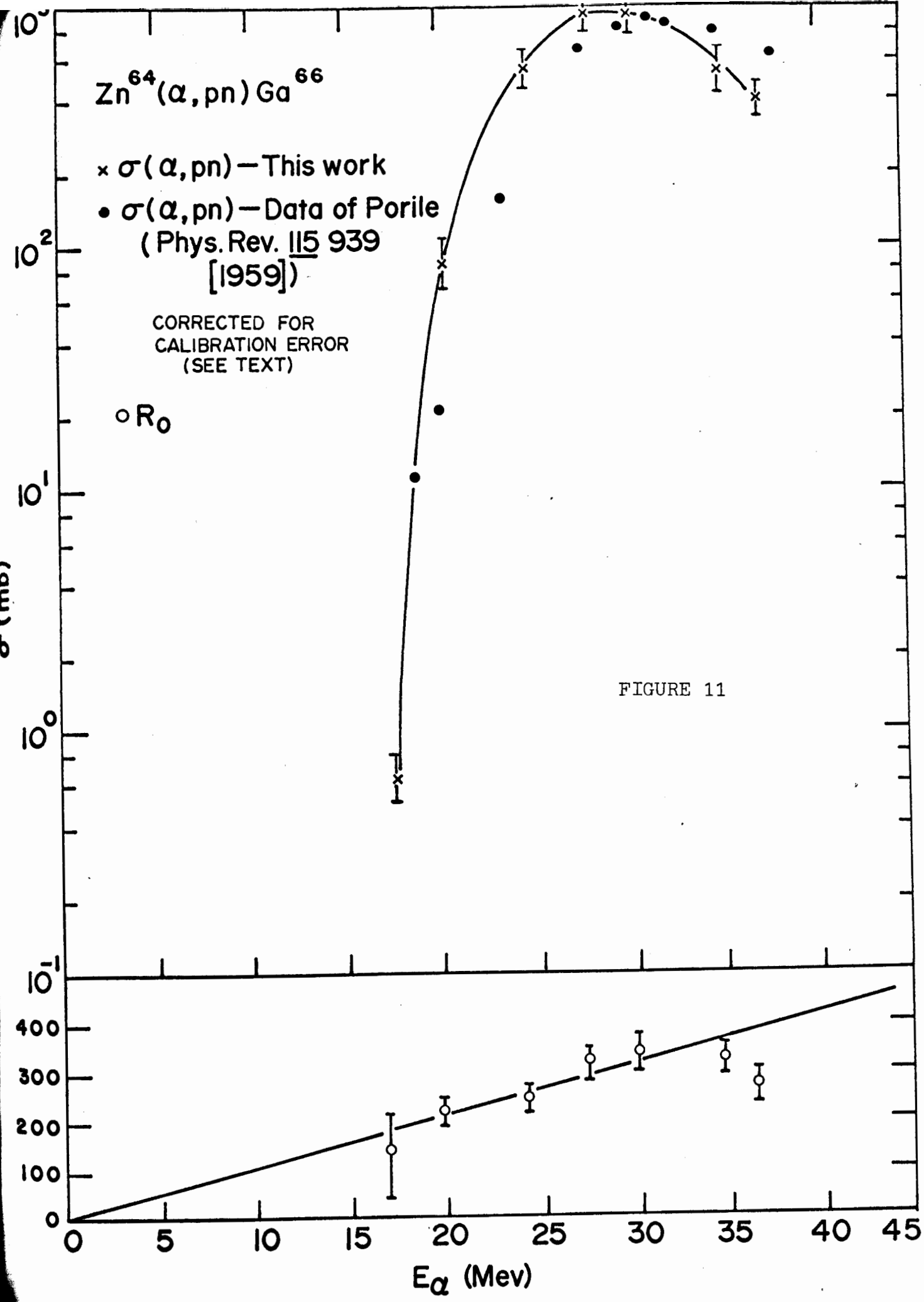
$Zn^{64}(\alpha, pn)Ga^{66}$
× σ(α, pn) — This work
• σ(α, pn) — Data of Porile (Phys. Rev. 115 939 [1959])
CORRECTED FOR CALIBRATION ERROR (SEE TEXT)
○ R_0
σ (mb)
10^2
10^1
10^0
10^{-1}
400
300
200
100
0
0
5
10
15
20
25
30
35
40
45
E_α (Mev)

FIGURE 11

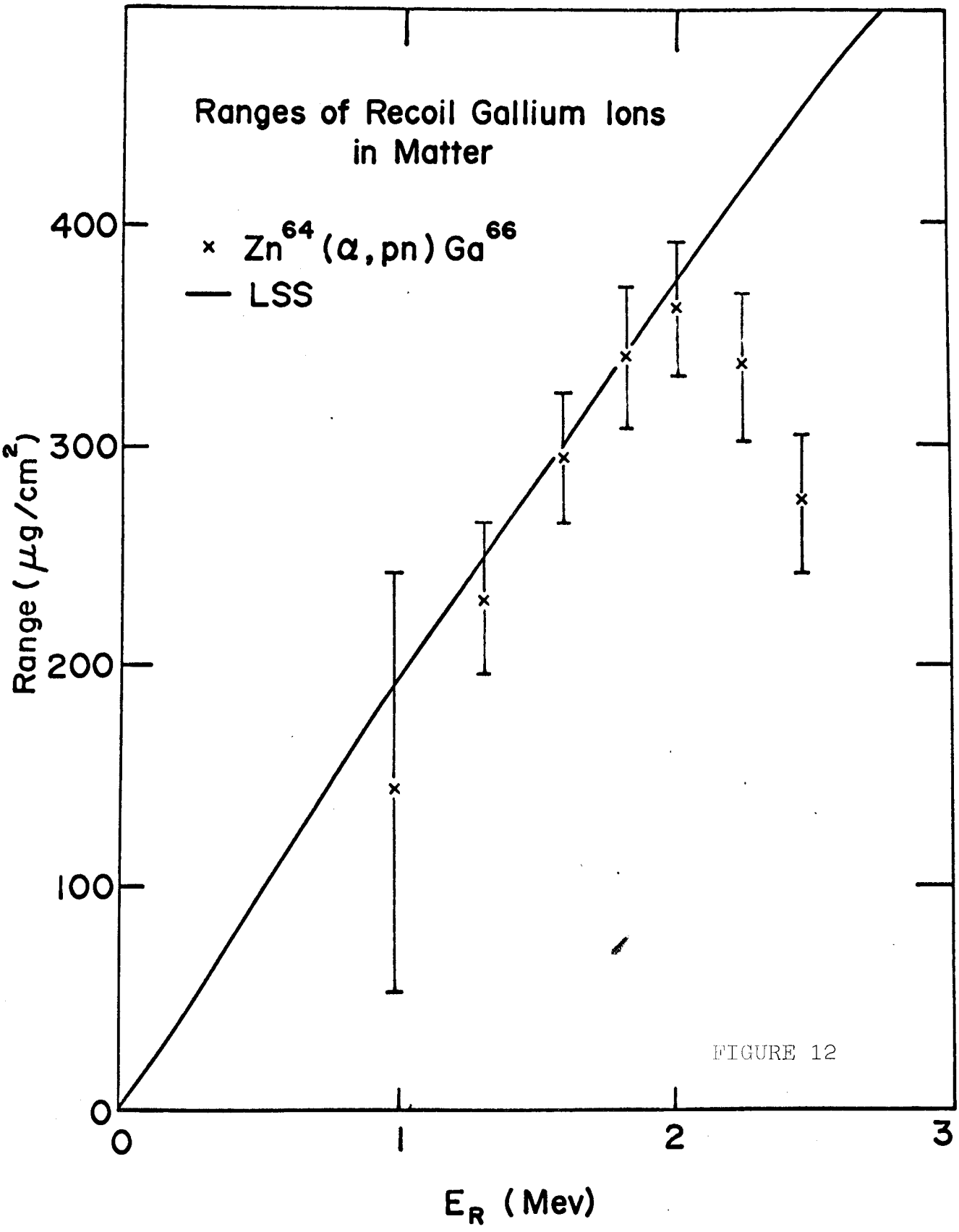
Ranges of Recoil Gallium Ions
in Matter
× $Zn^{64}(\alpha, pn)Ga^{66}$
— LSS
Range ($\mu g/cm^2$)
400
300
200
100
0
0
1
2
3
E_R (Mev)

FIGURE 12

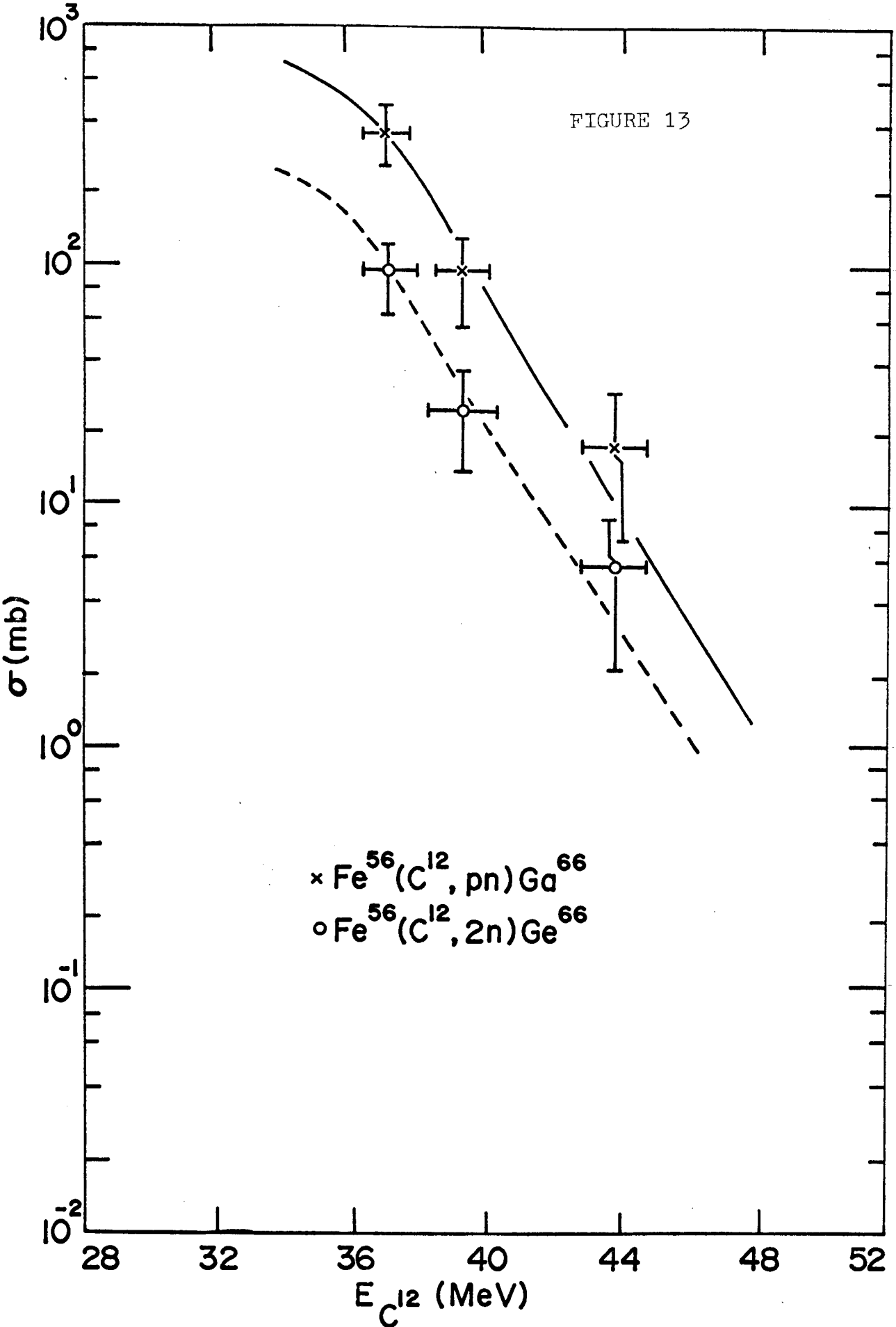
FIGURE 13
10^3
10^2
10^1
10^0
10^{-1}
10^{-2}
σ (mb)
× $Fe^{56}(C^{12}, pn)Ga^{66}$
○ $Fe^{56}(C^{12}, 2n)Ge^{66}$
28
32
36
40
44
48
52
$E_{C^{12}}$ (MeV)

FIGURE 14

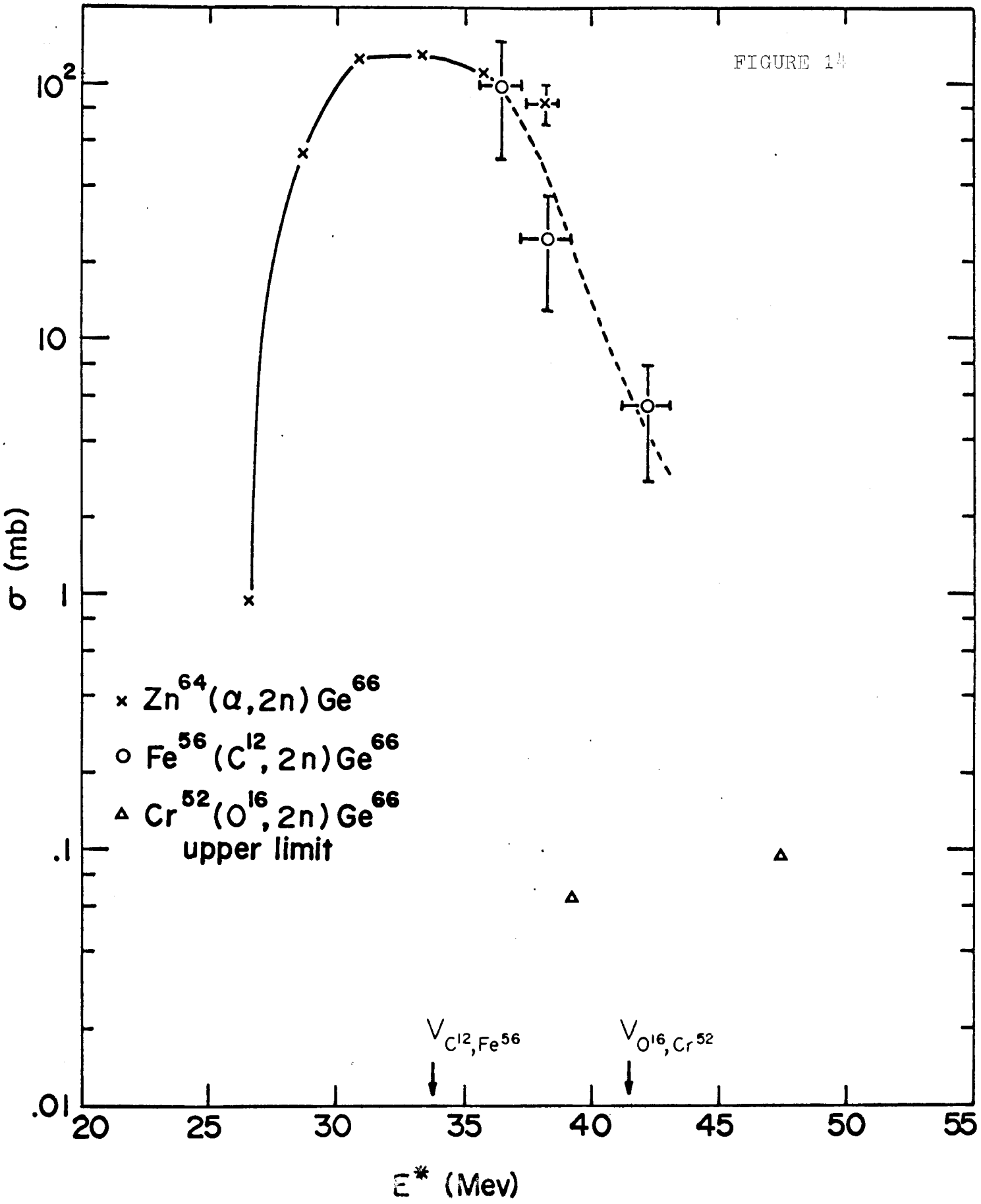
10^2
10
1
.1
.01
σ (mb)
× $Zn^{64}(\alpha,2n)Ge^{66}$
○ $Fe^{56}(C^{12},2n)Ge^{66}$
△ $Cr^{52}(O^{16},2n)Ge^{66}$
upper limit
$V_{C^{12},Fe^{56}}$
$V_{O^{16},Cr^{52}}$
20
25
30
35
40
45
50
55
E* (Mev)

FIGURE 15

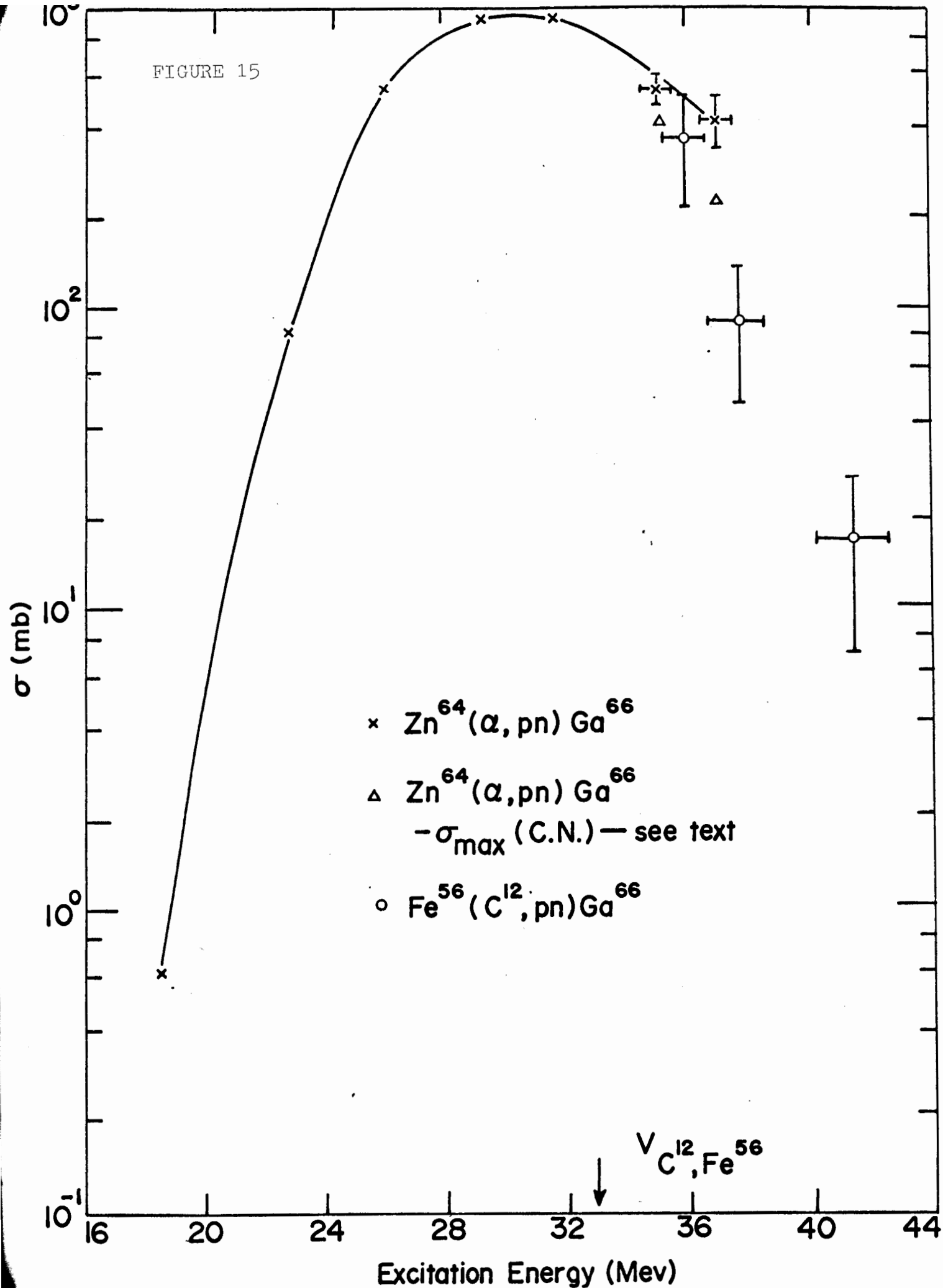
σ (mb)
10²
10¹
10⁰
10⁻¹
16
20
24
28
32
36
40
44
Excitation Energy (Mev)
× Zn⁶⁴(α, pn) Ga⁶⁶
△ Zn⁶⁴(α,pn) Ga⁶⁶
-σmax (C.N.) — see text
○ Fe⁵⁶(C¹², pn)Ga⁶⁶
V C¹², Fe⁵⁶

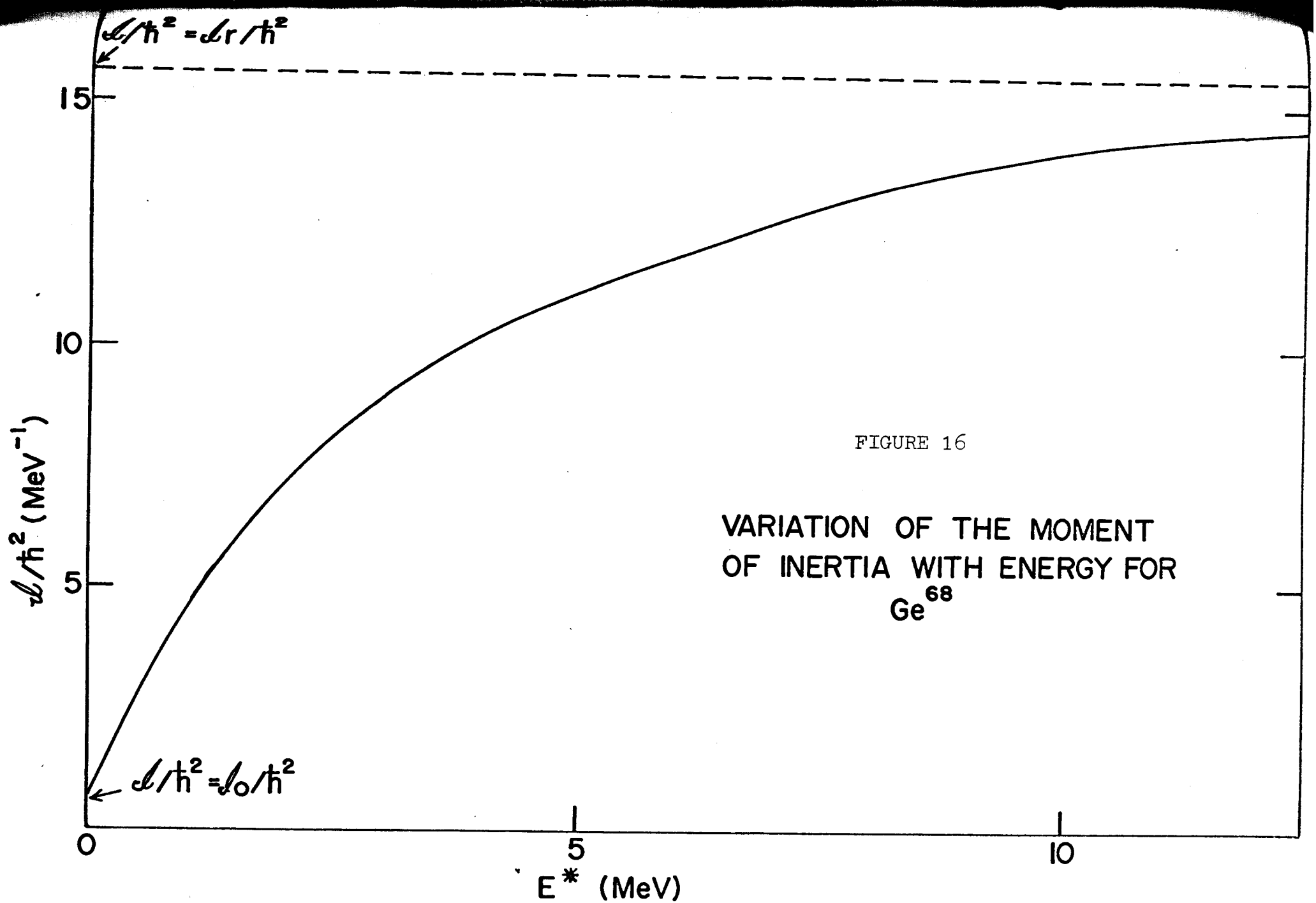

FIGURE 16

VARIATION OF THE MOMENT OF INERTIA WITH ENERGY FOR Ge^{68}

FIGURE 17

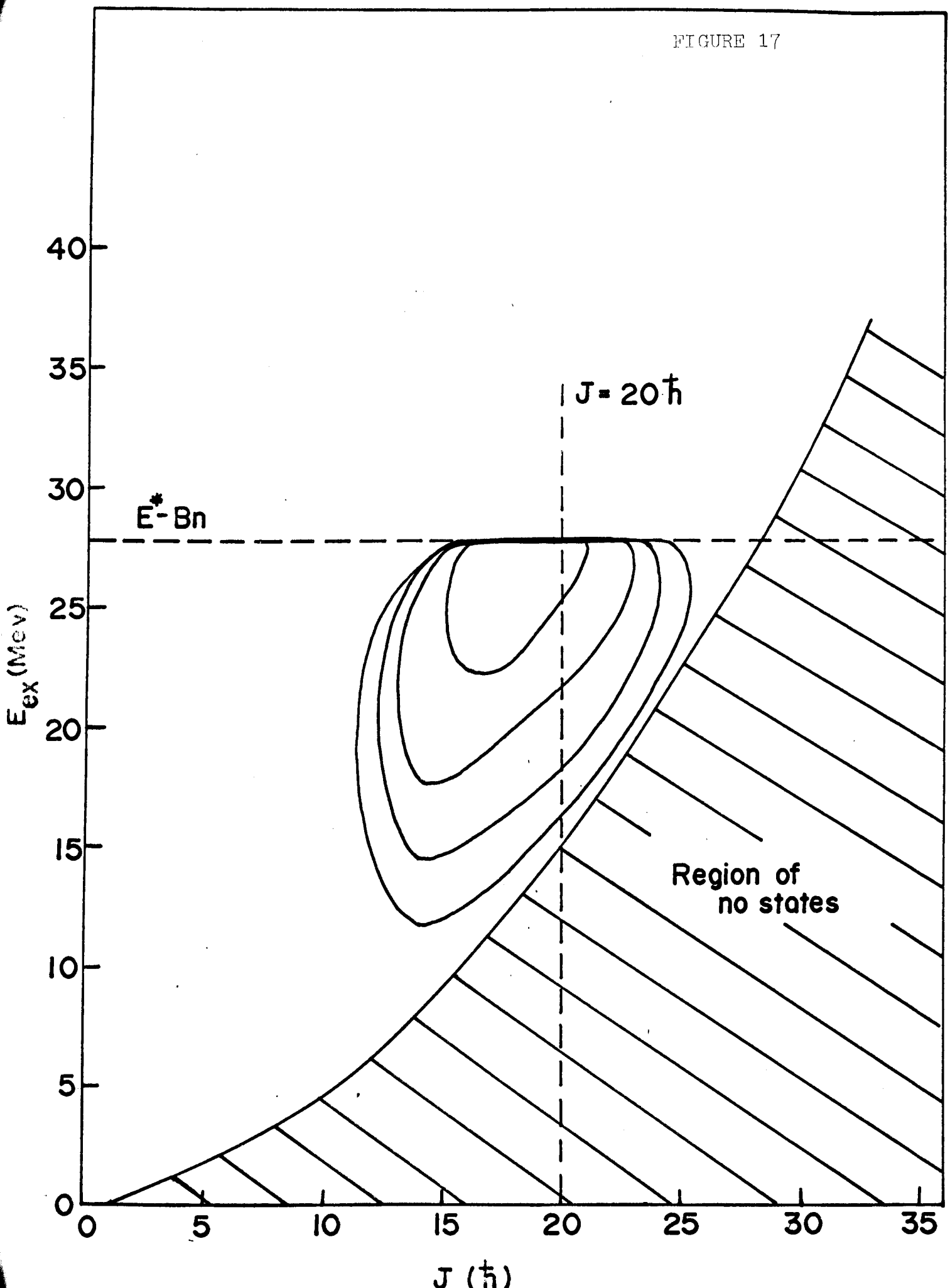
40
35
30
25
20
15
10
5
0
E_{ex} (Mev)
E^* - Bn
J = 20ħ
Region of
no states
0
5
10
15
20
25
30
35
J (ħ)

FIGURE 13

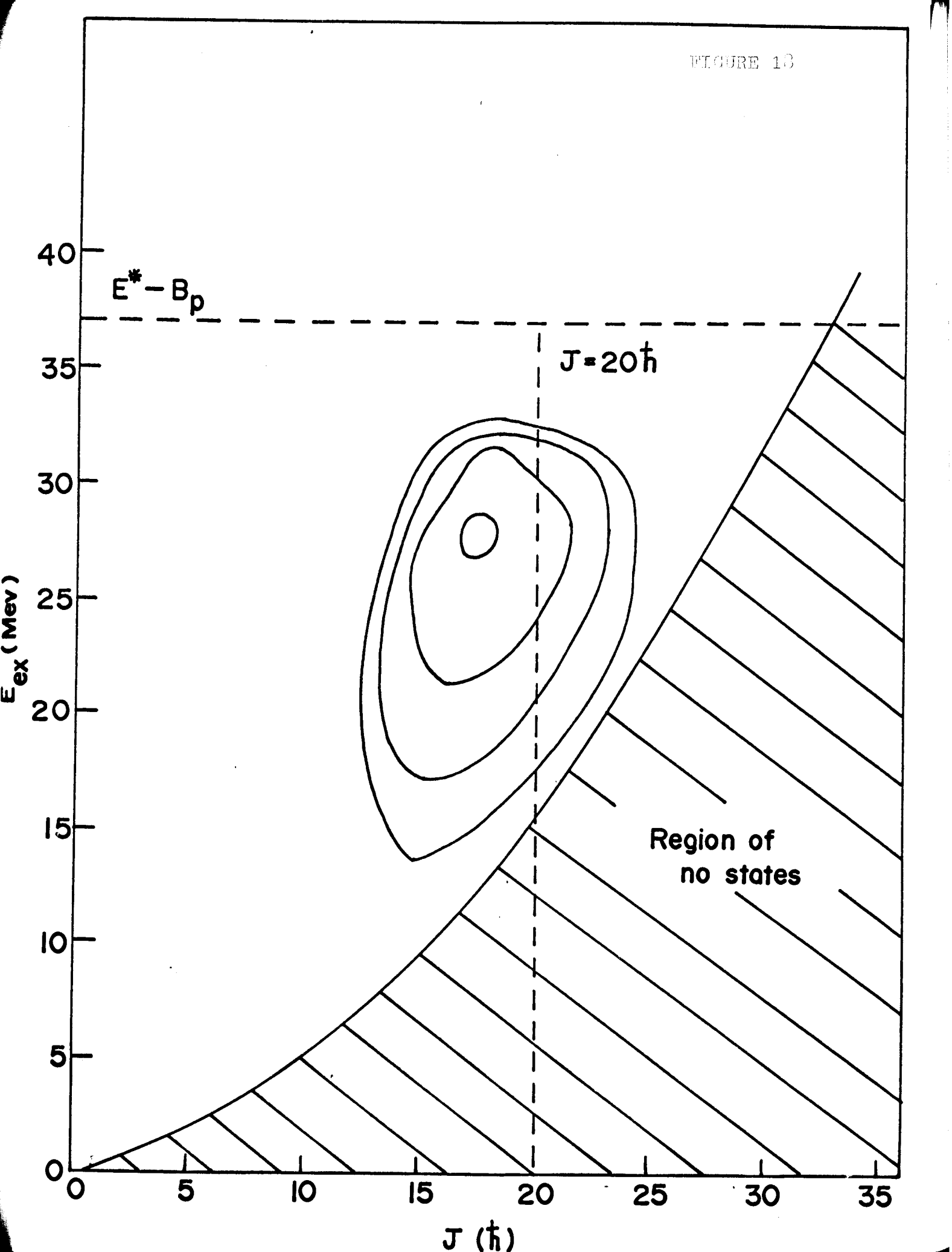
40
35
30
25
20
15
10
5
0
$E^* - B_p$
J = 20ħ
E_{ex} (Mev)
Region of
no states
0
5
10
15
20
25
30
35
J (ħ)

FIGURE 19

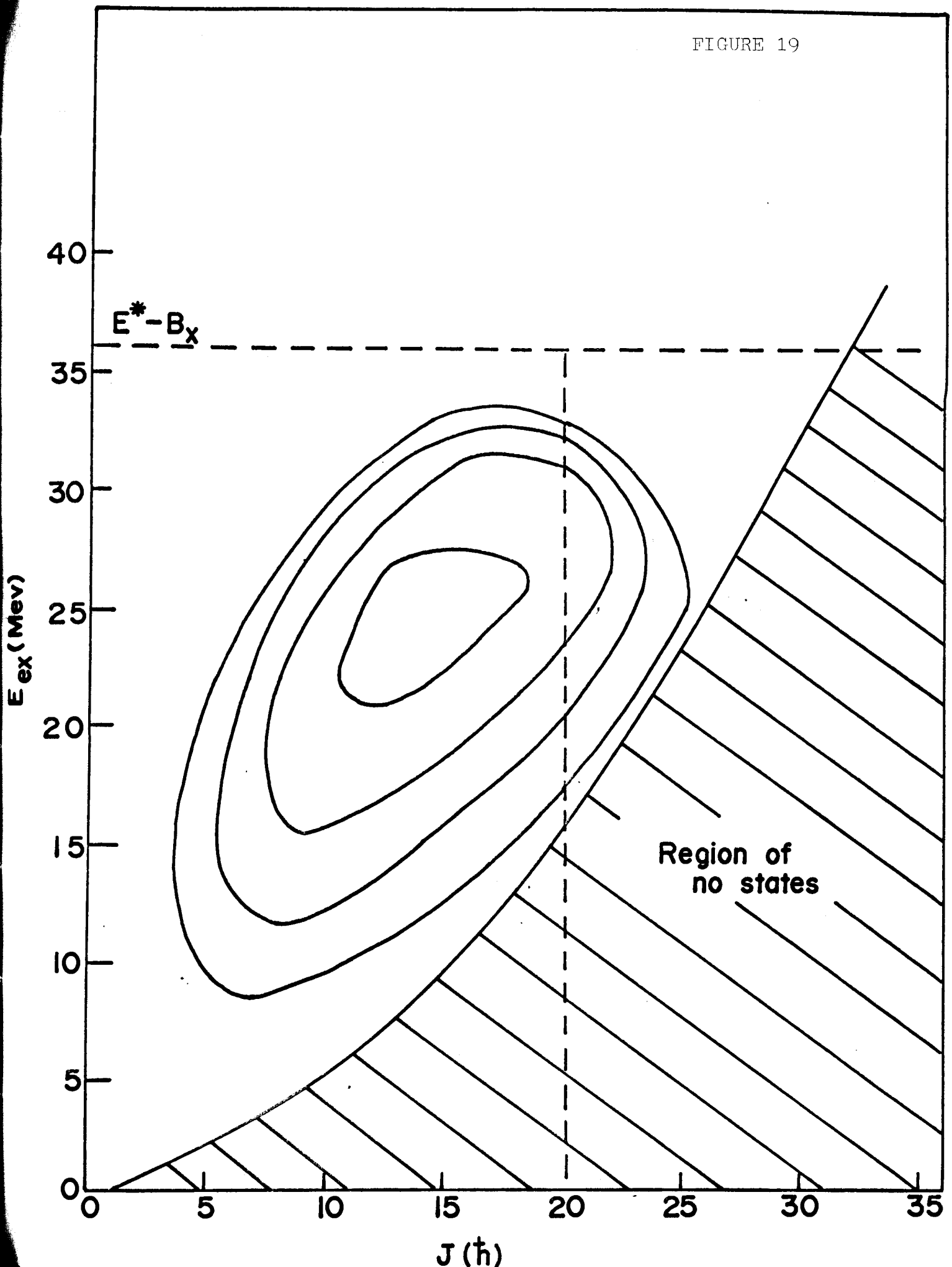
40
35
30
25
20
15
10
5
0
E^*-B_x
E_{ex} (Mev)
Region of
no states
0
5
10
15
20
25
30
35
J (ħ)

FIGURE 20

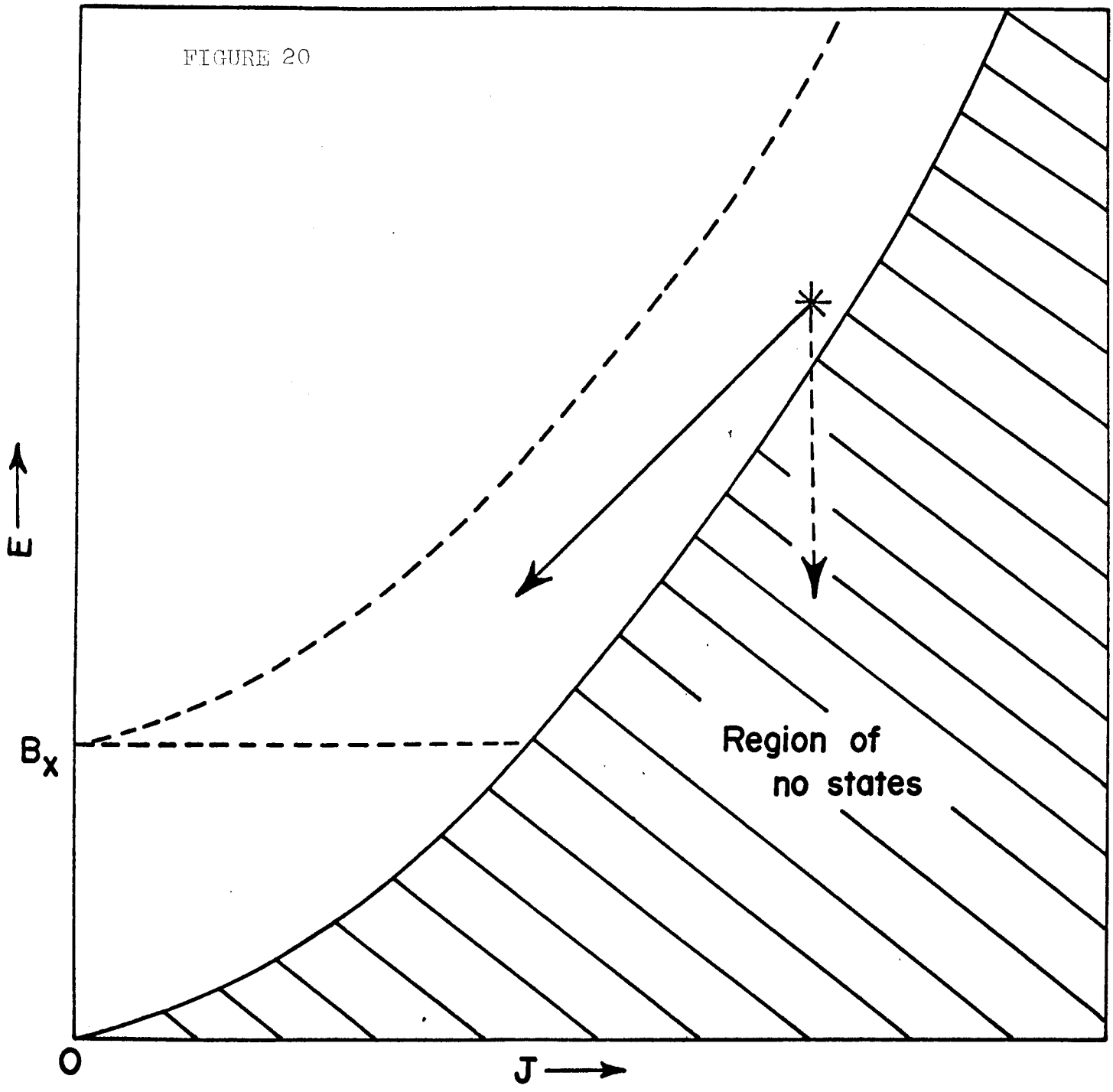

FIGURE 21

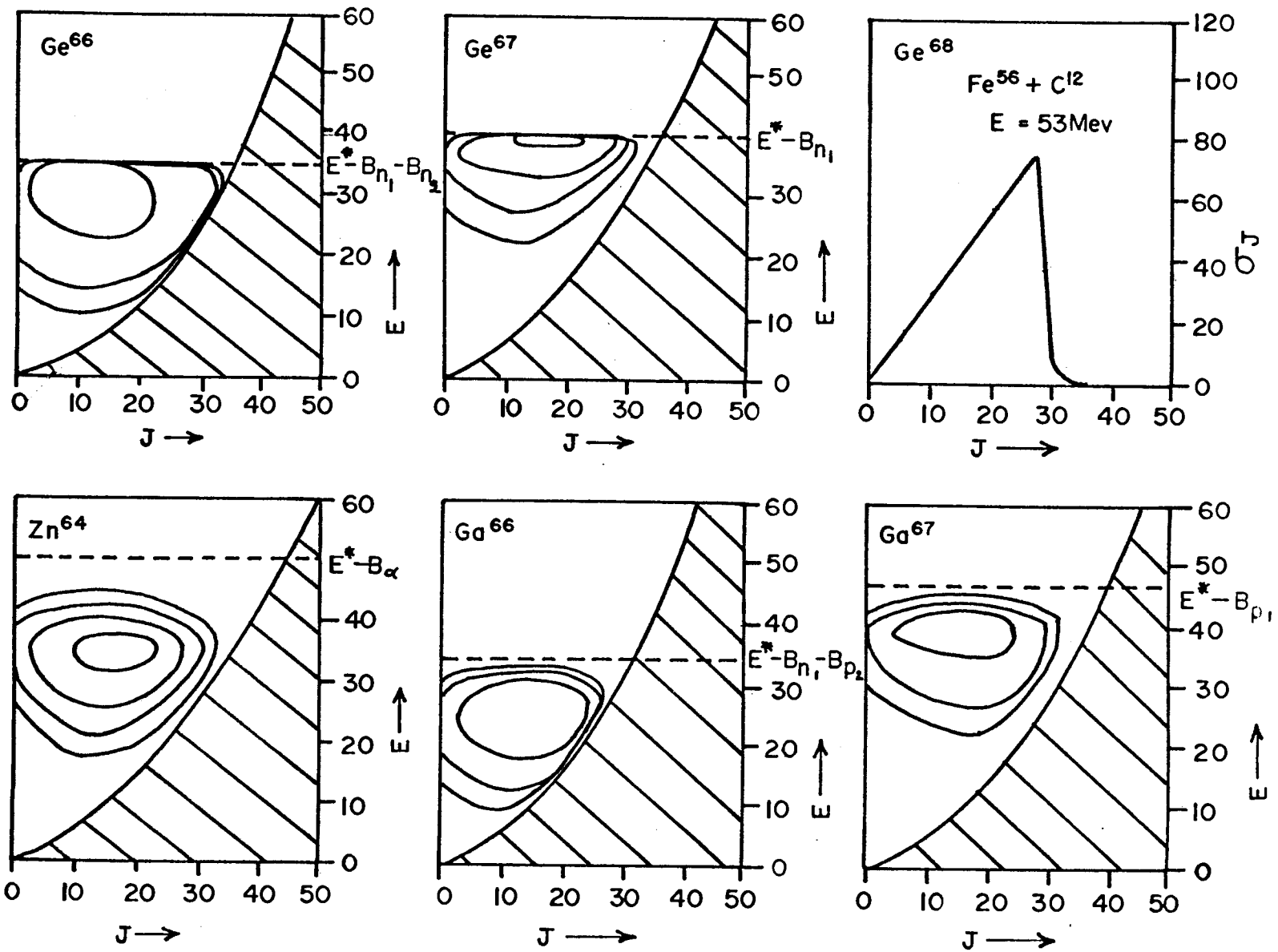
Ge66
Ge67
Ge 68
Fe56 + C12
E = 53Mev
Zn64
Ga 66
Ga67
E*-Bn1-Bn2
E*-Bn1
E*-Bα
E*-Bn1-Bp2
E*-Bp1
E
J
σJ
0 10 20 30 40 50
0 10 20 30 40 50 60
0 20 40 60 80 100 120

FIGURE 22

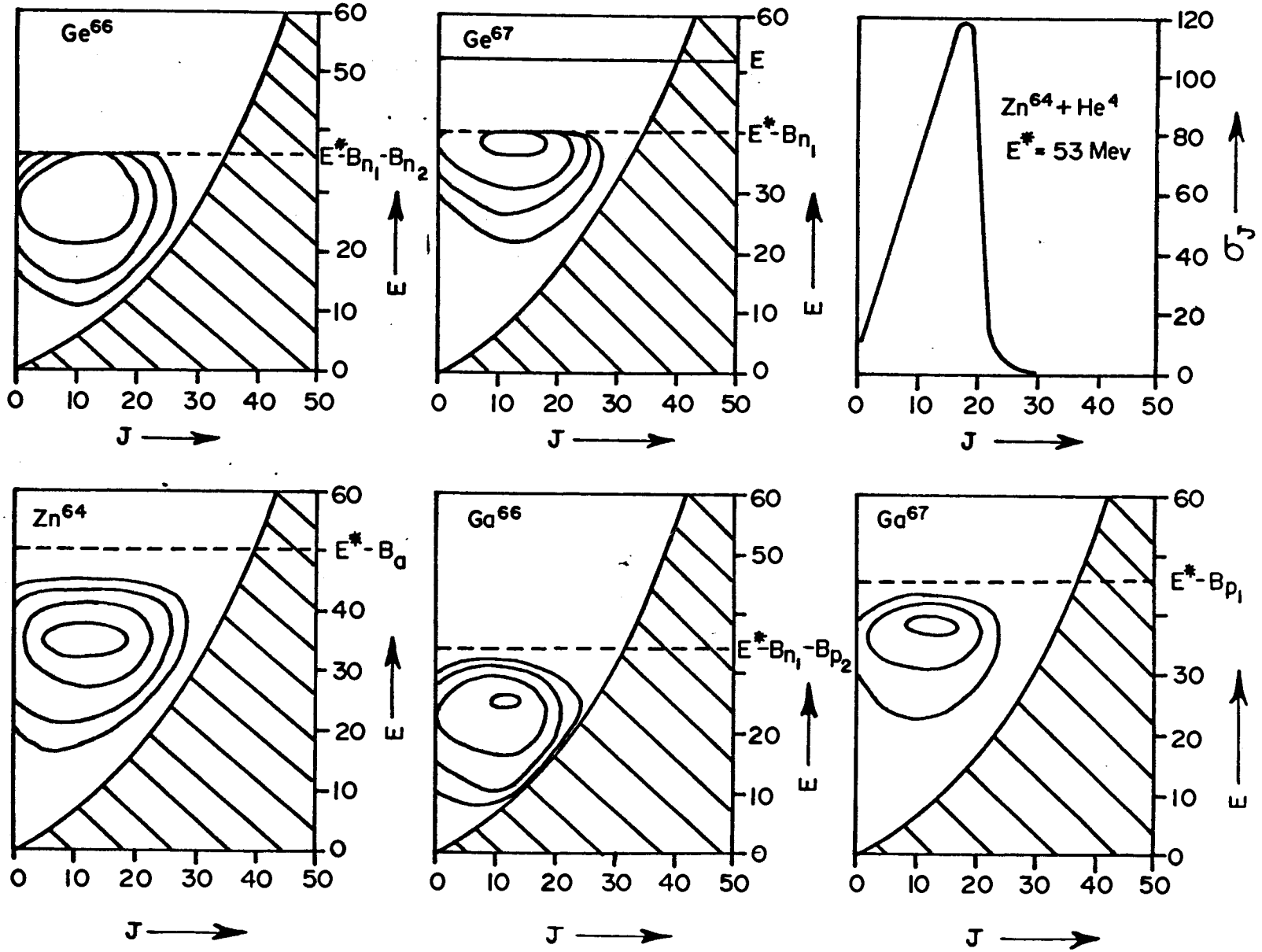
Ge66
E*-Bn1-Bn2
Ge67
E
E*-Bn1
Zn64 + He4
E* = 53 Mev
σJ
Zn64
E*-Ba
Ga66
E*-Bn1-Bp2
Ga67
E*-Bp1
E
J
0 10 20 30 40 50
0 10 20 30 40 50 60
0 20 40 60 80 100 120

FIGURE 23

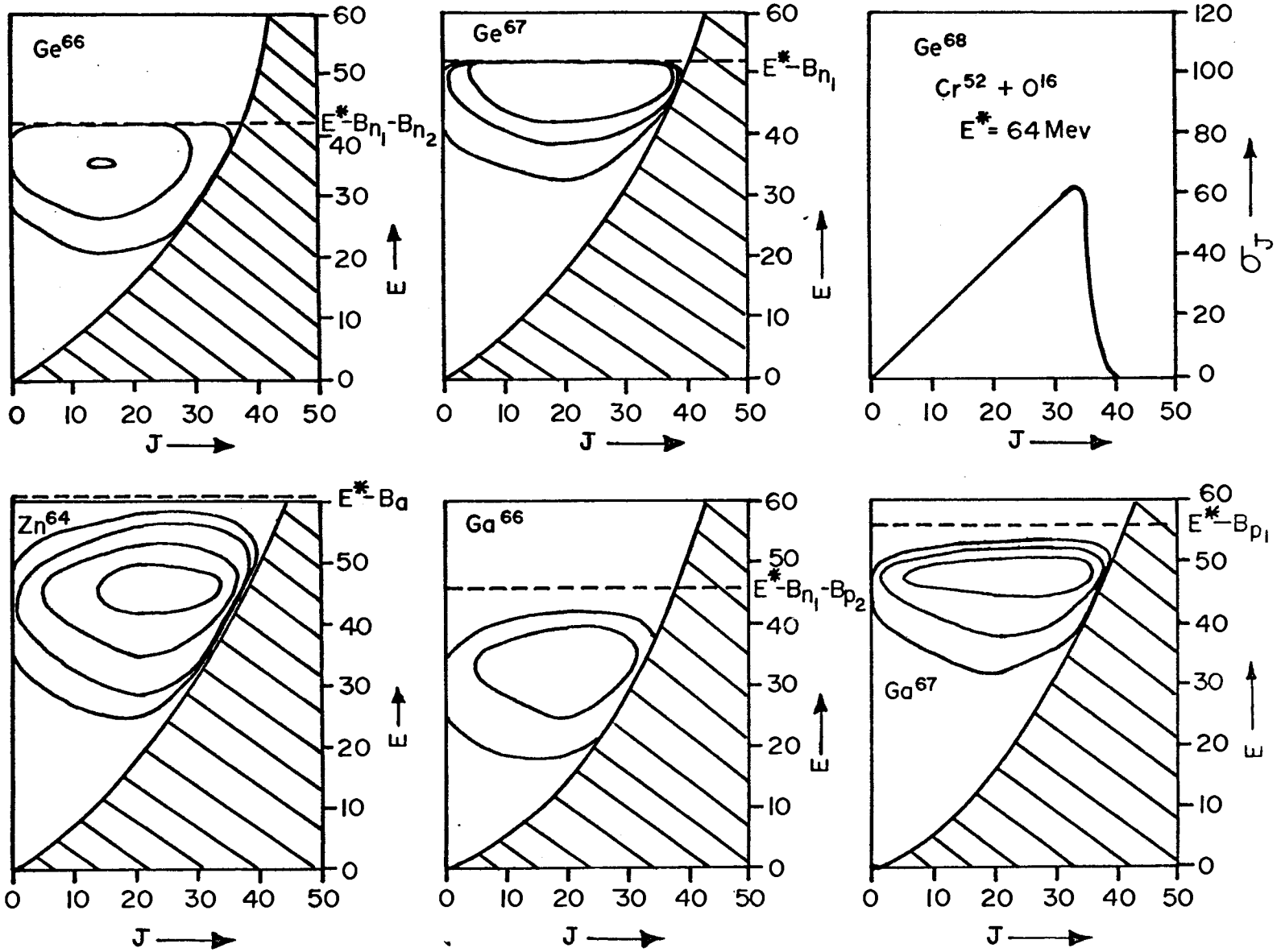
Ge66
E*-Bn1-Bn2
Ge67
E*-Bn1
Ge68
Cr52 + O16
E* = 64 Mev
Zn64
E*-Ba
Ga66
E*-Bn1-Bp2
Ga67
E*-Bp1
E
J
σJ
0 10 20 30 40 50
0 10 20 30 40 50 60
0 20 40 60 80 100 120

FIGURE 24

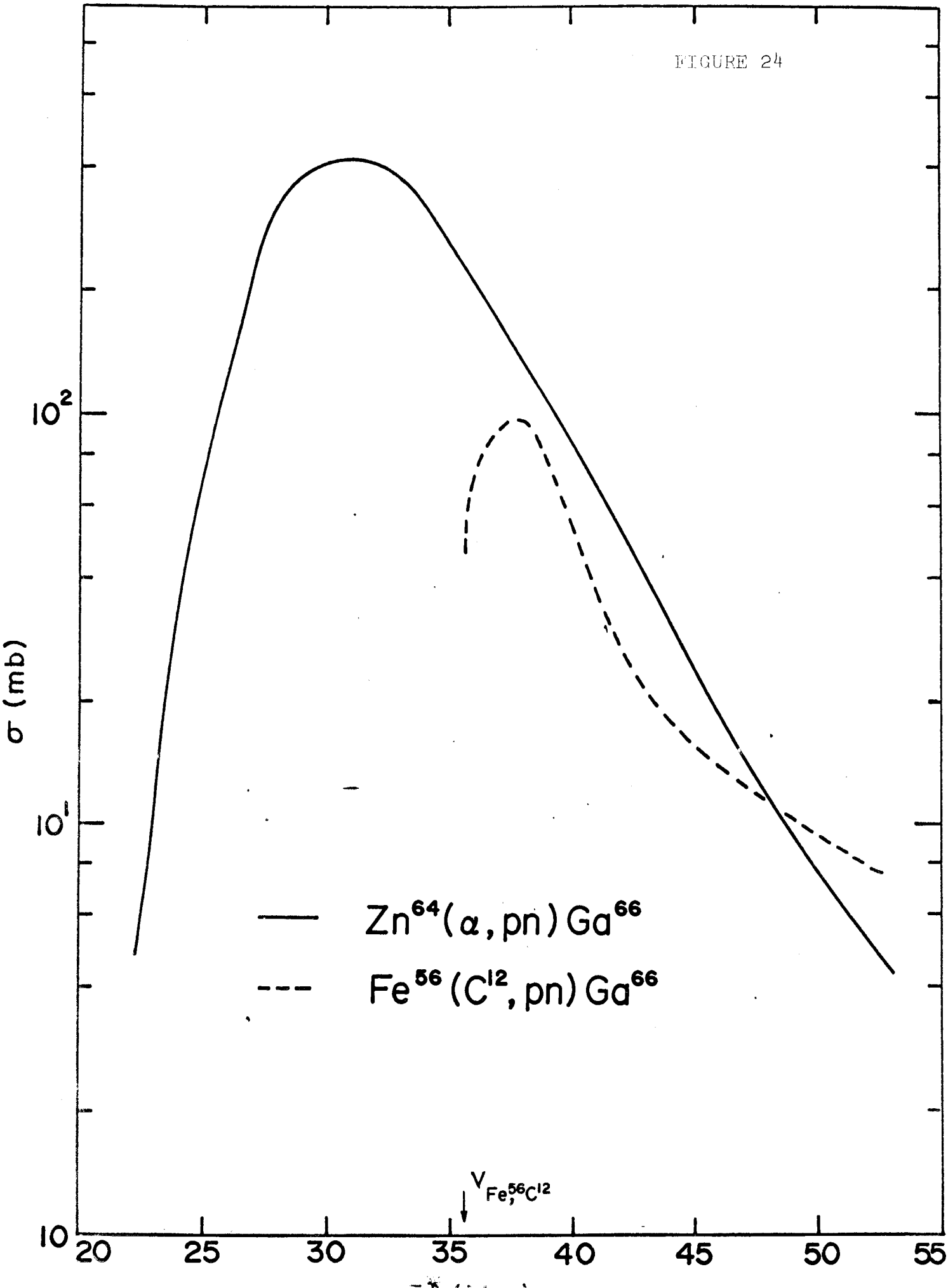
σ (mb)
10²
10¹
10
20
25
30
35
40
45
50
55
V Fe;56C12
Zn64(α, pn) Ga66
Fe56 (C12, pn) Ga66

FIGURE 25

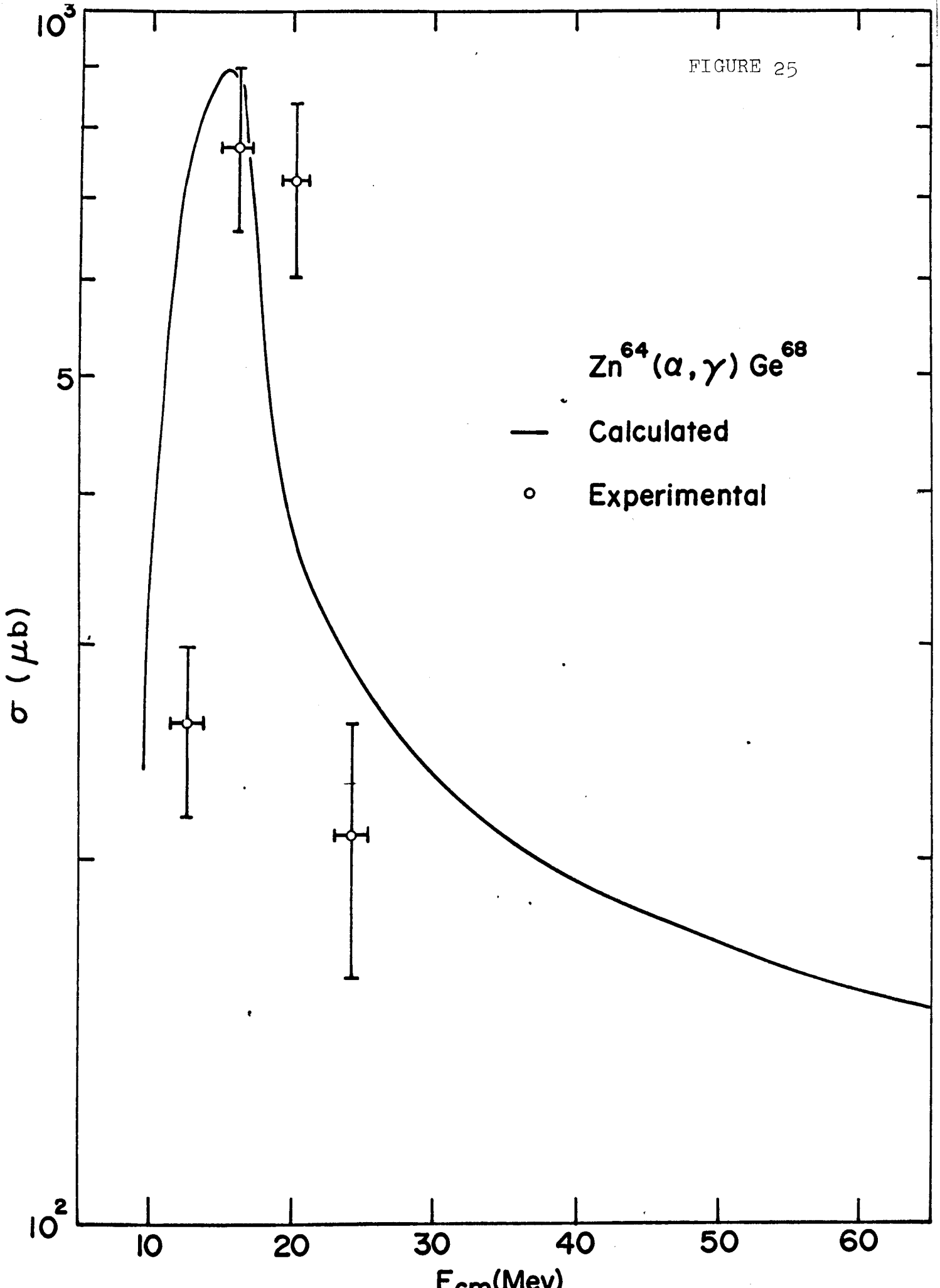
10^3
5
10^2
σ (μb)
10
20
30
40
50
60
E_{cm}(Mev)
$Zn^{64}(\alpha,\gamma)\ Ge^{68}$
Calculated
Experimental

FIGURE 26

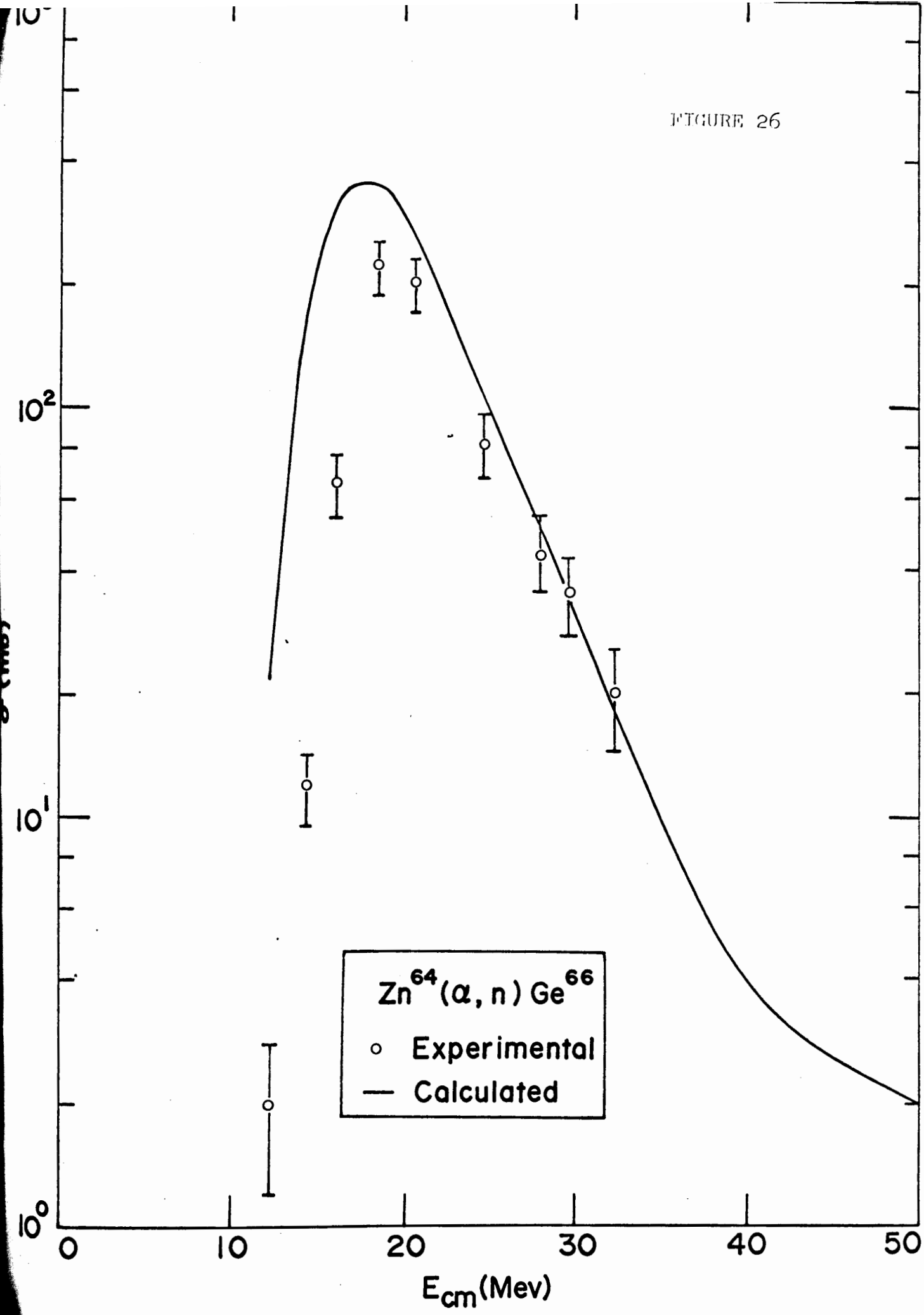
10^2
10^1
10^0
0
10
20
30
40
50
E_{cm}(Mev)
$Zn^{64}(\alpha, n)\,Ge^{66}$
Experimental
Calculated

FIGURE 2

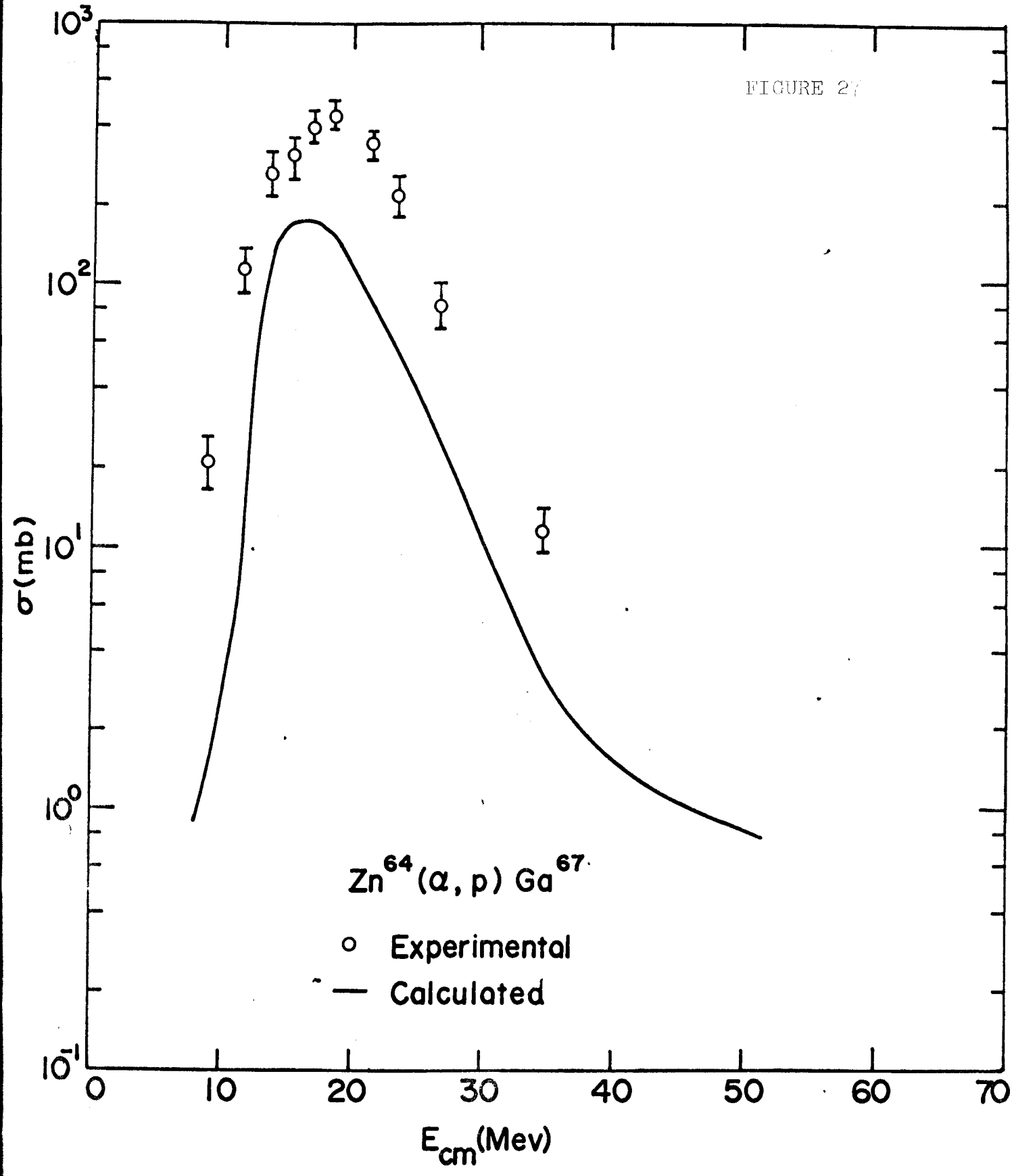
10^3
10^2
10^1
10^0
10^{-1}
σ(mb)
0
10
20
30
40
50
60
70
E_{cm}(Mev)
$Zn^{64}(\alpha, p)\ Ga^{67}$
Experimental
Calculated

FIGURE 28

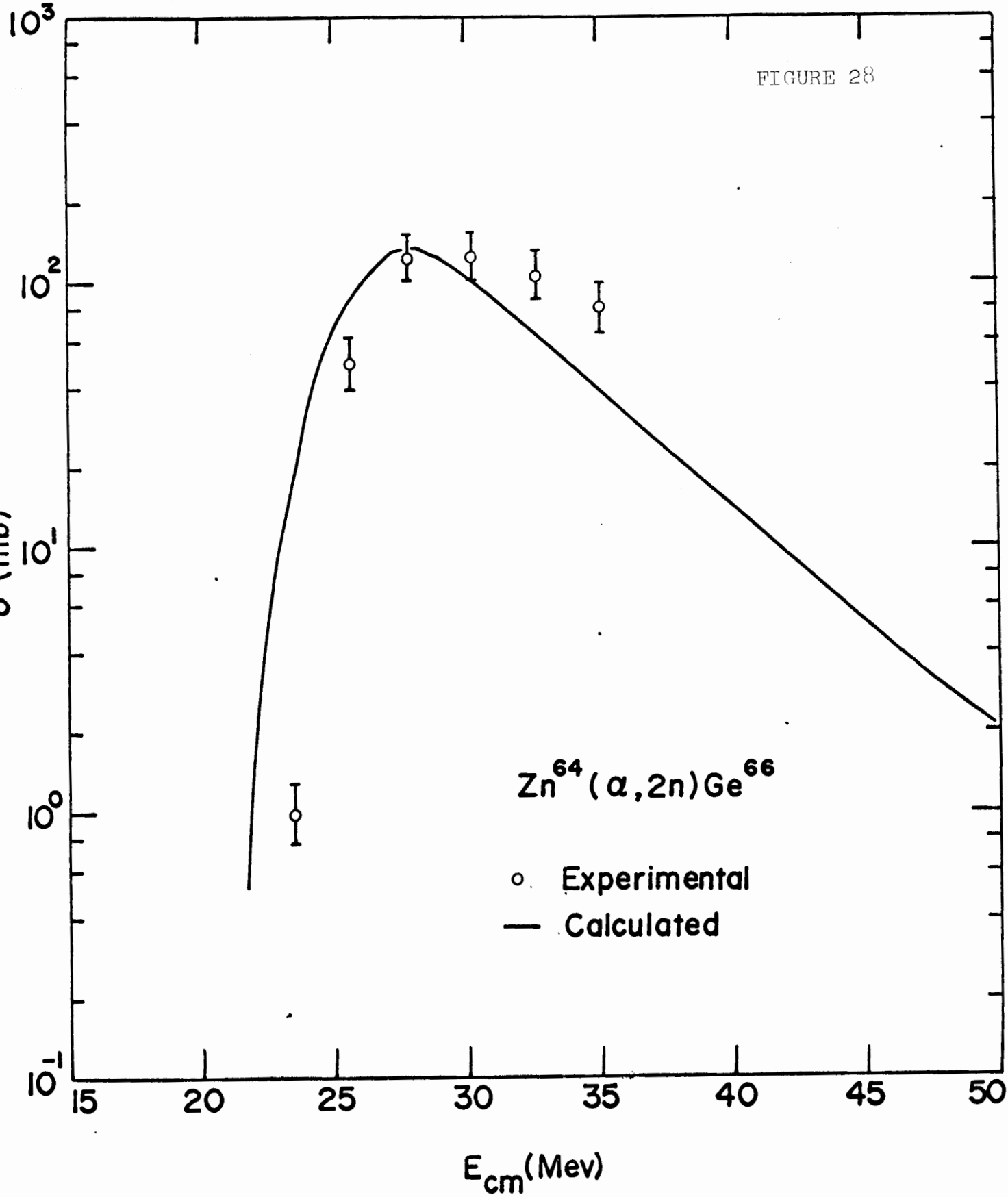
10^3
10^2
10^1
10^0
10^{-1}
σ (mb)
15
20
25
30
35
40
45
50
E_{cm}(Mev)
$Zn^{64}(\alpha,2n)Ge^{66}$
Experimental
Calculated

FIGURE 29

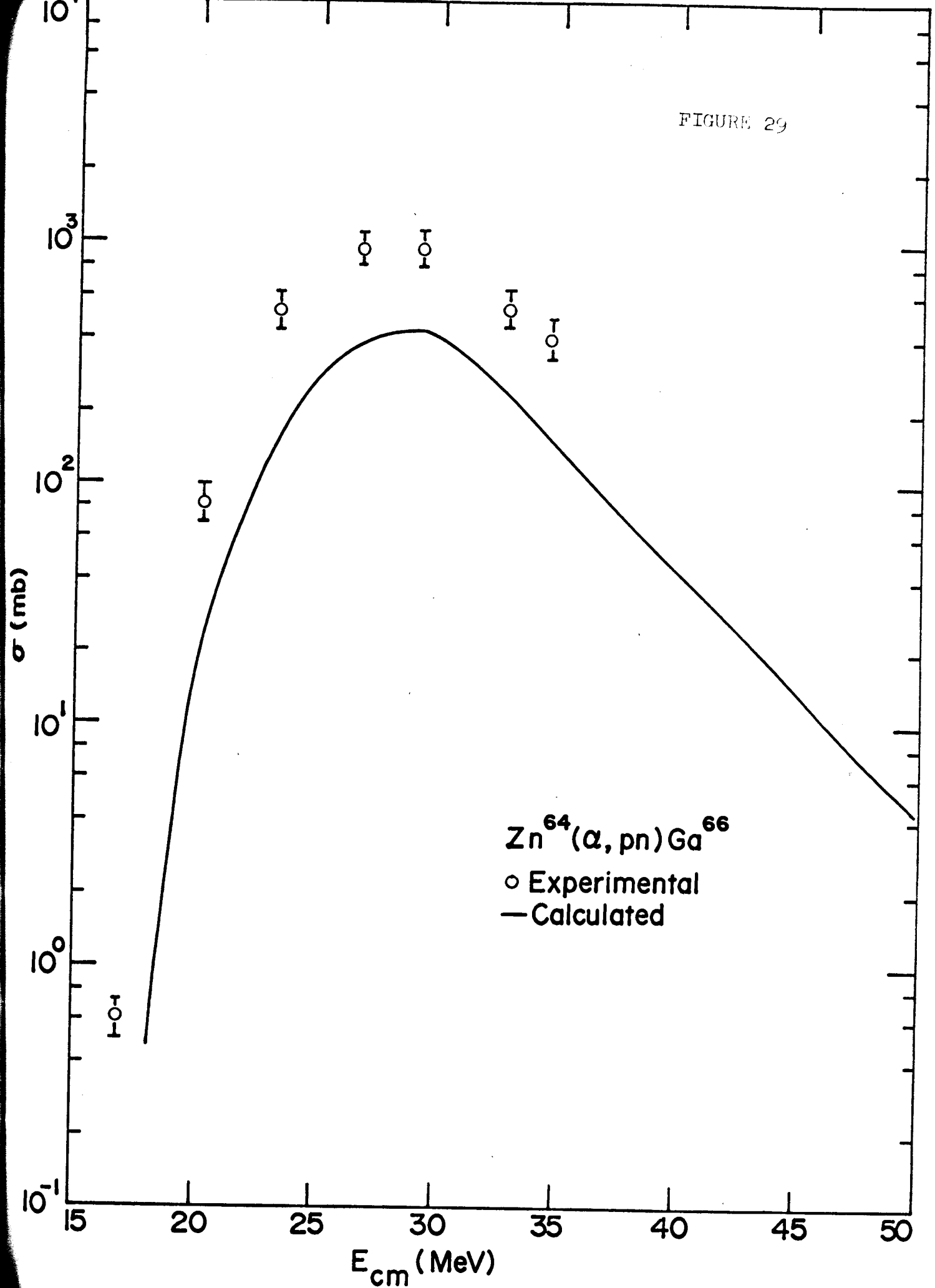
10^3
10^2
10^1
10^0
10^{-1}
σ (mb)
15
20
25
30
35
40
45
50
E_{cm} (MeV)
$Zn^{64}(\alpha, pn)Ga^{66}$
o Experimental
— Calculated

FIGURE 30

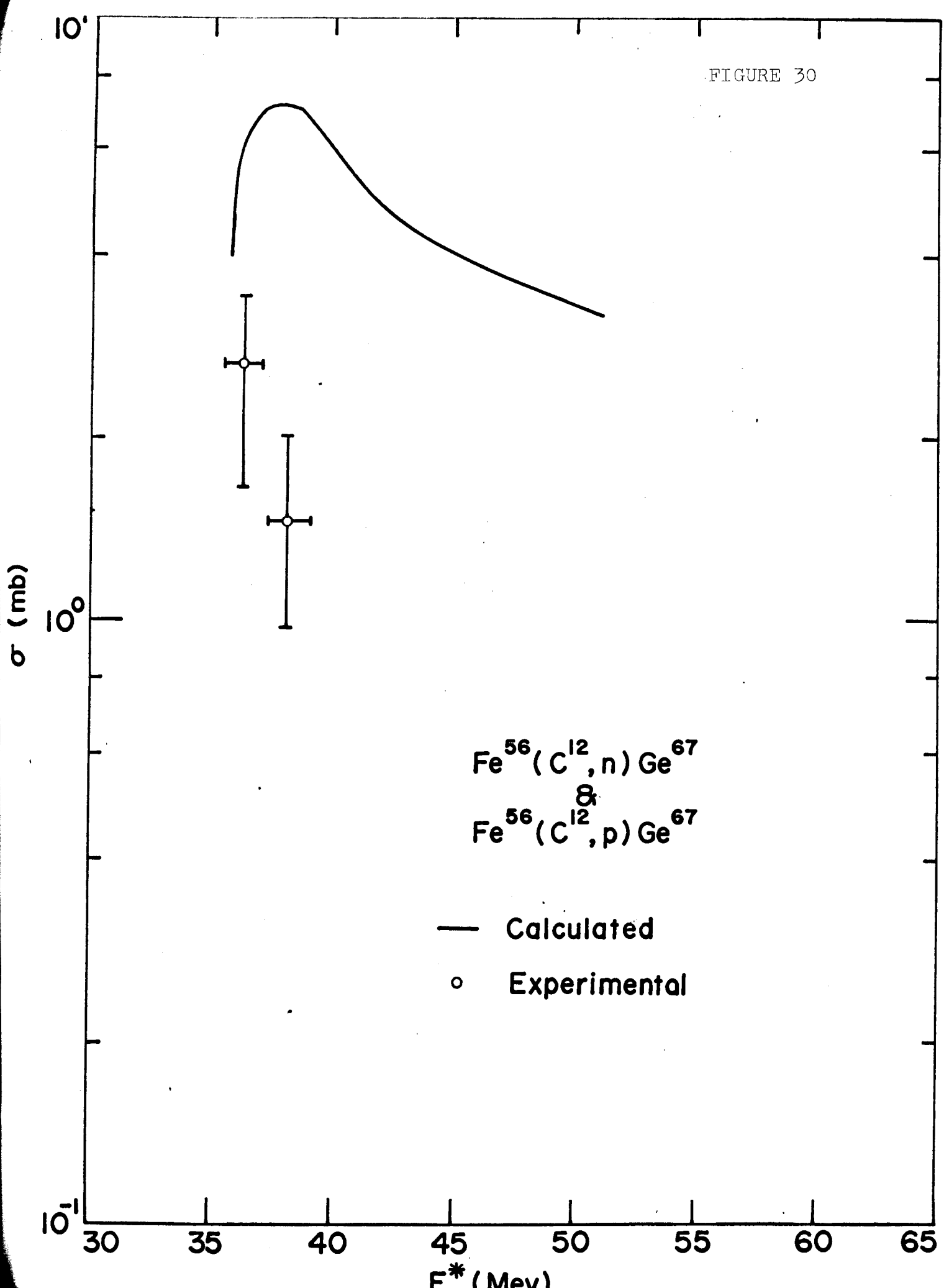
10'
10⁰
10⁻¹
σ (mb)
30
35
40
45
50
55
60
65
E* (Mev)
Fe⁵⁶(C¹², n) Ge⁶⁷
&
Fe⁵⁶(C¹², p) Ge⁶⁷
Calculated
Experimental

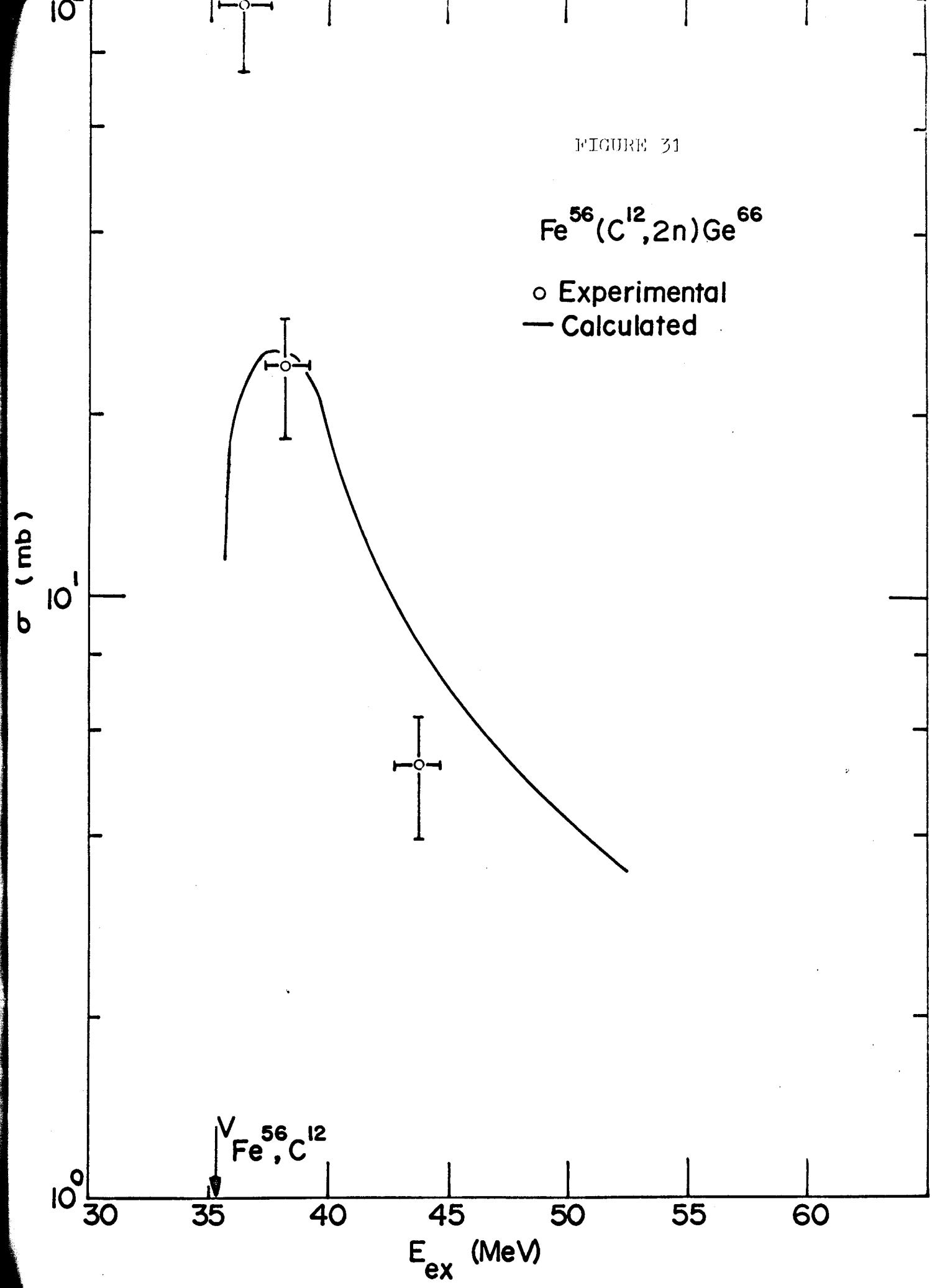
FIGURE 31
$Fe^{56}(C^{12},2n)Ge^{66}$
o Experimental
— Calculated
σ (mb)
10^1
10^0
$V_{Fe^{56},C^{12}}$
30
35
40
45
50
55
60
E_{ex} (MeV)

FIGURE 32

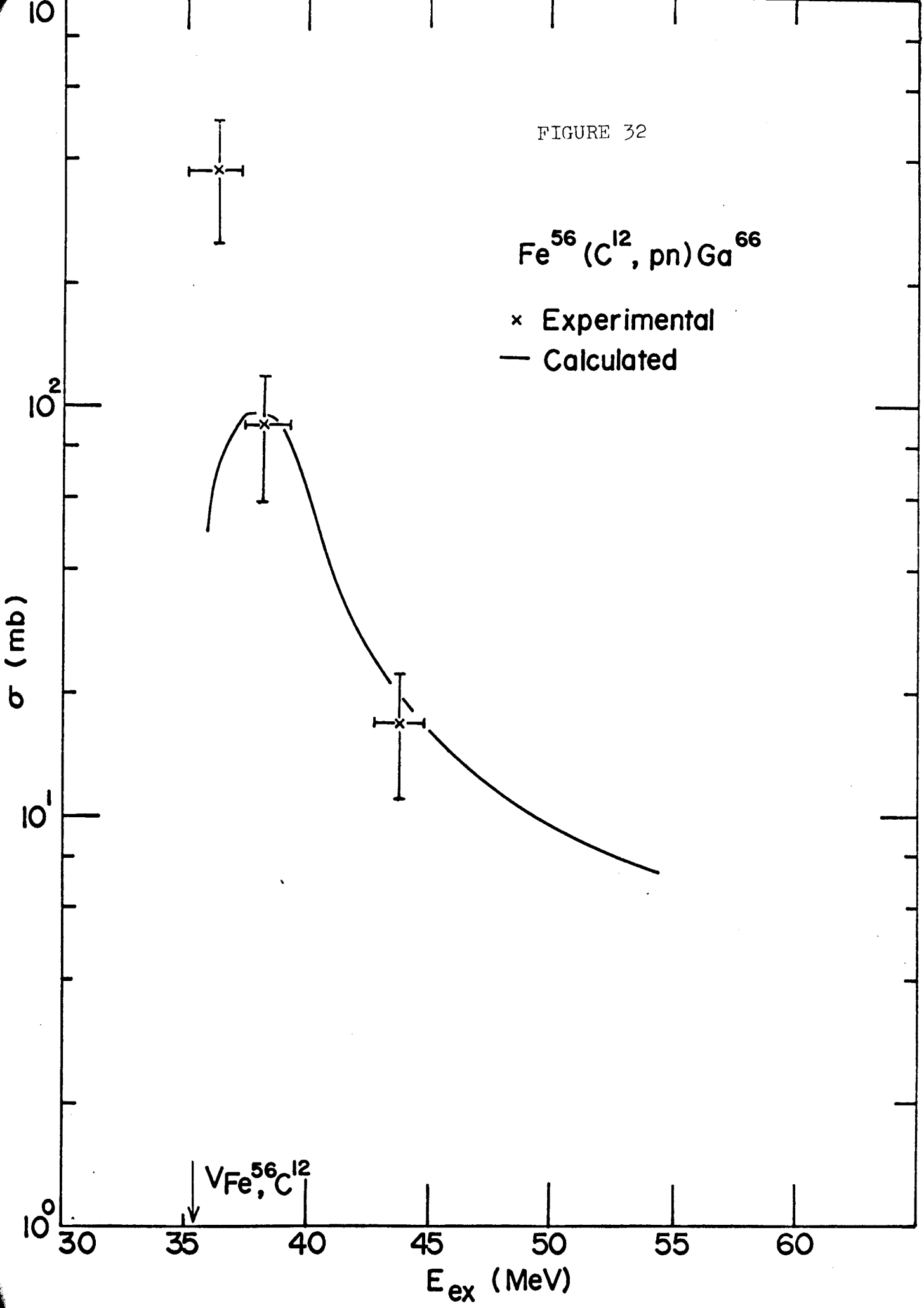
$Fe^{56}(C^{12}, pn)Ga^{66}$
× Experimental
— Calculated
10^2
10^1
10^0
σ (mb)
$V_{Fe,C}^{56,12}$
30
35
40
45
50
55
60
E_{ex} (MeV)

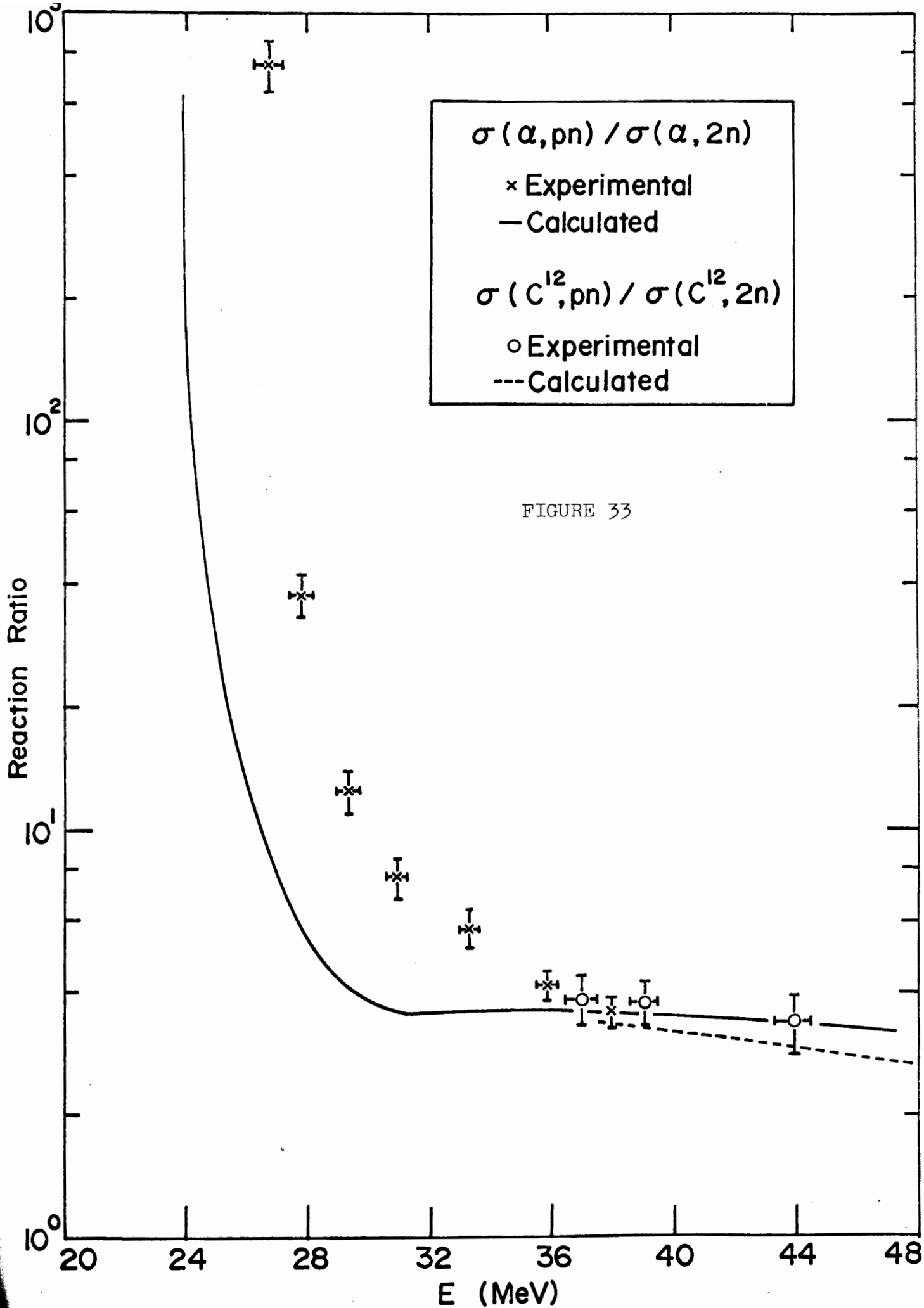
σ (α, pn) / σ (α, 2n)
× Experimental
— Calculated
σ (C12, pn) / σ (C12, 2n)
○ Experimental
--- Calculated
Reaction Ratio
10³
10²
10¹
10⁰
20
24
28
32
36
40
44
48
E (MeV)

FIGURE 33

REFERENCES

1. References to early neutron reaction studies may be found in the work cited in footnote 5.
2. H.A. Bethe, Phys. Rev. 47, 747 (1935)
3. N. Bohr, Nature 137, 344 (1936)
   N. Bohr & F. Kalckar, Mat. Fys. Medd. Dan. Vid. Selsk. 14, 10 (1937)
   N. Bohr, Science 86,2225, 161 (1937)
4. G. Breit and E. Wigner, Phys. Rev. 49, 519 (1936)
5. E. Vogt, "The Statistical Theory of Nuclear Reactions" (to be published)
6. J.M. Blatt & V.F. Weisskopf, Theoretical Nuclear Physics, (J. Wiley and Sons, New York, 1958) 313.
7. S. De Benedetti, Nuclear Interactions, (J. Wiley & Sons, New York, 1964) 329.
8. J.R. Oppenheimer & M. Phillips, Phys. Rev. 48, 500 (1935)
9. G. Friedlander, J.W. Kennedy, and J.M. Miller, Nuclear and Radiochemistry (J. Wiley & Sons, New York, 1964) 310
10. H.A. Bethe, Rev. Mod. Phys. 9, 69 (1937)
11. V.F. Weisskopf, Phys. Rev. 52, 295 (1937)
12. V.F. Weisskopf and D.H. Ewing, Phys. Rev. 57, 472 (1940)
13. I. Frenkel, Sov. Phys. 9, 533 (1936)
14. E. Segre, Nuclei and Particles (W.A. Benjamin, Inc., Amsterdam, 1964)

15. P.M. Morse, Thermal Physics, (rev. ed., W.A. Benjamin, New York, 1964)

16. P.C. Gugelot, Phys. Rev. 93, 425 (1945)
Eisberg, Igo, and Wegner, Phys. Rev. 100, 1309, (1955)

17. K.J. Le Couteur, Nuclear Reactions (ed. P.M. Endt and M. Demeur, North Holland Publishing Co., Amsterdam, 1959) - Other early references may be found in the works cited in footnote 6.

18. H. Hurwitz & H.A. Bethe, Phys. Rev. 81, 898 (1951)

19. A.G.W. Cameron, Can. J. Phys. 36, 1040 (1958)

20. T.D. Newton, Can. J. Phys. 34, 804 (1956)

21. I. Dostrovsky, Z. Fraenkel, and G. Friedlander, Phys. Rev. 116, 683 (1959)

22. E.g. preceding footnote and Dostrovsky, Rabinowitz, and Burns, Phys. Rev. 111, 1659 (1958)

23. E.H. Auerbach, ABACUS - 2, BNL, unpublished.

24. M.A. Melkanoff, D.S. Saxon, J.S. Nodvik, and D.G. Cantor, A Fortran Program for Elastic Scattering Analysis With the Nuclear Optical Model, (U. of California, Berkeley, 1961)

25. G.S. Mari, I. Iori, & M.A. Melkanoff, Neutron Penetrabilities Using an Optical Model Potential, Rapport C.E.A. No. 2380 (1963), Centre D'Etudes Nucleaires de Saclay and Proton Penetrabilities Using an Optical Model Potential, Rapport C.E.A. No. 2379 (1963)

26. R. Serber, Phys. Rev. 72, 1008 (1947)

27. S. Fernbach, R. Serber, and T.B. Taylor, Phys. Rev. 75, 1352 (1949)

28. H. Feshbach, C. Porter, and V.F. Weisskopf, Phys. Rev. 96, 448 (1954)

29. M.A. Preston, Physics of the Nucleus, (Addison - Welsey, Reading, Massachusetts, 1963)

30. R.D. Woods and D.S. Saxon, Phys. Rev. 95, 577 (1954)

31. D.G. Sarantits and B.D. Pate, Nuclear Physics A93, 545 (1967)

32. I. Kanestrøme, Nuclear Physics 83, 380 (1966)

33. D.W. Lang, Nuclear Physics 77, 545 (1966)

34. J.M. Lang, and K.J. Couteur, Proc. Phys. Soc. 67A, 586 (1954)

35. D. Bodansky, Ann. Rev. Nucl. Sci. 12, 79 (1962)

36. D.W. Lang, "High Angular Momentum Cutoff in Nuclear Level Densities", Proceedings of the Third Conference on Reactions Between Complex Nuclei, ed. by A. Ghiorso, R.M. Diamond, and H.E. Conzett, U. of Cal. Press, Berkeley, D-9, 248 (1963)

37. J. Bardeen, L.N. Cooper, and J.R. Schrieffer, Phys. Rev. 108, 1175 (1957)

38. N.N. Bogolyubov, J.E.T.P., U.S.S.R., 34, 58 & 73 (1958); Nuevo Cimento 7, 794 (1958)

39. A. Bohr, B.R. Mottelson, & D. Pines, Phys. Rev. 110, 936 (1958)

40. S.T. Belyaev, Mat. Fys. Medd. Dan. Vid. Selsk. 31, 11 (1959)

41. A. B. Migdal, Nuclear Physics 13, 655 (1959)

42. D.W. Lang, Nuclear Physics 42, 353 (1963)

43. H.K. Vonach, R. Vandenbosch, & J.R. Huizenga, Nuclear Physics 60, 70 (1964)

44. A. Bohr, and B. Mottelson, Dan. Mat. Fys. Medd. 30, 1 (1955)

45. W. Heisenberg, Z Physik 77, 1 (1932)

46. W.E. Burcham, "Isotopic Spin and Nuclear Relations", Progress in Nuclear Physics, Vol. 4 Ed. O.R. Frisch, 171 (1961)

47. D. Robson "Isobaric Spin in Nuclear Physics", Annual Review of Nuclear Science, Vol. 16 Ed. E, Segre', G. Friedlander, H.P. Noyes, 119 (1966)

48. C.J. Stevens, A.J. Gorski, & J.R. Huizenga, Bull. Am. Phys. Soc. BH4, 491 (1967)

49. J.M. D'Auria and J.M. Miller, Nuclear Physics (to be published)

50. N.T. Porile, Phys. Rev. 115, 939 (1959)

51. P.H. Stelson and F.K. M^{c}Gowan, Phys. Rev. 133, B911 (1964)

52. M. Cogneau and L. Gilly, Nuclear Physics 73, 122 (1965)

53. R.A. Esterlund and B.D. Pate, Nuclear Physics 69, 401 (1965)

54. L. Holland, Vacuum Deposition of Thin Films, Chapman & Hall, Ltd., London, 1961

55. J.F. O'Hanlon and R.R. Haering, personal communication.

56. Natural Abundances are from the Chart of the Nuclides, prepared by David T. Goldman, Knolls Atomic Power Laboratory, Schenectady, N.Y., 9th ed. (1966)

57. Enriched isotopes were obtained from Oak Ridge National Laboratory, Oak Ridge, Tennessee, who performed the isotopic analysis.

58. Obtained from A.D. MacKay, Inc., 198 Broadway, New York, N.Y. 10038.

59. M. Blann, F. M. Lanzafame, and R. A. Piscitelli, Phys. Rev. 133, B700(1964).

60. J. B. Cumming, personal communication (1967).

61. F. S. Houck and J. M. Miller, Phys. Rev. 123, 231 (1961).

62. J. H. Atkinson, Jr., and B. H. Willis, High Energy Particle Data, UCRL2426 Rev., vol. 2, 35-36 (June, 1957).

63. P. L. Reeder, personal communication (1966).

64. S. Amiel and N. T. Porile, Rev. Sci. Instr. 29, 1112 (1958).

65. J. B. J. Read, I.-M. Ladenbauer-Bellis, and R. Wolfgang, Phys. Rev. 127, 1722 (1962).

66. I. C. Northcliffe, Phys. Rev. 120, 1744 (1960).

67. I. C. Northcliffe, Ann. Rev. Nucl. Sci. 13, 67 (1963).

68. J. A. Marinsky, The Radiochemistry of Germanium, NAS-NS 3043, (July, 1961).

69. J. E. Lewis, The Radiochemistry of Aluminum and Gallium, NAS-NS 3032, (April, 1961).

70. R. L. Heath, Atomic Energy Commission Research and Development Report IDO-16408 (1957).

71. A. H. Sher, Ph. D. Thesis, Simon Fraser University (unpublished), (november, 1967).

72. M. K. Ramaswamy, Nuclear Physics 10, 205 (1959).

73. D. C. Camp and L. M. Langer, Phys. Rev. 129, 1782 (1963).

74. C. M. Lederer, J. M. Hollander, and I. Perlman, Table of Isotopes, 6th edition, Wiley and Sons, New York (1967).

75. J. B. Cumming, National Academy of Sciences - National Research Council, Washington 25, D. C., Nuclear Sciences Series NAS-NS 3107,25 (1962).

76. J.-P. Hazan and M. Blann, Phys. Rev. 137, B1202 (1965).

77. M. Blann and A. Ewart, Phys. Rev. 134, B783 (1964).

78. J. Lindhard, M. Scharff, and H. E. Schiøtt, Mat. Fys. Medd. Dan. Vid. Selsk. 33, no. 14 (1963).

79. J. H. E. Mattauch, W. Thiele, and A. H. Wapstra, Nuclear Physics 67, 1 (1965).

80. G. Breit, M. H. Hull, and R. L. Gluckstern, Phys. Rev. 74, 1828 (1952).

81. J. H. E. Mattauch, W. Thiele, and A. H. Wapstra, Nuclear Physics 67, 32 (1965).

82. E. Hayward, Rev. Mod. Phys. 35, 324 (1963).

83. R. V. Carlson and P. J. Daly, Nuclear Physics A102, 177 (1967).

84. C. F. Clement, A. M. Lane, and J. R. Rook, Nuclear Physics 66, 273 (1965).

85. A. M. Lane and J. E. Lynn, Nuclear Physics 11, 625,646 (1959).

86. F. S. Stephens, N. L. Lark, and R. M. Diamond, Nuclear Physics 63, 82 (1965).

87. E. V. Verdieck and J. M. Miller, to be published.

88. E. Vogt, personal communication (1968).

89. J. M. Miller, personal communication (1968).

90. T. W. Donnelly, Ph. D. Thesis, University of British Columbia (unpublished), (1967).

91. S. N. Ghoshal, Phys. Rev. 80, 939 (1959).

92. I. Preiss, personal communication, (1966).

93. D. Strominger, J. M. Hollander, and G. T. Seaborg, Revs. Mod. Phys. 30, 585 (;958).

94. D. W. Lang, Nuclear Physics 26, 434 (1961).

95. T. Ericson, Advan. Phys. 9, 425 (1960).

96. D. Sperber, Phys. Rev. 142, 478 (1966).

97. J. R. Huizenga and A. A. Katsanos, Nuclear Physics A98, 614 (1967).

98. J. H. Towle and R. O. Owens, Nuclear Physics A100, 257 (1967).

99. P. E. Hodgson, The Optical Model of Elastic Scattering, Clarendon Press, Oxford (1963).

100. E. Vogt, personal communication (1967).

101. T. W. Donnelly, personal communication (1967).

102. S. A. Moskowski in Alpha-, Beta-, and Gamma-Ray Spectroscopy, ed. K. Siegbahn, North-Holland Publishing Co., Amsterdam, vol. 2, 863 (1965).

103. J. R. Grover and J. Gilat, Phys. Rev. 157, 802 (1967).

104. J. R. Grover and J. Gilat, Phys. Rev. 157, 814 (1967).

105. J. R. Grover and J. Gilat, Phys. Rev. 157, 823 (1967).

106. N. V. Baggett, et al., Photonuclear Data Index, National Bureau of Standards Miscellaneous Publication, 277 (1966).

107. Photonuclear Reactions, Biographical Series No. 10, International Atomic Energy Agency, Vienna (1964).

108. J. Lindskog, T. Sundström, and P. Sparrman in Alpha-, Beta-, and Gamma-Ray Spectroscopy, ed. K. Siegbahn, North-Holland Publishing Co., Amsterdam, vol. 2, 1599 (1965).

109. M. Blann, Phys. Rev. 157, 860 (1967).

110. P. A. Seeger, Nuclear Physics 25, 1 (1961).

111. J. M. Alexander, "Studies of Nuclear Reactions by Recoil Techniques" in Nuclear Chemistry, ed. L. Yaffe, Academic Press, Inc., New York, Chapter IV (to be published).

112. J. M. Alexander and L. Winsberg, Phys. Rev. 121, 518 (1961).

113. J. M. Alexander and L. Winsberg, Phys. Rev. 121, 529 (1961).

114. J. M. Alexander and D. H. Sisson, Phys. Rev. 128, 2288 (1962).

115. N. Bohr, Kgl.Danske Videnskab Selskab Mat. Fys. Medd. 18, no. 8 (1948).

116. G. R. Piercy, M. McCargo, I. Brown, and J. A. Davies, Can. J. Phys. 42, 1116 (1964).

117. N. T. Porile, Phys. Rev. 135, A1115 (1964).

118. G. B. Saha and N. T. Porile, Phys. Rev. 149, 880 and 151, 907 (1966).

119. L. Bryde, N. O. Lassen, and R. Poulsen, Kgl. Danske Videnskab Selskab Mat. Fys. Medd. 33, no. 8 (;962).

120. T. Matsuo, J. M. Matuszek, Jr., N. D. Dudey, and T. T. Sugihara, Phys. Rev. 139, B886 (1965).

121. P. D. Croft and K. Street, Jr., Phys. Rev. 165, 1375 (1968).

122. L. Kowalski, J. C. Jodogne, and J. M. Miller, (to be published).

123. S. Cohen, F. Plasil, and W. J. Swiatecki, " Equilibrium Shapes of a Rotating Charged Drop and Consequences For Heavy Ion Nuclear Reactions ", Proceedings of the Third Conference on Reactions Between Complex Nuclei, ed. A. Ghiorso, R. M. Diamond, and H. E. Conzett, U. of California Press, Berkeley, D-9, 248 (1963).

Appendix I

Recoil Range Theories.

1. Recoil Range measurements.

Recoil ranges may be studied in a variety of ways,[111] the simplest of which is to measure projected ranges along the beam direction. For a given reaction at a specified energy, the observed ranges of nuclei recoiling from the target into some stopping medium will center about an average value R_o. Deviations from this average value, called range straggling, arise from a number of sources:[111-114]

(1.) Straggling from effects of the nuclear reaction, ie., resultant velocities of individual recoiling atoms will differ because of non-unique allignment of the velocity vectors of the emitted particles. (ρ_n)

(2.) Straggling inherent in the stopping process. (ρ_s)

(3.) Straggling caused by finite target thickness, ie., the individual recoiling nuclei originate from different depths in the target and escape with different degrees of the full range. (ρ_w)

(4.) Straggling caused by inhomogeneities in the stopping medium. (ρ_f)

The overall range straggling parameter is the resultant of parameters corresponding to the above combined in quadrature

$$\rho^2 = \rho_n^2+\rho_s^2+\rho_w^2+\rho_f^2$$

and the range straggling is given by $R_o\rho$. If the distribution

in range values is Gaussian, then[112].

$$P(R)dR = \frac{1}{R_o\rho\sqrt{2\pi}} \exp\left[-\left(\frac{R-R_o}{\sqrt{2R_o\rho}}\right)^2\right]dR \qquad (I\text{-}1)$$

Assuming uniform production of recoils across a layer of target atoms of thickness W, the fraction of recoils which remain in the target is[111,112].

$$F_W = \frac{1}{(2\pi)^{\frac{1}{2}}R_oW}\int_o^W\int_o^W \exp\left(-\left(\frac{r-s-R_o}{\sqrt{2R_o\rho}}\right)^2\right)drds \qquad (I\text{-}2)$$

where s is the distance from the edge of the layer to the point at which the recoiling atom originates and r-s is the distance that it travels. The integration of the above equation leads to the following[111,112].

$$F_W = \frac{\sqrt{2R_o\rho}}{W}\left[\mathfrak{F}\left(\frac{R_o-W}{\sqrt{2R_o\rho}}\right)-2\mathfrak{F}\left(\frac{R_o}{\sqrt{2R_o\rho}}\right)+\mathfrak{F}\left(\frac{R_o+iW}{\sqrt{2R_o\rho}}\right)\right] \qquad (I\text{-}3)$$

where

$$\mathfrak{F}(y) = \frac{1}{2\sqrt{\pi}}\exp(-y^2)-\tfrac{1}{2}[1-I(y)]y$$

and

$$I(y) = \frac{2}{\sqrt{\pi}}\int_o^y \exp(-u^2)du$$

F_W may be approximated by the first term for $W \gtrsim R_o$

$$F_W \cong \frac{\sqrt{2R_o\rho}}{W}\,\mathfrak{F}\left(\frac{R_o-W}{\sqrt{2R_o\rho}}\right) \qquad (I\text{-}4)$$

and if the thickness is many times the average range, (D-4) reduces to

$$R_o = W(1-F_W) \qquad (I\text{-}5)$$

If one bombards a thick target backed by a thick catcher foil, F_W is calculable from the activities observed in the target and catcher foils,

$$1-F_W = \frac{A_C}{A_T + A_C} \qquad \text{(I-6)}$$

and the calculation of R_o follows.

In practice, recoiling atoms will not be produced uniformly across the target thickness. If one assumes a linear variation of cross-section over the energy range corresponding to the target thickness, ie.,

$$\sigma_s = \frac{(\sigma_W-\sigma_o)s}{W}+\sigma_o \qquad \text{(I-7)}$$

where σ_o is the cross-section at the target-catcher interface (s=o) and σ_W is the cross-section at the opposite surface (s=w), and all recoiling ions are assumed to be formed within their range, R_o, from the surface, then[76].

$$1-F_W = \frac{A_C}{A_T+A_C} = \frac{\int_o^{R_o}\sigma_s ds}{\int_o^{W}\sigma_s ds} = \frac{R}{W^2}\cdot\frac{2\sigma_o W+(\sigma_W-\sigma_o)R_o}{\sigma_o+\sigma_W}$$

For small differences between σ_o and σ_W ($|\sigma_W-\sigma_o|<\sigma_o$), and $R<<W$.[76]

$$R_o = (1-F_W)W\frac{(\sigma_o+\sigma_W)/2}{\sigma_o} \qquad \text{(I-8)}$$

that is, the range must be corrected by a factor corresponding to the ratio of the average cross-section in the foil to the cross-section at the target-catcher interface.

Such thick target, thick catcher, or integral, range experiments provide a simple means for determining ranges if the variation of cross-section is small across available target thicknesses and the distribution in ranges is known to be Gaussian. If these conditions are not met, however, a differential method may be appropriate.

A convenient differential method for measuring average projected ranges in the beam direction is to bombard thin targets ($W \ll R_o$) backed by several thin catchers. If F_t, the fraction of activity that passes through thickness t, is plotted on a probability scale vs. t, the t value corresponding to $F_t = \frac{1}{2}$ defines R_o. The t value for F_t equals 0.0787 specifies $R_o(1+\sqrt{2}\rho)$[112]. Also, any deviation from Gaussian distribution about the average projected range may be observed directly in this type of experiment. However, one must be studying a product which is produced in high yield and the average range must be relatively large (>200mg/cm^2) in order for this type of differential measurement to be experimentally feasible.

2. The Stopping Process.

In order for interpretation of the results of recoil range measurements to be possible, the nature of the interactions of recoiling atoms with matter must be known. According to the formulation due to Bohr,[115] the stopping process is dependent on the velocity (v) of the moving atom.

If v is greater than the orbital velocities of the electrons of the stopping atoms, stopping is mainly by interaction with these electrons. If v is less than the orbital electron velocity, stopping is by interaction with the atoms as a whole (e.g. with the crystal lattice of the stopping medium.) In the latter case, Bohr derived the following formula[115.] for R_o expressed in mg/cm^2 and E in MeV.

$$R_o = 0.600 \frac{A_s(A_s+A_R)}{A_R} \cdot \frac{(Z_R^{\frac{2}{3}}+Z_s^{\frac{2}{3}})^{\frac{1}{2}}}{Z_s Z_R} E$$

which holds when the recoiling particle masses are much larger than the stopping atomic masses ($A_R >> A_s$).

In general, the stopping power may be represented (neglecting channeling effects) as the following[116.]

$$\frac{dE}{dX} = k[E^{\frac{1}{2}}+c_1]$$

The first term corresponds to electronic stopping and the second to elastic (atomic) stopping. Lindhard, Scharff, and Schiøtt[78.] (LSS) have derived a general stopping theory where atomic stopping was described by a Thomas-Fermi potential and the proportionality constant, k, for the electronic stopping term was given as[78.]

$$k = \xi_e \frac{0.0793 Z_R^{\frac{1}{2}} Z_s^{\frac{1}{2}} (A_R+A_s)^{\frac{3}{2}}}{(Z_R^{\frac{2}{3}}+Z_s^{\frac{2}{3}})^{\frac{3}{4}} A_R^{\frac{3}{2}} A_s^{\frac{1}{2}}} \qquad \text{(I-9)}$$

$$\xi_e = Z_R^{\frac{1}{6}}$$

The LSS theory makes use of dimensionless range and energy parameters, ρ and ϵ , given by

$$\rho = RNA_S 4\pi a^2 A_R (A_R+A_S)^{-2}$$
$$\epsilon = EaA_R[Z_R Z_S e^2 (A_R+A_S)]^{-1}$$
$$a = a_o\{0.8853(Z_R^{\frac{2}{3}}+Z_S^{\frac{2}{3}})^{-\frac{1}{2}}\}$$

Where N is the number of stopping atoms per unit volume, e is the electronic charge, and a_o is the first Bohr radius in the hydrogen atom. The LSS calculations produce a set of ρ-ϵ curves, each characterised by a value of k. The straggling, or mean square deviation from the mean, is given by plotting the quantity

$$\frac{(A_R+A_S)^2}{4A_R A_S} \quad \frac{\overline{\Delta R}^2}{\overline{R}^2}$$

vs. ϵ for different values of k. The range along the total path length of the recoiling atom is related to the projected range by the following correction factor given by LSS.

$$R = R_o \tfrac{1}{4}[-1-3\mu+(5+\mu)\cdot \frac{1+\mu}{2\mu^{\frac{1}{2}}} \arccos (\frac{1-\mu}{1+\mu})]$$

where $\mu = A_S/A_R$. LSS have given curves of $\frac{1}{\mu}\frac{R-R_o}{R_o}$ and $\frac{R}{R_o}-1$ vs. ϵ for several values of k.
At low energies

$$\frac{R}{R_o} \cong 1 + \frac{\mu}{3} \qquad \text{(I-11)}$$

although several inadequacies exist in the theories of LSS[111.], they have, in general, provided agreement within

experimental error with the type of integral and differential ranges measured by the previously described experiments.[76,77,117-121]

Appendix II

Coupling Schemes.

For the reaction X+b → Y+x, the target and projectile will have a mutual orbital angular momentum, $\vec{\imath}$, as will the products, $\vec{\imath}'$. X and Y will have spins $\vec{I}$ and $\vec{I}'$ and orbital angular momenta $\vec{L}$ and $\vec{L}'$, respectively, and b and x will have spins $\vec{s}$ and $\vec{s}'$, respectively. Angular momentum must be conserved; however, the method of addition of these vectors depends on the type of interaction assumed or "coupling" scheme used[29].

(a) j-j Coupling.

$$\vec{J} = \vec{I} + \vec{L} \qquad \vec{J}' = \vec{I}' + \vec{L}'$$

$$\vec{j} = \vec{\imath} + \vec{s} \qquad \vec{j}' = \vec{\imath}' + \vec{s}'$$

$$\vec{J} + \vec{j} = \vec{J}_c = \vec{J}' + \vec{j}'$$

(b) L-S (Russel Saunders) Coupling.

$$\vec{S} = \vec{I} + \vec{s} \qquad \vec{S}' = \vec{I}' + \vec{s}'$$

$$\vec{L}_1 = \vec{L} + \vec{\imath} \qquad \vec{L}_2 = \vec{L}' + \vec{\imath}'$$

$$\vec{S} + \vec{L}_1 = \vec{J}_c = \vec{S}' + \vec{L}_2$$

(c) Intermediate Coupling.

$$\vec{J} = \vec{I} + \vec{L} \qquad \vec{J}' = \vec{I}' + \vec{L}'$$

$$\vec{S} = \vec{J} + \vec{s} \qquad \vec{S}' = \vec{J}' + \vec{s}'$$

$$\vec{S} + \vec{\imath} = \vec{J}_c = \vec{S}' + \vec{\imath}'$$

The quantity S is called the channel spin[29].

If the intermediate coupling scheme is used, the distribution in angular momentum of intermediate states is given by[6].

$$\sigma_c(I,\epsilon,J_c) = \frac{\pi\lambda^2(2J_c+1)}{(2s+1)(2I+1)} \sum_{s=|I-s|}^{(I+s)} \sum_{t=|J_c-S|}^{(J_c+s)} T_t(\epsilon)$$

Appendix III.

The $Cu^{63}(\alpha,pn)Zn^{65}$ and $Cu^{63}(\alpha,2n)Ga^{65}$ Reactions.

The excitation function for the production of Zn^{65} in natural copper foils via the $Cu^{63}(\alpha,2n)Ga^{65}$ and $Cu^{63}(\alpha,pn)Zn^{65}$ reactions was measured by the bombardment of 3.64 mg/cm^2 natural copper foils[58]. backed by thick aluminium catchers and interspersed between aluminium degrading foils. The beam intensity was monitored via the production of Ga^{67} in zinc foils by the $Zn^{64}(\alpha,n)Ge^{67}$ and $Zn^{64}(\alpha,p)Ga^{67}$ reactions.

All 15 minute Ga^{65} activity was allowed to decay to 245 day Zn^{65}. A 7.6 cm x 7.6 cm NaI(Tl) detector was employed to monitor the intensity of the 511-kev and 1115-kev peaks. Efficency data due to Heath[70]. were employed. Positron emission was taken to occur in 51.7%[74]. of the decays and the intensity of the 1115-kev peak was taken as 0.49 photons/disintegration[74]. The disintegration rates determined seperately from the two peaks were found to agree within a few percent in all cases.

The measured excitation function is shown in figure 34.

Appendix IV.

Characterization of 280 day Ge^{68}.

The activity of 280 day Ge^{68} was determined by radioactivity assay of its 67 minute daughter after secular equilibrium had been established. Ge^{68} decays by pure electron capture, and therefore does not emit any easily detectable radiation. The radiations emitted during the decay of Ga^{68} are easily detectable, however.

The identity of Ga^{68} was established by a series of measurements immediately after separation of $GeCl_4$ from the dissolved target (several months after the irradiation to eliminate shorter lived Ge activities), followed by analysis of the radioactive growth curve. Figure 35 is such a curve. The crosses denote measured activity plotted versus time from the end of the separation to the time of the measurement of the activity. The open circles represent the difference between measured activity and the equilibrium activity. The half life was measured from the decay curve defined by the open circles in order to establish the identity of this isotope, and was found in all cases to agree well with the value measured in an independent study of the nuclide Ga^{68}.

Appendix V.

SFUSMAP

The Fortran VI statistical model program, SFUSMAP, consists of a main program, four subprograms, and a function subroutine.

a.) MAIN.

The main program reads the input data and performs the summations and multiplications of the various probabilities for populations of the E-J grids corresponding to the various nuclear states. Most of the written output from the program is executed by MAIN.

b.) Subroutine WRITE.

This subprogram was written as a result of core space restrictions on the main program and is used to write out the E-J matrix ONE.

c.) Subroutine BRANCH.

Probabilities for the population of final states are calculated for a specific compound nucleus energy and angular momentum by the subprogram. Most of the statistical model mathematics are performed by this subroutine which calls the remaining two subroutines and the function subroutine.

d.) Subroutine FURG.

Transmission coefficients (which are read in as data) are interpolated and summed to give inverse reaction cross-sections by this subroutine.

e.) Subroutine BIND.

This subroutine returns a value of the binding energy of a particular particle for a given compound nucleus.

f.) Function ALEVEL.

This function calculates the level density corresponding to a particular E and J.

A listing of SFUSMAP immediately follows this discussion. The program has been revised substantially since this listing to remove programming steps which were included to avoid inadequacies in early versions of the SFU system 360/40 compiler programs.

A typical input data deck consists of:

(1) 36 cards containing binding energies (punched in columns 1-6) for the nine nuclei surrounding (and including) the compound nucleus at lower neutron and proton numbers.

(2) 108 cards, each containing 8 transmission coefficients for alpha penetrations (punched in each group of 10 columns). Each group of four cards represents one energy value with each value separated by 2 MeV. This data designates the matrix TLA (J,JXE) where J and JXE signify angular momentum and energy respectively.

(3) 135 cards, each containing eight proton tansmission coefficients as above. Each group of five cards represents ane energy value. This data populates the matrix TPL(J,L,JXE) where L signifys orbital angular momentum.

(4) 135 cards containing neutron transmission coefficients, populating the matrix TLN (J,L,JXE).

(5) 1 card containing the four single-particle gamma strength constants (C_t') punched in the first four groups of 10 columns.

(6) An eight card packet which contains:

(a) The center of mass energy of the target-projectile system (punched in columns 1-8).

(b) The binding energy of the projectile and the target (columns 2-8).

(c) 5 cards containing the capture cross-sections for population of each J state from J=0 to J=39 for the energy specified by the first card in the packet (a). The data is puched in each group of 10 channels.

(d) The angular momentum value above which the capture cross-section is zero.

The number of data packets which may be used is not limited by the program. The last card in the deck should contain a zero punched in place of the energy.

```
FORTRAN IV G LEVEL 0, MOD 0             MAIN                DATE = 68017        30/13/41

            C  SFUSMAP, THE COMPUTER BOGGLER.
0001            DIMENSION GAMMA(4),CL(4)
0002            DIMENSION B(4,9)
0003            DIMENSION TLA(32,27), TLP(2,20,27) , TLN(2,20,27)
0004            REAL ONE
0005            DIMENSION ONE(30,20),TWO(30,20),THREE(30,20),FIVE(30,20)
0006            DIMENSION FOUR(30,20), SIG(9)
0007            DIMENSION SFUBAR(30,20,4)
0008            REAL NINE
0009            DIMENSION NINE(30,20)
0010            COMMON  B,AN,ZN,IX,EF
0011            COMMON U
0012            COMMON CL
0013            COMMON TLA,TLP,TLN
0014            COMMON SFUBAR
0015            READ(5,1)((B(IX,ICN),IX=1,4),ICN=1,9)
0016          1 FORMAT(1F6.3)
0017            READ(5,2) ((TLA(J,JXE),J=1,32),JXE=1,27)
0018            READ(5,2) (((TLP(J,L,JXE),J=1,2),L=1,20),JXE=1,27)
0019            READ(5,2) (((TLN(J,L,JXE),J=1,2),L=1,20),JXE=1,27)
0020            READ(5,6) (CL(L),L=1,4)
0021          6 FORMAT(4E10.3)
0022          2 FORMAT(8F10.8)
0023          3 FORMAT(8E10.3)
0024          4 FORMAT(2F8.3,I3,E20.8)
0025          5 FORMAT(8F15.8)
0026          9 FORMAT(2F12.8,5X,2F12.8,5X,2F12.8,5X,2F12.8)
0027          7 FORMAT(1F10.5)
0028       2008 FORMAT(E20.8)
0029        200 FORMAT(4E20.8)
           CONTROL PROGRAM STARTS HERE
0030            FDG=1.3E-07
0031            DIMENSION SIGCAP(40)
0032            READ(5,7) ECM
0033            READ(5,7) Q
0034            READ(5,3)(SIGCAP(JCN),JCN=1,40)
```

```
0035              READ(5,7) BB
0036              XY=BB
0037         7515 CONTINUE
0038              WRITE(6,7) ECM
0039              WRITE(6,7) Q
0040              WRITE(6,7) BB
0041              AA=ECM+Q
0042              DO 3000 I=1,30
0043              DO 3000 J=1,20
0044              JEF=I
0045              JJF=J
0046              ONE(JEF,JJF)=0.0
0047              TWO(JEF,JJF)=0.0
0048              THREE(JEF,JJF)=0.0
0049              FIVE(JEF,JJF)=0.0
0050              FOUR(JEF,JJF)=0.0
0051              NINE(JEF,JJF)=0.0
0052         3000 CONTINUE
0053              ICN=1
0054              SIG(ICN)=0.0
0055         4004 CONTINUE
0056              DO 10 K=1,30
0057              DO 10 J=1,20
0058              DO 10 I=1,4
0059              JEF=K
0060              JJF=J
0061              IX=I
0062              SFUBAR(JEF,JJF,IX)=0.0
0063           10 CONTINUE
0064              JCN=BB+1.
0065              SFURAB=0.0
0066              DO 20 IA=1,4
0067              IX=IA
0068              AN=68.
0069              ZN=32.
0070              CALL BRANCH(GAMMA,AA,BB)
0071              SFURAB=SFURAB+GAMMA(IX)
0072           20 CONTINUE
0073              IF((SFURAB).LE.0.0) GO TO 12002
0074              DO 2002 ID=1,30
```

```
0075                DO 2002 IE=1,20
0076                DO 2002 IF=1,4
0077                JEF=ID
0078                JJF=IE
0079                IX=IF
0080                SFUBAR(JEF,JJF,IX)=SFUBAR(JEF,JJF,IX)/SFURAB
0081             2002 CONTINUE
0082            12002 CONTINUE
0083                IX=1
0084                DO 2003 IG=1,30
0085                DO 2003 IH=1,20
0086                JEF=IG
0087                JJF=IH
0088                ONE(JEF,JJF)=ONE(JEF,JJF)+SFUBAR(JEF,JJF,IX)*SIGCAP(JCN)
0089                ICN=1
0090                SIG(ICN)=SIG(ICN)+SFUBAR(JEF,JJF,IX)*SIGCAP(JCN)
0091             2003 CONTINUE
0092                IX=4
0093                DO 2004 IO=1,30
0094                DO 2004 IP=1,20
0095                JEF=IO
0096                JJF=IP
0097                TWO(JEF,JJF)=TWO(JEF,JJF)+SFUBAR(JEF,JJF,IX)*SIGCAP(JCN)
0098             2004 CONTINUE
0099                IX=3
0100                DO 2005 IQ=1,30
0101                DO 2005 IR=1,20
0102                JEF=IQ
0103                JJF=IR
0104                FOUR(JEF,JJF)=FOUR(JEF,JJF)+SFUBAR(JEF,JJF,IX)*SIGCAP(JCN)
0105             2005 CONTINUE
0106                IX=2
0107                DO 2106 IS=1,30
0108                DO 2106 IT=1,20
0109                JEF=IS
0110                JJF=IT
0111                NINE(JEF,JJF)=NINE(JEF,JJF)+SFUBAR(JEF,JJF,IX)*SIGCAP(JCN)
0112             2106 CONTINUE
0113                BB=BB-1.
0114                IF((BB).GE.0.0) GO TO 4004
```

```
0115                ICN=1
0116                WRITE(6,4) ECM,Q,ICN,SIG(ICN)
0117                WRITE(6,101)
0118                CALL WRITE(ONE)
0119                WRITE(6,102)
0120                WRITE(6,204)
0121                DO 2104 I=1,30
0122                JEF=I
0123                WRITE(6,203)(JEF,(TWO(JEF,JJF),JJF=1,10))
0124          2104 CONTINUE
0125                WRITE(6,100)
0126                WRITE(6,205)
0127                DO 2105 I=1,30
0128                JEF=I
0129                WRITE(6,203)(JEF,(TWO(JEF,JJF),JJF=11,20))
0130          2105 CONTINUE
0131                WRITE(6,103)
0132                WRITE(6,204)
0133                DO 2111 I=1,30
0134                JEF=I
0135                WRITE(6,203)(JEF,(FOUR(JEF,JJF),JJF=1,10))
0136          2111 CONTINUE
0137                WRITE(6,100)
0138                WRITE(6,205)
0139                DO 2112 I=1,30
0140                JEF=I
0141                WRITE(6,203)(JEF,(FOUR(JEF,JJF),JJF=11,20))
0142          2112 CONTINUE
0143                WRITE(6,100)
0144                DO 2119 I=1,30
0145                JEF=I
0146                WRITE(6,203)(JEF,(NINE(JEF,JJF),JJF=1,10))
0147          2119 CONTINUE
0148                WRITE(6,100)
0149                DO 2113 I=1,30
0150                JEF=I
0151                WRITE(6,203)(JEF,(NINE(JEF,JJF),JJF=11,20))
0152          2113 CONTINUE
0153                ICN=2
0154                DO 9800 I=1,30
```

```
0155                DO 9800 J=1,20
0156                JEF=I
0157                JJF=J
0158                ONE(JEF,JJF)=0.0
0159          9800  CONTINUE
0160                ENSUM=0.0
0161                SIG(ICN)=0.0
0162                JA=1
0163          8500  CONTINUE
0164                JB=1
0165          2006  CONTINUE
0166                DO 3001 I=1,30
0167                DO 3001 J=1,20
0168                DO 3001 K=1,4
0169                JEF=I
0170                JJF=J
0171                IX=K
0172                SFURAB(JEF,JJF,IX)=0.0
0173          3001  CONTINUE
0174                SFURAB=0.0
0175                DO 4000 JC=1,4
0176                IX=JC
0177                AN=67.
0178                ZN=32.
0179                EEF=2*JA-1.75
0180                FJ=40.0-2*JB
0181                JJEF=EEF/2+1
0182                JJJF=FJ/2.0+1.5
0183                FUBAR=TWO(JJEF,JJJF)
0184                IF((FUBAR).LT.FDG) GO TO 12019
0185                IF((JA-3).LT.0) GO TO 700
0186                CALL BRANCH(GAMMA,EEF,FJ)
0187                SFURAB=SFURAB+GAMMA(IX)
0188          4000  CONTINUE
0189                IF((SFURAB).LT.FDG) GO TO 700
0190                GO TO 701
```

```
0191          700 IX=1
0192              SFUBAR(JJEF,JJJF,IX)=1.0
0193              GO TO 2109
0194          701 CONTINUE
0195              ENSUM=ENSUM+SFUBAB
0196              DO 2010 I=1,30
0197              DO 2010 J=1,20
0198              DO 2010 K=1,4
0199              JEF=I
0200              IX=K
0201              JJF=J
0202              SFUBAR(JEF,JJF,JX)=SFUBAR(JEF,JJF,IX)/SFUBAB
0203         2010 CONTINUE
0204         2109 CONTINUE
0205              DO 2007 JD=1,30
0206              DO 2007 JE=1,20
0207              JEF=JD
0208              JJF=JE
0209              IX=1
0210              SIG(ICN)=SIG(ICN)+SFUBAR(JEF,JJF,IX)*FUBAR
0211              ONE(JEF,JJF)=ONE(JEF,JJF)+SFUBAR(JEF,JJF,IX)*FUBAR
0212              IX=4
0213              THREE(JEF,JJF)=THREE(JEF,JJF)+SFUBAR(JEF,JJF,IX)*FUBAR
0214              IX=3
0215              FIVE(JEF,JJF)=FIVE(JEF,JJF)+SFUBAR(JEF,JJF,IX)*FUBAR
0216         2007 CONTINUE
0217        12019 CONTINUE
0218              JB=JB+1
0219              IF((JB-20).LE.0) GO TO 2006
0220         8520 CONTINUE
0221              JA=JA+1
0222              IF((JA-30).LE.0) GO TO 8500
0223         8510 CONTINUE
0224              ENORM=ENSUM
0225              WRITE(6,4) ECM, Q, ICN, SIG(ICN)
0226              WRITE(6,104)
0227              WRITE(6,204)
0228              DO 2107 I=1,30
0229              JEF=I
0230              WRITE(6,203)(JEF,(THREE(JEF,JJF),JJF=1,10))
```

```
0231          2107 CONTINUE
0232               WRITE(6,100)
0233               WRITE(6,205)
0234               DO 2108 I=1,30
0235               JEF=I
0236               WRITE(6,203)(JEF,(THREE(JEF,JJF),JJF=11,20))
0237          2108 CONTINUE
0238               WRITE(6,105)
0239               WRITE(6,204)
0240               DO 2115 I=1,30
0241               JEF=I
0242               WRITE(6,203)(JEF,(FIVE(JEF,JJF),JJF=1,10))
0243          2115 CONTINUE
0244               WRITE(6,100)
0245               WRITE(6,205)
0246               DO 2116 I=1,30
0247               JEF=I
0248               WRITE(6,203)(JEF,(FIVE(JEF,JJF),JJF=11,20))
0249          2116 CONTINUE
0250               WRITE(6,109)
0251               CALL WRITE(ONE)
0252               ICN=3
0253               ENSUM=0.0
0254               SIG(ICN)=0.0
0255               DO 9801 I=1,30
0256               DO 9801 J=1,20
0257               JEF=I
0258               JJF=J
0259               ONE(JEF,JJF)=0.0
0260          9801 CONTINUE
0261               IA=1
0262          8502 CONTINUE
0263               IB=1
0264          5006 CONTINUE
0265               DO 5001 I=1,30
0266               DO 5001 J=1,20
0267               DO 5001 K=1,4
0268               JEF=I
0269               JJF=J
0270               IX=K
```

```
0271            SFUBAR(JEF,JJF,IX)=0.0
0272       5001 CONTINUE
0273            SFURAB=0.0
0274            DO 5000 IC=1,4
0275            IX=IC
0276            AN=66.
0277            ZN=32.
0278            EEF=2*IA-1.75
0279            FJ=40.0-2*IB
0280            JJEF=EEF/2+1
0281            JJJF=FJ/2.0+1.5
0282            FUBAR=THREE(JJEF,JJJF)
0283            IF((FUBAR).LT.FOG) GO TO 15011
0284            IF((IA-3).LT.0) GO TO 702
0285            CALL BRANCH(GAMMA,EEF,FJ)
0286            SFURAB=SFURAB+GAMMA(IX)
0287       5000 CONTINUE
0288            IF((SFURAB).LT.FOG) GO TO 702
0289            GO TO 703
0290        702 IX=1
0291            SFUBAR(JJEF,JJJF,IX)=1.0
0292            GO TO 15010
0293        703 CONTINUE
0294            ENSUM=ENSUM+SFURAB
0295            DO 5010 I=1,30
0296            DO 5010 J=1,20
0297            DO 5010 K=1,4
0298            JEF=I
0299            JJF=J
0300            IX=K
0301            SFUBAR(JEF,JJF,IX)=SFUBAR(JEF,JJF,IX)/SFURAB
0302       5010 CONTINUE
0303      15010 CONTINUE
0304            DO 5007 ID=1,30
0305            DO 5007 IE=1,20
0306            JEF=ID
```

```
0307                    JJF=IE
0308                    IX=1
0309                    ICN=3
0310                    SIG(ICN)=SIG(ICN)+SFUBAR(JEF,JJF,IX)*FUBAR
0311                    ONE(JEF,JJF)=ONE(JEF,JJF)+SFUBAR(JEF,JJF,IX)*FUBAR
0312          5007 CONTINUE
0313         15011 CONTINUE
0314                    IB=IB+1
0315                    IF((IB-30).LE.0) GO TO 5006
0316          8522 CONTINUE
0317                    IA=IA+1
0318                    IF((IA-30).LE.0) GO TO 8502
0319          8512 CONTINUE
0320                    ENORM=ENSUM
0321                    WRITE(6,4) ECM, Q, ICN, SIG(ICN)
0322                    WRITE(6,110)
0323                    CALL WRITE(ONE)
0324                    ICN=4
0325                    ENSUM=0.0
0326                    SIG(ICN)=0.0
0327                    DO 9802 I=1,30
0328                    DO 9802 J=1,20
0329                    JEF=I
0330                    JJF=J
0331                    ONE(JEF,JJF)=0.0
0332          9802 CONTINUE
0333                    JA=1
0334          8501 CONTINUE
0335                    JB=1
0336          6006 CONTINUE
0337                    DO 6001 I=1,30
0338                    DO 6001 J=1,20
0339                    DO 6001 K=1,4
0340                    JEF=I
0341                    JJF=J
0342                    IX=K
0343                    SFUBAR(JEF,JJF,IX)=0.0
0344          6001 CONTINUE
0345                    SFUBAR=0.0
0346                    DO 6000 JC=1,4
```

```
0347                    IX=JC
0348                    AN=67.
0349                    ZN=31.
0350                    EEF=2*JA-1.75
0351                    FJ=40.0-2*JB
0352                    JJEF=EEF/2+1
0353                    JJJF=FJ/2.0+1.5
0354                    FUBAR=FOUR(JJEF,JJJF)
0355                    IF((FUBAR).LT.FDG) GO TO 16011
0356                    IF((JA-3).LT.0) GO TO 704
0357                    CALL BRANCH(GAMMA,EEF,FJ)
0358                    SFURAB=SFURAB+GAMMA(IX)
0359                6000 CONTINUE
0360                    IF((SFURAB).LT.FDG) GO TO 704
0361                    GO TO 705
0362                 704 IX=1
0363                    SFUBAR(JJEF,JJJF,IX)=1.0
0364                    GO TO 16010
0365                 705 CONTINUE
0366                    ENSUM=ENSUM+SFURAB
0367                    DO 6010 I=1,30
0368                    DO 6010 J=1,20
0369                    DO 6010 K=1,4
0370                    JEF=I
0371                    JJF=J
0372                    IX=K
0373                    SFUBAR(JEF,JJF,IX)=SFUBAR(JEF,JJF,IX)/SFURAB
0374                6010 CONTINUE
0375               16010 CONTINUE
0376                    DO 6007 ID=1,30
0377                    DO 6007 IE=1,20
0378                    JEF=ID
0379                    JJF=IE
0380                    IX=4
0381                    FIVE(JEF,JJF)=FIVE(JEF,JJF)+SFUBAR(JEF,JJF,IX)*FUBAR
0382                    IX=1
0383                    SIG(ICN)=SIG(ICN)+SFUBAR(JEF,JJF,IX)*FUBAR
0384                    ONE(JEF,JJF)=ONE(JEF,JJF)+SFUBAR(JEF,JJF,IX)*FUBAR
0385                6007 CONTINUE
0386               16011 CONTINUE
```

```
0387                JB=JB+1
0388                IF((JB-20).LE.0) GO TO 6006
0389          8521  CONTINUE
0390                JA=JA+1
0391                IF((JA-30).LE.0) GO TO 8501
0392          8511  CONTINUE
0393                ENORM=ENSUM
0394                WRITE(6,4) ECM, Q, ICN, SIG(ICN)
0395                WRITE(6,106)
0396                CALL WRITE(ONE)
0397                WRITE(6,107)
0398                WRITE(6,204)
0399                DO 2306 I=1,30
0400                JEF=I
0401                WRITE(6,203)(JEF,(FIVE(JEF,JJF),JJF=1,10))
0402          2306  CONTINUE
0403                WRITE(6,100)
0404                WRITE(6,205)
0405                DO 2307 I=1,30
0406                JEF=I
0407                WRITE(6,203)(JEF,(FIVE(JEF,JJF),JJF=11,20))
0408          2307  CONTINUE
0409                ICN=5
0410                ENSUM=0.0
0411                SIG(ICN)=0.0
0412                DO 9803 I=1,30
0413                DO 9803 J=1,20
0414                JEF=I
0415                JJF=J
0416                ONE(JEF,JJF)=0.0
0417          9803  CONTINUE
0418                IA=1
0419          9502  CONTINUE
0420                IB=1
0421          9006  CONTINUE
0422                DO 9001 I=1,30
```

```
0423                DO 9001 J=1,20
0424                DO 9001 K=1,4
0425                JEF=I
0426                JJF=J
0427                IX=K
0428                SFUBAR(JEF,JJF,IX)=0.0
0429             9001 CONTINUE
0430                SFURAB=0.0
0431                DO 9000 IC=1,4
0432                IX=IC
0433                AN=66.
0434                ZN=31.
0435                EEF=2*IA-1.75
0436                FJ=40.0-2*IB
0437                JJEF=EEF/2+1
0438                JJJF=FJ/2.0+1.5
0439                FUBAR=FIVE(JJEF,JJJF)
0440                IF((FUBAR).LT.FOG) GO TO 19011
0441                IF((IA-3).LT.0) GO TO 706
0442                CALL BRANCH(GAMMA,EEF,FJ)
0443                SFURAB=SFURAB+GAMMA(IX)
0444             9000 CONTINUE
0445                IF((SFURAB).LT.FOG) GO TO 706
0446                GO TO 707
0447              706 IX=1
0448                SFUBAR(JJEF,JJJF,IX)=1.0
0449                GO TO 19010
0450              707 CONTINUE
0451                ENSUM=ENSUM+SFURAB
0452                DO 9010 I=1,30
0453                DO 9010 J=1,20
0454                DO 9010 K=1,4
0455                JEF=I
0456                JJF=J
0457                IX=K
0458                SFUBAR(JEF,JJF,IX)=SFUBAR(JEF,JJF,IX)/SFURAB
0459             9010 CONTINUE
0460            19010 CONTINUE
0461                DO 9007 ID=1,30
0462                DO 9007 IE=1,20
```

```
0463                JEF=ID
0464                JJF=IE
0465                IX=1
0466                ICN=5
0467                ONE(JEF,JJF)=ONE(JEF,JJF)+SFUBAR(JEF,JJF,IX)*FUBAR
0468                SIG(ICN)=SIG(ICN)+SFUBAR(JEF,JJF,IX)*FUBAR
0469             9007 CONTINUE
0470            19011 CONTINUE
0471                IB=IB+1
0472                IF((IB-20).LE.0) GO TO 9006
0473             9522 CONTINUE
0474                IA=IA+1
0475                IF((IA-30).LE.0) GO TO 9502
0476             9512 CONTINUE
0477                WRITE(6,108)
0478                CALL WRITE(ONE)
0479                ENORM=ENSUM
0480                WRITE(6,4) ECM, Q, ICN, SIG(ICN)
0481                ICN=1
0482                WRITE(6,4) ECM,Q,ICN,SIG(ICN)
0483                ICN=4
0484                WRITE(6,4) ECM, Q, ICN, SIG(ICN)
0485                ICN=3
0486                WRITE(6,4) ECM, Q, ICN, SIG(ICN)
0487                ICN=2
0488                WRITE(6,4) ECM, Q, ICN, SIG(ICN)
0489                ICN=5
0490                WRITE(6,4) ECM, Q, ICN, SIG(ICN)
0491                READ(5,7) ECM
0492                IF((ECM).LT.1.0) GO TO 11111
0493                READ(5,7) Q
0494                READ(5,3)(SIGCAP(JCN),JCN=1,40)
0495                READ(5,7) BB
0496                XY=BB
0497                GO TO 7515
0498            11111 CONTINUE
0499              100 FORMAT(1H1///)
0500              101 FORMAT(1H1,6X,58HPOPULATION OF STATES IN GERMANIUM 67 AFTER GAMMA
                     1EMMISSION//)
0501              102 FORMAT(1H1,6X,39HPOPULATION OF STATES IN GERMANIUM 67 AFTER EMISS
```

```
      1ION OF A NEUTRON BY THE COMPOUND NUCLEUS//)
0502  103 FORMAT(1H1,6X,87HPOPULATION OF STATES IN GALLIUM 67 AFTER EMMISSIO
      1N OF A PROTON BY THE COMPOUND NUCLEUS.//)
0503  104 FORMAT(1H1,6X,88HPOPULATION OF STATES IN GERMANIUM 66 AFTER NEUTRO
      1N EMMISSION FROM STATES IN GERMANIUM 67//)
0504  105 FORMAT(1H1,6X,85HPOPULATION OF STATES IN GALLIUM 66 AFTER PROTON E
      1MMISSION FROM STATES IN GERMANIUM 67//)
0505  106 FORMAT(1H1,6X,56HPOPULATION OF STATES IN GALLIUM 67 AFTER GAMMA EM
      1MISSION//)
0506  107 FORMAT(1H1,6X,95HPOPULATION OF STATES IN GALLIUM 66 AFTER NEUTRON
      1EMMISSION FROM STATES IN GALLIUM 67 %ADDITIVE<//)
0507  108 FORMAT(1H1,6X,56HPOPULATION OF STATES IN GALLIUM 66 AFTER GAMMA EM
      1MISSION//)
0508  109 FORMAT(1H1,6X,58HPOPULATION OF STATES IN GERMANIUM 67 AFTER GAMMA
      1EMMISSION//)
0509  110 FORMAT(1H1,6X,58HPOPULATION OF STATES IN GERMANIUM 66 AFTER GAMMA
      1EMMISSION//)
0510  203 FORMAT(//13,5X,10E12.3)
0511  8505 FORMAT(2F10.5)
0512  204 FORMAT( 3HJEF,10X,3HJ#C,9X,3HJ#1,9X,3HJ#2,9X,3HJ#3,9X,3HJ#4,9X,3HJ
      1#5,9X,3HJ#6,9X,3HJ#7,9X,3HJ#8,9X,3HJ#9//)
0513  205 FORMAT( 3HJEF,9X,4HJ#10,8X,4HJ#11,8X,4HJ#12,8X,4HJ#13,8X,4HJ#14,8X
      1,4HJ#15,8X,4HJ#16,8X,4HJ#17,8X,4HJ#18,8X,4HJ#19//)
0514  206 FORMAT( 3HJEF,9X,4HJ#20,8X,4HJ#21,8X,4HJ#22,8X,4HJ#23,8X,4HJ#24,8X
      1,4HJ#25,8X,4HJ#26,8X,4HJ#27,8X,4HJ#28,8X,4HJ#29//)
0515  207 FORMAT( 3HJEF,9X,4HJ#30,8X,4HJ#31,8X,4HJ#32,8X,4HJ#33,8X,4HJ#34,8X
      1,4HJ#35,8X,4HJ#36,8X,4HJ#37,8X,4HJ#38,8X,4HJ#39//)
0516        STOP
0517        DEBUG UNIT(6), INIT(ENORM)
0518        AT 9001
0519        END
```

TOTAL MEMORY REQUIREMENTS 007700 BYTES

```
FORTRAN IV G LEVEL 0, MOD 0          WRITE          DATE = 68017          30/13/41

0001                  SUBROUTINE WRITE(ONE)
0002                  DIMENSION ONE(30,20)
0003                  DO 1 I=1,30
0004                  JEF=I
0005                  WRITE(6,203)(JEF,(ONE(JEF,JJF),JJF=1,10))
0006                1 CONTINUE
0007                  WRITE(6,100)
0008                  DO 2 I=1,30
0009                  JEF=I
0010                  WRITE(6,203)(JEF,(ONE(JEF,JJF),JJF=11,20))
0011                2 CONTINUE
0012              100 FORMAT(1H1///)
0013              203 FORMAT(//I3,5X,10E12.3)
0014                  RETURN
0015                  END

TOTAL MEMORY REQUIREMENTS 000264 BYTES
```

```
FORTRAN IV G LEVEL 0, MOD 0          BRANCH          DATE = 68017          30/13/41

0001                  SUBROUTINE BRANCH(GAMMA,AA,BB)
0002                  DIMENSION GAMMA(4),CL(4)
0003                  DIMENSION B(4,9)
0004                  DIMENSION TLA(32,27), TLP(2,20,27) , TLN(2,20,27)
0005                  DIMENSION SFUBAR(30,20,4)
0006                  REAL JF
0007                  REAL JR
0008                  COMMON  B,AN,ZN,IX,EF
0009                  COMMON U
0010                  COMMON CL
0011                  COMMON TLA,TLP,TLN
0012                  IF((AA).LE.0.0) GO TO 33
0013                  AB=.96
0014                  CC=3.0
0015                  RI=15.58
0016                  C=(1.-AB*EXP(-0.693*CC*AA))*RI
0017                  AJR=-0.5+0.5*SQRT(1.0+8.0*AA*C)
0018                  IF((BB-AJR).GT.0.0) GO TO 33
0019                  COMMON SFUBAR
0020                  GAMMA(IX)=0.0
0021                  SFUSUM=0.0
0022              1113 CONTINUE
0023                  DIMENSION PN(6), PZ(6)
0024                  PZ(1)=-1.36
0025                  PZ(2)=0.0
0026                  PZ(3)=-1.09
0027                  PZ(4)=0.0
0028                  PZ(5)=-1.47
0029                  PZ(6)=0.0
0030                  PN(1)=-1.46
0031                  PN(2)=0.0
0032                  PN(3)=-1.44
0033                  PN(4)=0.0
0034                  PN(5)=-1.46
0035                  PN(6)=0.0
0036                  ACN=68.
```

```
0037            ZCN=32.
0038            IZ=ZCN-ZN+1.
0039            IN=ACN-AN-ZCN+ZN+1.
0040            IF(AA-3.0) 4000,4000,4001
0041       4000 E=3.0+PN(IN)+PZ(IZ)
0042            W=ALEVEL(E,BP)*AA**2.0/9.0+(3.0-AA)*10.0
0043            GO TO 4002
0044       4001 E=AA+PN(IN)+PZ(IZ)
0045            W=ALEVEL(E,BB)
0046       4002 CONTINUE
0047            GO TO 17
0048         33 GAMMA(IX)=0.0
0049            GO TO 20
0050         17 CONTINUE
0051            GO TO (4,5,6,7),IX
0052          4 BX=0.0
0053            DZ=0.0
0054            DA=0.0
0055            GO TO 9
0056          5 CALL BIND(BX)
0057            DZ=2.0
0058            DA=4.0
0059            GO TO 8
0060          6 CALL BIND(BX)
0061            DZ=1.0
0062            DA=1.0
0063            GO TO 8
0064          7 CALL BIND(BX)
0065            DZ=0.0
0066            DA=1.0
0067          8 CONTINUE
0068            U=AA-BX
0069            IF((U).GT.0.0) GO TO 19
0070            GO TO 33
0071         19 CONTINUE
0072            AN=AN-DA
0073            ZN=ZN-DZ
0074            FACTA=AN*DA/(AN+DA)
0075            IZ=ZCN-ZN+1.
0076            IN=ACN-AN-ZCN+ZN+1.
```

```
0077                DO 111 I=1,30
0078                DO 2 K=1,20
0079                EF=2*I-1.75
0080                XE=AA-EF-BX
0081                IF((XE).LT.0.0) GO TO 3
0082                JEF=EF/2+1
0083                C=(1.-AB*EXP(-.693*CC*EF))*RI
0084                JR=-0.5+0.5*SQRT(1.0+8.0*EF*C)
0085                JF=40-2*K
0086                JJF=JF/2.0+1.5
0087                IF((JF-JR).GT.0.0) GO TO 2
0088                IF((JF).LT.0.0) GO TO 2
0089                CALL FURG(IX,XE,BB,JF,TLA,TLP,TLN,SIGMA,AN,ZN)
0090                IF(EF-3.0) 3000,3000,3001
0091          3000  E=3.0+PN(IN)+PZ(IZ)
0092                YAJ=SIGMA*(ALEVEL(E,JF)*EF**2.0/9.0+10.0*(3.0-EF))
0093                GO TO 3002
0094          3001  E=EF+PN(IN)+PZ(IZ)
0095                YAJ=SIGMA*ALEVEL(E,JF)
0096          3002  CONTINUE
0097                SFUBAR(JEF,JJF,IX)=FACTA*XE*YAJ/W
0098                IF((IX).EQ.2) GO TO 3012
0099                EF=2*I-0.75
0100                XE=AA-EF-BX
0101                IF((XE).LT.0.0) GO TO 3012
0102                IF((XE).GT.10.0) GO TO 3012
0103                CALL FURG(IX,XE,BB,JF,TLA,TLP,TLN,SIGMA,AN,ZN)
0104                IF(EF-3.0) 3010,3010,3011
0105          3010  CONTINUE
0106                E=3.0+PN(IN)+PZ(IZ)
0107                YAJ=SIGMA*(ALEVEL(E,JF)*EF**2.0/9.0+10.0*(3.0-EF))
0108                GO TO 3013
0109          3011  CONTINUE
0110                E=EF+PN(IN)+PZ(IZ)
0111                YAJ=SIGMA*ALEVEL(E,JF)
0112          3013  CONTINUE
0113                SFUBAR(JEF,JJF,IX)=(SFUBAR(JEF,JJF,IX)+FACTA*XE*YAJ/W)/2.0
0114          3012  CONTINUE
0115                SFUSUM=SFUSUM+SFUBAR(JEF,JJF,IX)
0116             2  CONTINUE
```

```
0117          111    CONTINUE
0118            3    GAMMA(IX)=SFUSUM
0119                 GO TO 20
0120              9 CONTINUE
0121                 U=AA-BX
0122                 IZ=ZCN-ZN+1.
0123                 IN=ACN-AN-ZCN+ZN+1.
0124                 DO 13 LL=1,4
0125                 L=LL
0126                 DO 11 I=1,30
0127                 EF=2*I-1.75
0128                 XE=AA-EF
0129                 IF((XE+2.0).LT.0.0) GO TO 13
0130                 IF((XE).GT.0.0) GO TO 7000
0131                 XE=0.20
0132                 EF=AA-XE
0133          7000 CONTINUE
0134                 JEF=EF/2+1
0135                 C=(1.-AB*EXP(-.693*CC*EF))*2I
0136                 JR=-0.5+0.5*SQRT(1.0+8.0*EF*C)
0137                 DJ=L
0138                 JD=BB+DJ+0.5
0139                 LF=BB-DJ+0.5
0140                 DO 12 K=LF,JD
0141                 JF=K
0142                 JJF=JF/2+1
0143                 IF((JF).LT.0.0) GO TO 12
0144                 IF((JF-JR).GT.0.0) GO TO 12
0145                 IF(EF-3.0) 2000,2000,2001
0146          2000 E=3.0+PN(IN)+PZ(IZ)
0147                 YAJ=ALEVEL(E,JF)*EF**2.0/9.0+(3.0-EF)*10.0
0148                 GO TO 2002
0149          2001 E=EF+PN(IN)+PZ(IZ)
0150                 YAJ=ALEVEL(E,JF)
0151          2002 CONTINUE
0152                 IF((L).EQ.1) GO TO 5000
0153                 IF((BB).LT.4.0) GO TO 202
0154                 IF((AA).LT.3.0) GO TO 202
0155                 IF((L).EQ.2) GO TO 200
0156           202 CONTINUE
```

```
0157                GO TO 5001
0158           5000 CONTINUE
0159                GIDIP=410.26/((20.1-AA)**2+6.25)
0160                SFUBAR(JEF,JJF,IX)=SFUBAR(JEF,JJF,IX)+GIDIP*CL(L)*XE**(2.*OJ+1.)
                   1*YAJ/W
0161                GO TO 5002
0162           5001 CONTINUE
0163                SFUBAR(JEF,JJF,IX)=SFUBAR(JEF,JJF,IX)+CL(L)*XE**(2.*OJ+1.)*YAJ/W
0164           5002 CONTINUE
0165                SFUSUM=SFUSUM+SFUBAR(JEF,JJF,IX)
0166                GO TO 204
0167            200 CONTINUE
0168                DELJ=ABS(JF-BB)
0169                IF((DELJ).EQ.2.0) GO TO 201
0170                GO TO 202
0171            201 CONTINUE
0172                CONJ=2.*(2.*BB+1.)/((BB+1.)*((BB-1.)**2-1.))
0173                WD=1.0/ALEVEL(F,BB)
0174                WE=1.0/YAJ
0175                ETWO=CONJ*(WD/(WD+WE))**5
0176                SFUBAR(JEF,JJF,IX)=SFUBAR(JEF,JJF,IX)+CL(L)*XE**(2.*OJ+1.)*YAJ/W
                   1ETWO
0177                ETMAX=ZN**2
0178                IF((ETWO-ETMAX).GT.0.0) GO TO 250
0179                GO TO 251
0180            250 ETWO=ETMAX
0181            251 CONTINUE
0182                GO TO 5002
0183            204 CONTINUE
0184             12 CONTINUE
0185             11 CONTINUE
0186             13 CONTINUE
0187                GAMMA(IX)=SFUSUM
0188             20 RETURN
0189                END

 TOTAL MEMORY REQUIREMENTS 001396 BYTES
```

```
FORTRAN IV G LEVEL 0, MOD C            ALEVEL          DATE = 68017          30/13/41

0001                  FUNCTION ALEVEL(E,J)
0002                  REAL M
0003                  REAL J
0004                  CC=3.0
0005                  AB=.96
0006                  RI=15.58
0007                  CCC=CC*5.0
0008                  IF(E-CCC)4,5,5
0009                5 C=RI
0010                  GO TO 6
0011                4 C=(1.-AB*EXP(-.693*CC*E))*RI
0012                6 CONTINUE
0013                2 A=8.5
0014                  FACT=5.282
0015                  T=(1.5+SQRT(2.25+4.*A*E))/(2.*A)
0016               10 CONTINUE
0017                  M=J+.5
0018                  ET=(E+1.5*T)
0019                  ALEVEL=FACT*2.*M*EXP(2.*SQRT(A*E)-M*M/(2.*C*T))/(ET*ET)
0020                3 RETURN
0021                  END


TOTAL MEMORY REQUIREMENTS 0002F2 BYTES
```

```
FORTRAN IV G LEVEL 0, MOD 0          FURG                    DATE = 68017          30/13/41

0001                SUBROUTINE FURG(IX,XE,BB,JF,TLA,TLP,TLN,SIGMA,AN,ZN)
0002                DIMENSION TLA(32,27), TLP(2,20,27) , TLN(2,20,27)
0003                REAL JF
0004                JIX=IX-1
0005                JXE=XE
0006                JXEA=JXE/2+1
0007                JXEB=JXEA+1
0008                XEA=2*(JXEA-1)
0009                INTER=0.5*(XE-XEA)
0010                GO TO (2,1,1), JIX
0011              1 S=0.0
0012                DA=1.0
0013                GO TO 3
0014              2 S=0.5
0015                IF((XE).LE.5.0) GO TO 7
0016                DA=4.0
0017              3 JS=ABS(JF-S)
0018                JJS=JF+S
0019                FACTA=.6566*(2.*BB+1.)*(AN+DA)/((2.*JF+1.)*(2.*S+1.)*AN*DA*XE)
0020             20 CONTINUE
0021                SIGSUM=0.0
0022                DO 4 JJ=JS,JJS
0023                BJ=JJ
0024                LL=ABS(BB-BJ)
0025                LLL=BB+BJ
0026                TALLY=0.0
0027                DO 5 L=LL,LLL
0028                J=JJ-JS+1
0029                GO TO (11,12,13),JIX
0030             11 IF((L-32).GT.0) GO TO 6
0031                TLX=TLA(L,JXEA)-(TLA(L,JXEA)-TLA(L,JXEB))*INTER
0032                GO TO 14
0033             12 IF((L-20).GT.0) GO TO 6
0034                TLX=TLP(J,L,JXEA)-(TLP(J,L,JXEA)-TLP(J,L,JXEB))*INTER
0035                GO TO 14
0036             13 IF((L-20).GT.0) GO TO 6
```

```
0037                TLX=TLN(J,L,JXEA)-(TLN(J,L,JXEA)-TLN(J,L,JXEB))*INTER
0038          14    TALLY = TALLY+TLX
0039              5 CONTINUE
0040              6 SIGSUM=SIGSUM+TALLY
0041              4 CONTINUE
0042                SIGMA=SIGSUM*FACTA
0043                GO TO 8
0044              7 SIGMA=0.0
0045              8 CONTINUE
0046                RETURN
0047                END
```



```
FORTRAN IV G LEVEL 0, MOD 0          FORG          DATE = 68017          30/13/41

 TOTAL MEMORY REQUIREMENTS 00076E BYTES
```

```
FORTRAN IV G LEVEL 0, MOD 0          BIND                DATE = 68017          20/13/41

0001                  SUBROUTINE BIND(BX)
0002                  DIMENSION B(4,9)
0003                  COMMON  B,AN,ZN,IX,EF
0004                  ACN=68.0
0005                  ZCN=32.0
0006                  ICN=ACN-AN+2.0*(ZCN-ZN)+1.0
0007                  BX=B(IX,ICN)
0008                  RETURN
0009                  END

TOTAL MEMORY REQUIREMENTS 000196 BYTES
```

Appendix VI. The Ar^{40} + Si^{28} Target-Projectile System.

Extension of the study of the compound nucleus Ge^{68} to reactions induced by the target-projectile pair Si^{28} and Ar^{40} would provide a test of the effects of extremely high angular momentum on the decay of this compound nucleus.

The pertinant data for this target-projectile system are contained in table VIII. The large negative binding energy makes possible the extension of measurements to much lower Ge^{68} excitation energies than were possible for either the C^{12} or O^{16} systems. However, the high projectile energies necessary to form the compound nucleus might present a problem, since recent work[122]. has shown that the cross-section for complete fusion processes above 100 MeV decreases with increasing energy of the bombarding particle. Attempts were made[122]. to explain this behavior by considering a sharp cut-off in the spin distribution of the compound nucleus. Collisions which would lead to higher compound nucleus spins were assumed to result instead in noncomplete fusion processes.

Obvious experimential difficulties would be expected for this system (e.g. low beam currents and beam energy uncertainty), however theoretical problems might be even more formidable. For instance, the optical model description of nuclear interactions will likely prove to be inadequate for a complex system such as this. A model which considers interactions with two potential wells might be more appropriate

Also, for higher angular momentum states, fission may become a predominant mode of de-excitation for the compound nucleus[123].

The reactions studied would be those leading to products one or two mass units removed from the compound nucleus, in order to avoid reactions which would proceed predominantly via direct interaction mechanisms.

TABLE VIII

$Ar^{40} + Si^{28}$

V(MeV)	E_{BE}(MeV)[79].	$E_{Ar^{40}}$(MeV)‡	E*(MeV)‡
37.7	-10.042	91.5	27.7

‡ Listed values are minimum energies required to overcome the coulomb barrier.

Element	Isotope	Natural Abundance (atomic %)[56].
Si	→ 28	92.21
	29	4.70
	30	3.09
Ar	36	0.337
	38	0.063
	→ 40	99.60

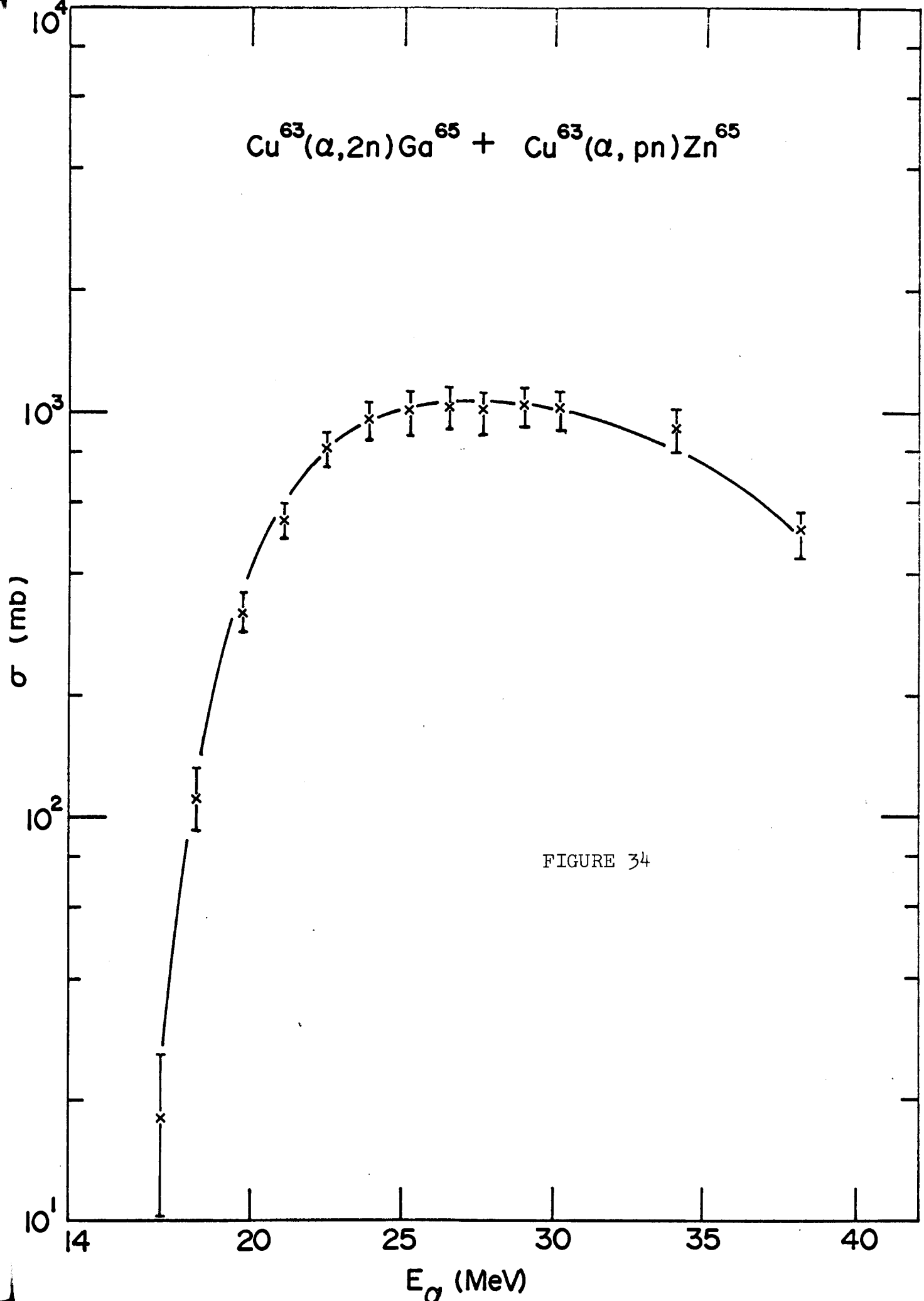
$Cu^{63}(\alpha,2n)Ga^{65} + Cu^{63}(\alpha,pn)Zn^{65}$
10^4
10^3
10^2
10^1
σ (mb)
14
20
25
30
35
40
E_α (MeV)

FIGURE 34

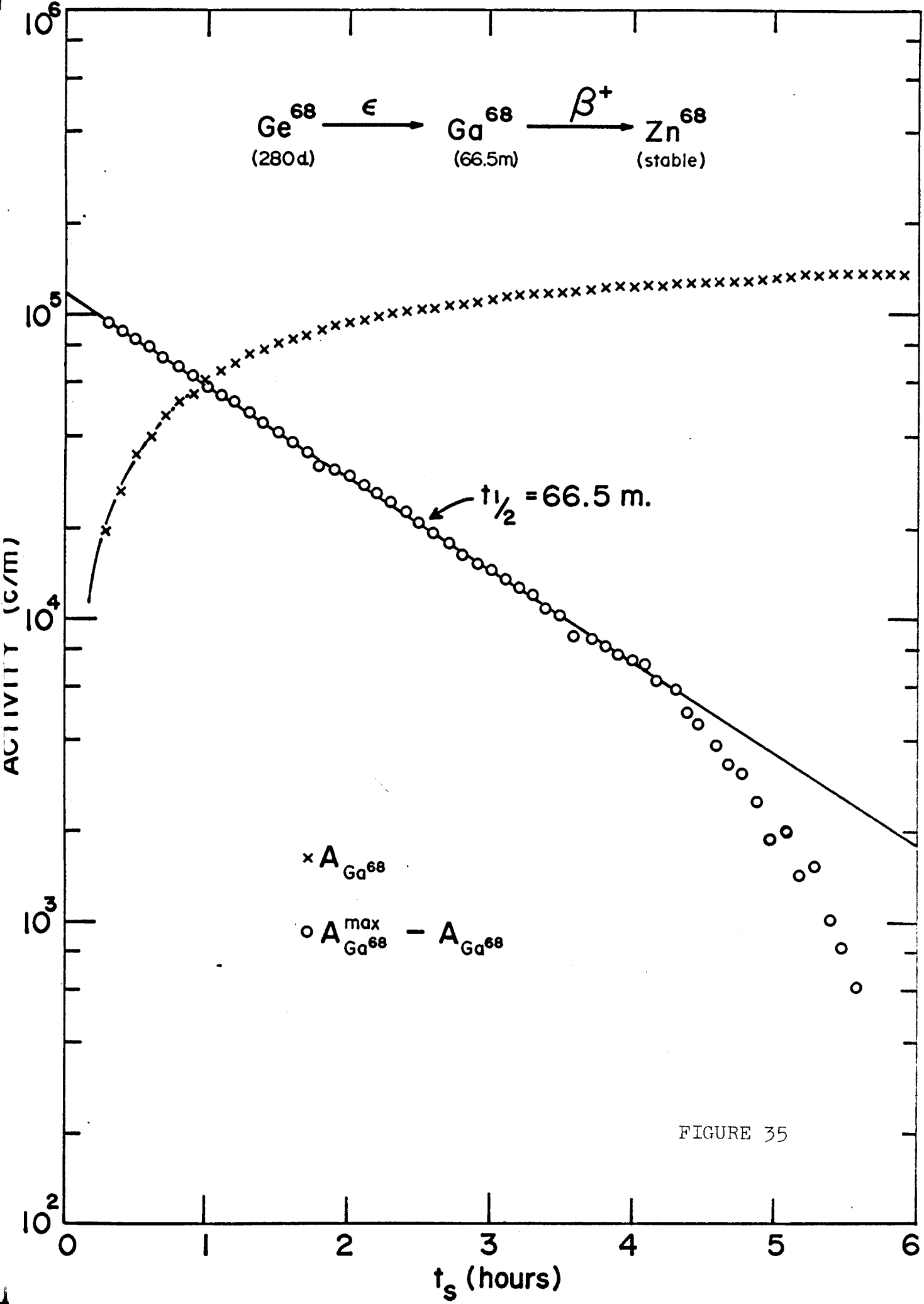
Ge^{68} (280d) $\xrightarrow{\epsilon}$ Ga^{68} (66.5m) $\xrightarrow{\beta^+}$ Zn^{68} (stable)
$t_{1/2}$ = 66.5 m.
$\times A_{Ga^{68}}$
$\circ A^{max}_{Ga^{68}} - A_{Ga^{68}}$
ACTIVITY (c/m)
10^6
10^5
10^4
10^3
10^2
0
1
2
3
4
5
6
t_s (hours)

FIGURE 35